2-D HORIZONTAL AND VERTICAL NEARSHORE CIRCULATION

by

Dadang Ahmad Suriamihardja

February 1989

2-D HORIZONTAL AND VERTICAL NEARSHORE CIRCULATION

by

Dadang Ahmad Suriamihardja

February 1989

ABSTRACT

This study was undertaken to develop a model of the nearshore 2-D horizontal (2-DH) and vertical (2-DV) circulation system. Based on interaction between waves and currents and employing the driving forces concept in the momentum equations, the field equations for the 2-DH circulation are formulated. The mild-slope equation is used to express the gradient of radiation stress which results in the formulation of the driving forces. The field equations consist of the depth-integrated conservation of mass, momentum and wave action, as well as wave number conservation. These equations are linearized by a perturbation method, where the beach slope is selected as an ordering parameter. Owing to the difference in wave characteristics, the nearshore zone is regionalized into the surf and shoaling zones. The boundary condition at the breaking point is used to match the solution of both zones. In the zeroth-order, this condition results in the maximum run-up position, and the characteristic equation by which the eigenvalues related to the rip current spacings are determined in the first order.

In comparing field observations with the rip current spacings derived herein, reasonable agreement is found. Comparing with Dalrymple and Lozano's parameter, calculated curves of the rip current spacings monotonically increase as the parameter decreases, and remains relatively constant as the parameter increases. This trend is also noted when comparing with the surf similarity parameter evaluated at the breaking point. Furthermore, the influence of littoral reflective boundaries on rip current spacing are investigated both theoretically and experimentally. Theoretical results indicate that the boundary influence decreases as the

ratio of rip current spacing to beach span decreases. Moreover, the rip current spacings become smaller as the distances from the boundaries to the center of rip current become larger. This agrees with the experimental observations. The rip current spacing significantly characterizes the profile of the rip current velocity distribution. As the rip current spacing increases the rip current velocity decreases and the circulation pattern extends offshore.

In the 2-DV circulation, a two layer model is proposed to stratify the vertical dynamics into surface and inner layers. The surface layer provides the time-averaged kinematic and dynamic boundary conditions for the inner layer along mean water level. The governing equations in the inner layer consist of time-averaged mean flow motion and turbulence. The mean flow motion is expressed in terms of the vorticity and stream function. The k-ε equations are employed to govern the turbulent motion.

The conformal mapping method is used to transform a planar beach into two parallel straight lines. In the transformed coordinate the mean flow motion is numerically calculated using an eddy viscosity similar to Svendsen (1984). The side boundary conditions are proposed to specify the undertow with slip condition on the bottom. The results are in good agreement with the Stive and Wind's (1982) experiments.

LIST OF FIGURES

CONTINUED

CONTINUED

LIST OF TABLES

ACKNOWLEDGEMENTS

I would like to express my sincere gratitude to Professor Y. Tsuchiya, Disaster Prevention Research Institute, Kyoto University for his continual supervision and encouregement, which extended far beyond the duties of his post, during my graduate and post graduate education at Kyoto University. It was through Professor Tsuchiya that I was first introduced to coastal engineering research, consequently, the culmination of this work is largely owe to him.

My appreciation also goes to Dr Y. Kawata, Associate Professor, and Dr T. Yamashita, Instructor, for their guidance and support in carrying out this study. Dr Yamashita's advise and persistence were often found to be of crucial importance.

I am also grateful to all graduate and doctor course students, for their help on several occassions, especially in the completion of this manuscript. To Mr J.R. Tallent M.sc for his kindness in correcting the draft, and to Mr T. Shishikura for his cooperation in this reseach work, I am greatly indebted. Mrs Shoko Tsuchiya is deserved thanks for the numerous occasions on which she and her husband so graciously entertained my family and I.

Lastly, I would like to dedicate this work to the mother of Indonesian nature, who served as friend, foe, and instructor to my children during the nearly 7 years of their youth that I was absent.

CONTENTS

CONTENTS

CHAPTER 1 INTRODUCTION

1.1 The Role of Nearshore Circulations

The shoreline, being simply defined as the boundary of the land, sea and air, is continually changing under the actions of waves and nearshore currents, as well as winds. Therefore, the shoreline as a whole, or the beaches which include the foreshore and backshore regions, are of a dynamic system. The beaches themselves are composed of many kinds of sediment, such as sand, silt, clay and gravel, these materials being of both organic and inorganic origins. The combined action of waves and nearshore currents incessantly works at shaping the beach into a complex geometry which is often observed along the shoreline as cyclic pattern of cusps and bays. The process of forming the beach will continue for the duration over which wave and current actions exist. This phenomenon is typically observed in nature.

Mans activities often result in partial disruption of these natural processes, which frequently leads to the acceleration of beach erosion. Consequently, coastal communities will continue to implement coastal defence methods erosion in order to maintain their residential, industrial and recreational areas. In order for coastal engineers to meet their needs, it is necessary to understand the forces which govern beach change. Most importantly are the behaviour of waves and nearshore currents, and their interaction with the beach sediment. Therefore, wave transformation in shallow water, i.e. wave refraction, diffraction, reflection, shoaling, and wave breaking is of primary importance. Once the above mentioned transformation phenomena have been adequately determined it is possible to

predict the nearshore circulations. The wave and current combined motion generates an action force which is mainly responsible for the sediment transport. The objective of the present study is to investigate the wave induced nearshore circulations more precisely, which includes their driving forces, and circulation patterns, in the horizontal and vertical planes. The nearshore circulation currents are of course one of the most important problems in coastal engineering since they are closely related to sedimentation in the nearshore zone. The present study therefore deals with the so-called nearshore dynamics. The mathematical formulation of the nearshore circulation will greatly contribute to the establishment of the nearshore dynamics.

It is well known that the water mass carried shoreward by waves often generates nearshore currents which are sometimes divided into longshore and on-offshore directed currents. They form the horizontal circulation cells in the nearshore zone. The seaward current is called the "rip current". In addition, there is a seaward current close to the bottom which is also fed by the water mass transported by breakers, this current is termed the "undertow", signifying the vertical circulation in the surf zone. Both circulations have been intensively investigated in terms of field observations and laboratory experiments. It is also well known that these circulations greatly contribute to the sediment transport in the surf zone.

1.2 Literature Review of Earlier Work on the Horizontal Nearshore Circulation

The central theme of the study on a horizontal circulation is classified into two main categories, i.e., the structure of rip currents

by which the horizontal circulation pattern can be explained and the driving mechanism by which the circulation phenomena can be generated.

1.2.1 Rip current structure

The first category was first examined theoretically by Arthur (1962). Tam (1973) utilized the qualitative description of the previously observed circulation patterns by Shepard and Inman (1951), i.e., the observed circulation was classified into three parts in order to propose a mathematical model of the rip current structure in the surf zone: the rip feeder current (longshore current), the rip current and the rip head. In Tam's model, the existence of the rip current was assummed and the energy and momentum transfer mechanism from the incident waves via feeder currents were formulated. By assuming steady state condition, shallow water approximation, boundary layer type approximation for the narrow rip current, and energy dissipation through horizontal mixing, he obtained the governing equations for nearshore currents which is identical to those of a two-dimensional incompressible jet derived by Schlichting (1933,1960) and Bickley (1939). His solution on a plane beach yields a rip currrent width which is linearly proportional to the distance from the shoreline with a constant fluid entrainment rate. To describe the rip head formation process, a sudden increase in the bottom slope is imposed, which dramatically reduces the rip current velocity, and increases the width of the rip current.

Ozaki and Sasaki (1977) experimentally examined the structure of the horizontal circulation pattern. Their experiment was related to the so-called instability region proposed by Horikawa and Sasaki (1975). According to their experimental results, two types of the horizontal

circulation pattern exist, the regular type such as Bowen's (1969) linearized solution, and the free jet type such as Tam's (1973) solution. Conclusively, they stated that, for small dimensionless rip current spacings the generated rip currents may form the former type of circulation, and if the dimensionless rip spacing becomes larger the latter circulation may be formed. Sasaki and Ozaki (1979), and Sasaki (1984) presented papers which considered theoretically their experimental conclusions. Sasaki included the lateral mixing in his theory and revealed that, as the values of the dimensionless rip spacing and the Reynolds number increase, the rip current becomes narrower and more intense, while the shoreward current in the shoaling zone becomes wider and slower.

1.2.2 Driving mechanism

The second category of the study of nearshore circulation, which focuses on the driving mechanisms of rip currents is divided into two main causes as proposed by Dalrymple (1975), i.e., wave interaction and structural interaction.

1) Driving mechanism by wave interaction

The wave interaction model includes the interaction of, synchronous edge waves and incident gravity waves (Bowen, 1969; Bowen and Inman, 1969; Sasaki, 1975); synchronous trains of incident waves with different directions (Dalrymple, 1975; Horikawa and Maruyama, 1976); wave-current interaction (Le Blond and Tang, 1974; Iwata, 1976; Mizuguchi, 1976; Dalrymple and Lozano, 1978). It is important to note that the driving mechanism which is subject to a hydrodynamic instability can be included in the wave interaction model, where the onset of the circulation occurs

when a destabilizing constraint is infinitesimaly exeeded (Hino, 1974; Tsuchiya, Yasuda and Tokuda, 1979; Tsuchiya, Yasuda and Katayama, 1980; Tsuchiya and Yasuda, 1983; Tsuchiya, Kawata, Shibano, Dadang and Shishikura, 1986).

One of the first theoretical models of rip currents and the associated nearshore circulation patterns was given by Bowen (1969). The rip current in his model developed on a plane beach under the influence of normal incidence waves. The driving mechanism for circulation pattern in the nearshore region was assumed to be due to a longshore variation in the radiation stress field. He then investigated these longshore variations produced by longshore changes in either the bottom topography or the wave heights, which are caused by the presence of edge waves (the normal mode of longshore oscillation in the nearshore zone).

Sonu (1972) carried out the detail field measurements of the nearshore circulation and meandering longshore current patterns together with beach profile data, wave characteristics, and mean water surface elevation. From the field observations, he concluded that the driving mechanism of the nearshore circulation is related to the characteristics of waves and bottom topography. He also presented a figure which describes the distribution of velocities and streamlines in the circulation cell. This figure shows that shoreward currents in the circulation cell typically occur over the shoals, and the rip currents start from the embayment. Shepard and Inman (1951) observed the inverse situation of Sonu on Scrips Beach. To explain this discrepancy Sonu argued that the phenomena should be viewed in terms of two features: 1) when incident waves have variable heights alongshore, and the surf zone bottom profile is plane, the longshore currents near the shoreline move from high-wave to low-wave areas, as observed by Shepard

and Inman, however, 2) when incident waves are uniform at the bar (or the breaker line) and the surf zone bottom profile has undulations, the currents flow from shallow to deep areas, like his observation.

Sonu further explained the wave climate during his field observation that spilling breakers entering the shoals tended to maintain the breaking crest across the surf zone, and plunging breakers was observed in a narrow strip of the rip near the bar, and unbroken crest traveled the remainder of the surf zone. As a consequence, wave heights near the shoreline were small at the shoal and large near the embayment. This feature indicates that the mean currents near the shoreline flowed from areas of small wave elevation to areas of large wave elevation.

The next development was by Le Blond and Tang (1974). They introduced the effects of the interaction between the incoming waves and the resulting rip currents, in which the plane beach and normal incidence of wave was assumed. Through a perturbation expansion, they obtained the first-order solution which included the effects of rip current-wave interaction. Their results indicate that the circulation field is not greatly modified by this interaction, except the change in wave energy distribution across the surf zone. This coupling effect may reduce the rip current velocity. However, Dalrymple and Lozano (1978) pointed out that Le Blond and Tang's calculation contained significant numerical error.

Similar to the work of Le Blond and Tang (1974), Iwata (1976) developed the theory for steady state rip current generation, in which the non-uniformity of bottom friction was assumed. But his theory failed in obtaining the eigenvalues of the governing equations, which are related to the non-dimensional alongshore spacing of the rip current system. In his characteristic equation the eigenvalue was not determined. He further

attempted to find an asymptotic solution for both the offshore and onshore stream functions which were matched at the breaking point. Finally, he obtained the real eigenvalue as a function of a parameter determined by the bottom friction, the surf zone width and the breaker height.

Mizuguchi (1977) attempted to obtain the eigenvalues from the characteristic equation similar to Iwata's theory. He considered both the uniformity and non-uniformity of the bottom friction, however, no eigenvalue was obtained. He conclude that this failure occurred due to ignoring the lateral mixing and the contribution of the bottom friction is not sufficient to represent the dissipative effect in the nearshore current. Consequently, he modified the bottom friction term to be a function of the distance from shoreline similar to the lateral mixing. Dalrymple and Lozano (1978) commented that no reason exists to justify this modificaton, so that the real eigenvalue obtained as a function of a parameter proportional to the so-called surf zone similarity parameter and inversely to the bottom friction is invalid.

Dalrymple and Lozano (1978) presented two models. One was similar to the theory of Le Blond and Tang (1974), in which changes in local wave length due to currents were considered. However their assumption of the extremely small refraction angle, which implied that no longshore variation in wave orthogonals was allowed, resulted in no rip current formation.

In the second model, the wave-current interaction effect was considered, i.e., the wave refraction due to current, in which the formation of longshore periodic nearshore circulation cells were calculated. The obtained eigenvalue was a function of a parameter expressed by the ratio of the beach slope to bottom friction coefficient. The relationship between the eigenvalue and this parameter showed that the rip current spacing

increased as the parameter increased and vice versa. The field data of Balssilie (1975) was compared with their theoretical results and found to be relatively small. According to their statement, that 59% of the field data obtained were spilling breaker. Therefore if most of the incoming waves were the so-called infragravity waves, the rip currents with small spacing can be generated as have been empirically shown by Sasaki(1977).

Rip currents have been observed in the absence of significant wave-topography, wave-wave, or wave-structure interaction. However, there is no obvious external reason for longshore variation in breaker height. Bowen and Inman (1969) stated that, theoretically, the wave set-up and the radiation stress gradient of a uniform wave train are in equilibrium over any width of beach. However, the equilibrium may not be stable; a small temporary disturbance may cause a complete breakdown of the two-dimensional equilibrium. They then presummed that a small disturbance could excite edge waves. It is also conceivable that a purely hydrodynamic instability, i.e. an initial disturbance (or perturbation), can extract potential energy from the set-up regime and convert it into horizontal circulation patterns and rip currents (Basco, 1982).

Hino (1974) proposed a theoretical model of rip current generation based on the hydrodynamic instability. Through his analysis, it was found that the unperturbed motion was related to longshore currents, and the perturbed one to rip currents. The onset of rip current excitation was subject to an infinitesimal disturbance. When the amplitude of the disturbances exponentially grew or deteriorated with respect to time, it ment that the motion became unstable or stable. These trends depended on the sign of their eigenvalues. From the governing equations together with boundary conditions at the shoreline and infinity, he obtained the

characteristic equation to determine eigenvalues. He suggested that the longshore spacing of rip currents of the most stable mode was about four times the width of breaker zone.

Tsuchiya, Yasuda and Tokuda (1979), Tsuchiya, Yasuda and Katayama (1980), and Tsuchiya and Yasuda (1983) presented a model using the cnoidal wave theory and employing the concept of hydrodynamic instability. The importance of their works was that the mass transport due to wave was included in the inertial terms of the governing equations. As previously mentioned, shoreward mass transport is compensated by seaward currents. Their analysis revealed that the solution of the longshore current was a trivial solution, while the solution of the rip currents or meandering type currents was a bifurcation solution. Finally, they obtained the rip current spacing as a function of bottom slope and bottom friction. Based on this model Tsuchiya, Kawata, Shibano, Dadang and Shishikura (1986) experimentally showed that rip currents were generated by the mechanism of hydrodynamic instability. The crest line of a normally incident wave was observed to retain its uniformity up to the third incoming wave, after the third, instability occured. It is evident that the rip currents initiate immediately following destabilization of the wave field. The current field will stabilize itself, once its interaction with the wave fields reaches an equilibrium state. Here, the need to more exactly reformulate the driving forces becomes important in qualifying the mechanism of the rip current generation through a hydrodynamic instability produced by the wave-current interaction.

2) Driving mechanism by structural interaction

The concept of structural interaction for rip current generation probably accounts for the majority of rip currents that are observed on many

sandy beaches of the world. The structural boundary, such as bottom topography, coastal littoral boundaries, and longshore bars, strongly contribute to the formation of the nearshore circulation. Variations in wave heights due to structural boundaries causes variations of radiation stresses alongshore. Consequently, the gradient of the mean water level in the surf zone initiates currents which flow from the highest to the lowest areas of wave heights. This mechanism of longshore current generation is previously discussed in the review of Sonu's(1972) work.

Noda(1974) presented the steady state nearshore circulation by considering the interaction of an incoming wave system of uniform waves with a variable bottom topography, for both normal and oblique incidence of waves. The nearshore bottom topography was approximated by Sonu's (1972) field observations. In his model, the longshore variation in the radiation stresses due to wave refraction and shoaling produce the driving mechanism of nearshore circulation. Applying this model, he obtained a maximum rip current velocity of 4 m/s which was significantly larger than field measurements. He commented this unrealistic velocity arised from neglecting the effects of wave-current interaction and lateral mixing, in his mathematical model.

Mei and Liu (1977) developed a linear theory in which the effects bottom topography on nearshore circulation was considered. They show that the depth perturbation causes variations in the mean sea level and in the radiation stresses components both in the offshore and longshore directions. The combined effects tend to drive rip currents near the shoals. The depth perturbation affects the local wave direction due to refraction and the variation of wave field causes variation in the radiation stress in turn. This tend to drive rip currents near the embayment. A

criterion was proposed in their paper to classify the mechanism of nearshore currents. This criterion, Z_B, was defined by the ratio of the surf zone width to minor longshore undulation length of the beach profile. Their analysis showed that in the case of small alongshore variation in the bottom topography, which was confined in and near the surf zone, the position of the rip currents strongly depended on the configuration of the bottom topography, as well as the parameter Z_B. They concluded that, when the value of Z_B is approximately 2 the wave-topography interaction is the controling factor in the directing the longshore currents towards the embayment, which supports Sonu's field observation. When the value of Z_B is near 10 the refraction effect becomes dominant, then the longshore currents are directed towards the shoals, which corresponds to the field observation of Shepard and Inman (1951) at the Scripps Beach.

The present study investigates rip currents excited by wave-current interaction. The model was pioneered by Le Blond and Tang (1974) and improved by Dalrymple and Lozano (1978) and Tsuchiya, Yasuda and Tokuda (1979), Tsuchiya, Yasuda and Katayama (1980), and Tsuchiya and Yasuda (1983).

1.3 Literature Review of Earlier Work on the Vertical Circulation in the Surf Zone

The first qualitative analysis of the vertical circulation in the surf zone was presented by Dyhr-Nielsen and Sørensen (1970), in which the radiation stresses in the surf zone act on the upper region of the control volume, while the hydrostatic pressure distribution is assumed. In order

to achieve an equilibrium state of the momentum in the control volume, however, two additional stresses were required, shoreward and seaward stresses acting on the water body and the bottom boundary, respectively. Hence under breaking waves, the wave motion was superposed in a resulting seaward bottom current which was termed as the "undertow".

Svendsen (1984a), and Buhr-Hansen and Svendsen (1984) extended the dynamic and mathematical model of the undertow. The former developed a theoretical model based on the first order appoximation of wave quantities in the surf zone, such as radiation stresses, wave energy dissipation and shape function. The latter emphasized the physical aspects and presented some new measurements of the undertow considering the interaction with the bottom boundary layer. Both studies developed the mechanism of the 2-D vertical nearshore circulation under the steady state. Essentially, the proposed mechanism is established as a balance among three different forces: the gradients of radiation stress, static pressure, and the shear stresses induced by breaking waves and bottom wall turbulence.

In the water column, the radiation and Reynolds stresses act dominantly shoreward and the static pressure is uniform in the whole depth, consequently, net seaward-directed horizontal forces exist over an averaging of wave period. This is the mechanism of generation of undertow.

The undertow distribution is calculated in both studies by using the linearized momentum equation which consists of the depth-integrated balances between the Reynolds and radiation stresses induced by the breaking waves and the pressure gradient of wave set-up. As far as using the zero equation model of turbulence, the Prandtl- Boussinesq gradient model is employed and the solution of the vertical distribution of undertow velocity is obtained by the integration. However, this solution includes several

parameters to be determined, such as the vertical distribution of the eddy viscosity and boundary conditions at the trough of breaking waves and the bottom. By the same concept, minor modifications in the model were made by Stive and Wind (1985) and more recently by Tsuchiya, Yamashita and Uemoto (1986).

1.4 Objectives and Outlines

The present nearshore circulation investigation is divided into two categories, the 2-D horizontal and 2-D vertical circulations. Furthermore, a theoretical investigation for both cases is performed. The objectives of this study are outlined in the following sections.

1.4.1 2-D Horizontal circulation in the nearshore zone

In Chapter 2, for the 2-D horizontal circulation in the nearshore zone, a mathematical formulation of rip currents on a planar beach is made by means of the wave-current interaction model. The theoretical results of the rip current characteristics, such as the rip current spacing and flow patterns, are compared with both the previous theoretical results, laboratory and field data, as well as the experimental results of this study.

The governing equations of 2-D nearshore currents on the plane beach are first established by employing the conservation laws of mass, momentum, energy and wave number. The so-called mild slope equation is applied to calculate wave transformation interacting with the nearshore currents. By using a perturbation method for a small parameter of beach slope, the governing field equations of rip currents are formulated. At the first-order approximation, the field equations of rip currents are obtained

in both the surf zone and shoaling zone, where the wave refraction due to currents is fully considered.

With some additional assumptions, solutions to the field equation of the 2-D nearshore currents both in the surf zone and shoaling zone are obtained in terms of the Gaussian hypergeometric function and the modified Bessel function of the 1st and 2nd kind, respectively. The matching condition for these solutions at the breaking point makes it possible to determine the eigenvalues of the characteristic equation of the derived field equation. The obtained eigenvalues determine the rip current spacings theoretically and they are compared with laboratory and field data with satisfactory agreement. Current patterns in a nearshore circulation cell are also calculated numerically based on the field equations.

In the case of nearshore circulation with littoral reflective boundary conditions, a series of experiments of rip current generation are conducted to determine the the effect of littoral boundaries on the generation of rip currents. A theoretical formulation to the rip current spacing with littoral boundaries is developed and the derived solution is compared with experiments.

1.4.2 2-D Vertical circulation in the surf zone

In Chapter 3, the 2-D vertical nearshore circulation model is developed in terms of the simplified 2-layer models of mean currents, waves and turbulence. The model is divided into the surface and inner layers.

The surface layer model provides the time-average boundary conditions for the inner layer model by simplifying the mass and momentum conservation in the surface layer. Instead of the energy conservation in this layer, the turbulent bore model is employed to provide the boundary condition for

turbulent kinetic energy model in the inner layer.

The inner layer model consists of three models, they include : the mean current model described by the stream function and vorticity equations, the turbulence model by the k-ε equations, and the time and depth-averaged momentum and energy conservation model which is modified the Svendsen model (1984.a). The numerical solution method of these three models for the 2-D vertical circulation in the surf zone is also developed by employing the grid-generation method (conformal mapping) and the model calibration is attempted by comparing the numerical results and Stive and Wind's(1985) experiment.

REFERENCES

Arthur, R.S., 1962, A note on the dynamics of rip currents, Jour. Geophys. Res., Vol. 67, pp. 2777-2779.

Basco, D.R., 1982, Surf zone currents Volume I, Miscellaneous Report No. 82-7 (I), U.S. Army, Virginia.

Basco, D.R., 1983, Surf zone currents, Coastal Engineering, Vol.7, pp. 331-355.

Beer, T., 1983, Environmental oceanography, Pergamon Press, New York, pp. 20-36.

Bowen, A.J., 1969, Rip currents, I, Theoretical investigation, Jour. Geophys. Res., Vol.74, pp.5479-5490.

Bowen, A.J., and D.L. Inman, 1969, Rip currents,II, Laboratory and field observations, Jour. Geophys. Res., Vol.74, pp. 5479-5490.

Buhr-Hansen, J. and I.A. Svendsen, 1984, A thoretical and experimental study of undertow, Proc. 19th Inter. Conf. on Coastal Eng.,

pp.2246-2262.

Dalrymple, R.A., and C.J. Lozano, 1978, Wave-current interaction model for rip currents, 83, C12, pp. 6063-6071.

Dyhr-Nielsen, M., and T. Sørensen, 1970, Sand transport phenomena on coasts with bars, Proc. 12th Inter. Conf. on Coastal Eng., pp.855-866.

Hino, M., 1974, Theory on formation of rip current and cuspidal coast, Proc. 16th Inter. Conf. on Coastal Eng., pp. 901-919.

Horikawa, K., and Y. Maruyama, 1976, On the generation of rip current in laboratory, Proc. 23rd Japanese Conf. on Coastal Eng., pp. 464-469. (in Japanese)

Horikawa, K., and M. Mizuguchi, 1975, Experiment on nearshore currents on a plane beach, Proc. 22nd Japanese Conf. on Coastal Eng., pp. 141-153. (in Japanese)

Iwata, N., 1976, Rip current spacing, Jour. of the Oceanographical Society of Japan, 32, pp. 1-10.

Le Blond, P.H. and C.L. Tang, 1974, On energy coupling between wave and currents, Jour. Geophys. Res., Vol.79, 6, pp. 811-816.

Mei, C.C., and L-F P. Liu, 1977, Effects of topography on the circulation in and near the surf zone - linear theory, Estuarine and Coastal Marine Science, 5, pp. 25-37.

Mizuguchi, M., 1976, Eigenvalue problems for rip current spacing, Proc. JSCE, 248, pp. 83-88. (in Japanese)

Mizuguchi, M., 1977, On the mechanism of nearshore circulation, Proc. 24th Japanese Conf. on Coastal Eng., pp. 591-595. (in Japanese)

Noda, E.K., 1974, Wave-induced nearshore circulation, Jour. Geophys. Res., Vol.79, 27, pp. 50-59.

Ozaki, A., M. Sasaki and Y. Usui, 1976, On the rip currents(Experiment

on steep planar beach), Proc. 23rd Japanese Conf. on Coastal Eng., pp. 471-476. (in Japanese)

Sasaki, M., 1984, Coastal Engineering in Japan, Vol. 27, pp. 139-149

Sasaki, M., and A. Ozaki, 1979, Rip currents of free jet type and regular circulation type, Proc. JSCE, 288, pp. 95-106. (in Japanese)

Sasaki, T., 1977, Field Investigations of nearshore currents on gently sloping bottom, PhD Disertation, NERC, Tokyo University, Japan.

Shepard, F.P., and D.L. Inman, 1951, Nearshore circulation, Proc. 1st Conf. on Coastal Eng., pp. 4097-4106.

Sonu, C.J., 1972, Field observation of nearshore circulation and meandering currents, Jour. Geophys. Res., Vol.77, 18, pp. 3232-3247.

Stive, M.J.F., and H.G. Wind, 1982, A Study of radiation stress and set-up in the nearshore region, Coastal Engineering, Vol.6, pp.1-25

Stive, M.J.F. and H.G. Wind, 1985, Cross-shore mean flow in the surf zone, Delft Hydraulics Laboratory-Report R1351, 15p.

Svendsen, I.A., 1984a, Wave heights and set-up in a surf zone, Coastal Engineering, Vol.8, pp.303-329.

Svendsen, I.A., 1984b, Mass flux and undertow in a surf zone, Coastal Engineering, Vol.8, pp.347-365.

Tam, C.K.W., 1973, Dynamic of Rip currents, Jour. of Geophys. Res., 78, 12, pp. 1937-1943.

Tsuchiya, Y., Y. Kawata, T. Shibano, A.S. Dadang and T. Shishikura, 1986, Proc. 33rd Japanese Conf. on Coastal Eng., pp. 36-40.(in Japanese)

Tsuchiya, Y. and A.S. Dadang, 1989, Studies on the formation of rip currents in a plane beach, Annual Dis. Prev. Res. Ins., Kyoto University, No. 32 B-2. (in press in Japanese)

Tsuchiya, Y., T. Yamashita and M. Uemoto, 1986, On the undertow in the surf

zone, Conf. on Coastal Eng. in Japan, pp.31-35. (in Japanese)

Tsuchiya, Y., T. Yasuda and K. Tokuda, 1979, Rip current theory (1), Proc. 26th Japanese Conf. on Coastal Eng., pp. 459-499. (in Japanese)

Tsuchiya, Y., T. Yasuda and A. Katayama, 1980, Rip current theory (2), Proc. 27th Japanese Conf. on Coastal Eng., pp. 158-162. (in Japanese)

Tsuchiya, Y. and T. Yasuda, 1983, Rip current theory (3), Proc. 30th Japanese Conf. on Coastal Eng., pp. 465-469. (in Japanese)

Yamashita,T., A.S. Dadang, T. Shishikura and Tsuchiya,Y.,1988, The 2VD circulation model in the surf zone, Proc.35th Japanese Conf. on Coastal Eng.,pp.267-271. (in Japanese)

Wanstrath, J.J., R.E. Whitaker, R.O. Reid, A.C. Vastano, 1976, Storm surge simulation in transformed coordinates, Volume I, Technical Report No.76-3, U.S. Coastal Engineering Research Center, 166p.

Wanstrath, J.J., 1976, Storm surge simulation in transformed coordinates, Volume II, Technical Report No.76-3, U.S. Coastal Engineering Research Center, 176p.

CHAPTER 2 HORIZONTAL CIRCULATION IN THE NEARSHORE ZONE

2.1 Introduction

At the onset of surf zone wave energy dissipation, which is defined as a momentum flux transfer from wave motion to turbulence resulting in the production of nearshore currents. The change in momentum flux can be described by the offshore and longshore gradients of the radiation stresses which act as the driving forces in the nearshore current system.

In order that the vertical integration of governing equations becomes possible, the horizontal components of the motion are assumed to be independent of water depth. The governing equations of the nearshore current system are composed of the equations of mass, momentum and energy conservation. Wave diffraction, shoaling and refraction are described by employing the so-called mild slope equation (MSE). Wave refraction due to the wave-current interaction is considered in this study, by which the mechanism of rip current formation is investigated. The steady state rip current is calculated assuming the local balance between the frictional forces and the wave-induced driving forces.

In order to obtain a set of linearized governing equations the bottom slope, s, is chosen as the scaling parameter in the perturbation method. Regionalization with the surf zone and the shoaling zone, is employed by considering the characteristics of the wave propagation in the nearshore zone. Eigenvalues of the equations in both zones are matched at the breaking point to obtain the values of the the run-up distance in the zeroth-order solution and of the alongshore spacing of the rip currents in the first-order solution. However, in order to obtained physically

reasonable values, two additional boundary conditions are required, i.e. the radiation condition for the solutions in the shoaling zone and the condition at the maximum run-up position in the surf zone, respectively.

The present study is dealing with the steady nearshore circulation system induced by normally incident waves on a uniformly sloping beach. In the latest theoretical investigation of this problem Dalrymple and Lozano (1978) extended the work of Le Blond and Tang (1974), as previously discussed no rip currents occur. However, after taking into consideration the refraction of the waves by the resulting current, steady longshore periodic nearshore current cells were formed. Consequently, the effect of the current-refracted waves should be associated with the driving forces in order to introduce it into the formulation of the nearshore current circulations, such as rip currents. It is noted, however, that the theoretical rip current spacing they obtained was not in good agreement with field data. It is therefore decided to employ the MSE in the reformulation of the driving forces in order to obtain a more reliable solution for rip current formation.

2.2 Basic Equations of Nearshore Current

To investigate the generation of nearshore currents one normally begins with the momentum equations in the wave-current system. These equations consist of the momentum conservation including radiation stress gradient, horizontal mixing, bottom friction, and convective terms, together with the mass conservation equation. The radiation stress terms can be transformed to the so-called driving force terms by using the mild slope equation to evaluate spatial distribution of wave height and direction

in the nearshore zone.

The equation of mass conservation is given as

$$\frac{\partial \rho}{\partial t} = -\frac{\partial (\rho q_j)}{\partial x_j} \tag{2.1}$$

where $d\rho/dt=0$ must be maintained due to the incompressibility of water, and the velocity vectors $q_i = U_i + u_{wi} + u_i'$. U_i represents the mean current velocity components, u_{wi} the water particle velocity components induced by wave motion, and u_i' the fluctuating components of velocities.

The momentum conservation equations are written as

$$\frac{\partial}{\partial t}(\rho q_i) = -\frac{\partial}{\partial x_j}\sigma_{ij} \tag{2.2}$$

where σ_{ij} is the momentum flux tensor of the motion which may be represented as

$$\frac{1}{\rho}\sigma_{ij} = U_iU_j + \overline{U_iu_{wj}} + \overline{u_{wi}U_j} + \overline{u_{wi}u_{wj}} + \overline{u_i'u_j'} + (\frac{1}{\rho}p+gz)\delta_{ij} \tag{2.3}$$

In this relation, the characteristic time scales of the two velocities u_{wi} and u_i' are assumed to be significantly different, such that they are uncorrelated. The over bar indicates time averaging.

For simplicity, the horizontal components of the nearshore current motion are assumed to be independent of the local depth. By depth-integrating (2.1) and (2.2) over the water column, Phillips (1966), Dolata and Rosenthal (1984), and Crapper (1984), the mass and momentum conservation equations can be written in the form by Crapper (1984), which include the bottom frictions and lateral mixing terms in the form as:

$$\frac{\partial}{\partial t}(\rho d) + \frac{\partial}{\partial x_j}(\rho U_j d + M_j) = 0 \tag{2.4}$$

$$\frac{\partial}{\partial t}(\rho U_i d) + \frac{\partial}{\partial x_j}(\rho U_i U_j + U_i M_j + U_j M_i + S_{ij} + \rho \tau_{ij} d) + g d \rho \delta_{ij} \frac{\partial \bar{\eta}}{\partial x_j} + \rho f_{ij} U_i = 0 \tag{2.5}$$

where M_i and M_j, S_{ij}, τ_{ij}, f_{ij} represent the mass transport due to waves, the so-called excess momentum fluxes due to waves (radiation stress), the lateral mixing terms and the bottom friction coefficients.

Modifying the momentum equation (2.5) in the steady state case results in

$$\rho U_j \frac{\partial U_i}{\partial x_j} + \rho \tau_{ij} + \rho f_{ij} U_i + \rho g \delta_{ij} \frac{\partial \bar{\eta}}{\partial x_j} = - \frac{\partial}{\partial x_j}(S_{ij} + U_j M_i) - M_j \frac{\partial}{\partial x_j} U_i \tag{2.6}$$

where the right hand side of (2.6) represents the so-called driving forces. Assuming the isotropic eddy viscosity, Longuet-Higgins (1970) expressed τ_{ij} as

$$\tau_{ij} = - \frac{N}{s} d^{3/2} \frac{\partial^2 U_i}{\partial x_j^2} - \frac{5}{2} N m d^{1/2} \delta_{ij} \frac{\partial U_i}{\partial x_j} \tag{2.7}$$

For the bottom friction $f_{ij}U_i$, Iwata's (1976) formulation is employed, which are written as:

$$f_{xx}U + f_{yx}V = \frac{2}{\pi} K_* (gd)^{1/2} \{ (1 + \cos^2\theta) U + \frac{1}{2} \sin 2\theta V \}$$

$$f_{yx}V + f_{yy}U = \frac{2}{\pi}K_*(gd)^{1/2}\{(1 + \sin^2\theta)V + \frac{1}{2}\sin 2\theta U\} \qquad (2.8.a)$$

In the case of normal incidence of waves, $\theta=0$, (2.8.a) is reduced to:

$$(f_{xx}U, \quad f_{yy}V) = \frac{2}{\pi}K_*(gd)^{1/2}(2U, V) \qquad \text{for} \quad x<x_B$$

$$(f_{xx}U, \quad f_{yy}V) = \frac{2}{\pi}K_*(gd_B)^{1/2}(2U, V) \qquad \text{for} \quad x>x_B \qquad (2.8.b)$$

where $K_* = 1.41\ (\gamma/kk_e)^{-2/3}$, k_e is bottom roughness, k wave number, γ the ratio of wave amplitude to the local depth, x_B wave breaking point.

2.3 Formulation of Driving Forces

The velocity potential of the linear wave theory, Φ is expressed in the form

$$\Phi = \frac{ga}{i\omega_r}\exp(i\psi) \qquad (2.9)$$

where ψ is the function which is related to the absolute angular frequency ω and to the wave number k as

$$\frac{\partial\psi}{\partial t} = -\omega \quad \text{and} \quad \frac{\partial\psi}{\partial x_j} = k_j \qquad (2.10)$$

and the relative angular frequency ω_r is defined by

$$\omega_r = \omega - k_jU_j \qquad (2.11)$$

The MSE formulated by Kirby (1984) which includes an additional wave energy dissipation term, $\omega_r W\Phi$, is written as

$$\frac{D^2\Phi}{Dt^2} + \frac{\partial U_j}{\partial x_j}\frac{D\Phi}{Dt} - \frac{\partial}{\partial x_j}(cc_g\frac{\partial \Phi}{\partial x_j}) + (\omega_r{}^2 - k^2cc_g - \omega_r W)\Phi = 0 \qquad (2.12)$$

where c and c_g are the wave celerity and group velocity respectively, W is the ratio of the wave energy dissipation D to the wave energy E, and the Lagrangian derivative $D/Dt = \partial / \partial t + U_j \partial / \partial x_j$.

By writting (2.9) in the form:

$$\Phi = \varphi\exp(-i\omega t) \qquad (2.13.a)$$

$$\varphi = \frac{ga}{i\omega_r}\exp(i\$) \qquad (2.13.b)$$

where $\$$ is phase function, the eikonal equation is written as

$$\frac{\partial \$}{\partial x_j} = k_j \qquad (2.14)$$

Substituting (2.13) into (2.12), the MSE can be transformed to

$$\frac{\partial}{\partial x_j}(cc_g\frac{\partial \varphi}{\partial x_j}) = -i\omega_r W\varphi - i\omega\varphi\frac{\partial U_j}{\partial x_j} - 2i\omega U_j\frac{\partial \varphi}{\partial x_j}$$

$$-(\omega^2 + k^2cc_g - \omega_r{}^2)\varphi \qquad (2.15)$$

When the wave celerity c is assumed to be nearly equal to the wave group velocity c_g, (2.15) becomes

$$\frac{\partial}{\partial x_j}(c^2\frac{\partial \varphi}{\partial x_j}) = -i\omega_r W\varphi - i\omega\varphi\frac{\partial U_j}{\partial x_j} - 2i\omega U_j\frac{\partial \varphi}{\partial x_j} - \omega^2\varphi \qquad (2.16)$$

Because φ in (2.16) contains effects of wave amplitude decay and changing in wave direction, it is possible to modify radiation stresses of Dingemans (1987) by assuming the shallow water condition. We get the expression of the radiation stresses as

$$S_{ij} = \frac{\rho}{4g}\left[c^2\left\{\frac{\partial \varphi^*}{\partial x_i}\frac{\partial \varphi}{\partial x_j} + \frac{\partial \varphi}{\partial x_i}\frac{\partial \varphi^*}{\partial x_j}\right\} + 2\varphi\varphi^* d\omega_r\frac{\partial \omega_r}{\partial d}\delta_{ij}\right] \qquad (2.17)$$

where φ^* is the complex conjugate of φ, and $\partial\omega_r/\partial d \fallingdotseq \omega_r/2d$. Recalling the right hand side of (2.6) results in the expression for the so-called driving forces which is written as

$$F_i = -\frac{\partial}{\partial x_j}\{S_{ij} + U_j M_i\} - M_j\frac{\partial}{\partial x_j}U_i \qquad (2.18)$$

where M_i is the depth-integrated mass transport due to waves which is formulated by Crapper (1984) as

$$M_i = \frac{\rho\omega_r}{2g}\varphi\varphi^*\frac{\partial S}{\partial x_i} \qquad (2.19)$$

Equation (2.18) can be modified by using (2.16), (2.17) and (2.19). Following lengthty algebraic procedures the (2.18) becomes

$$F_i = \frac{\rho\omega_r}{2g}W\varphi\varphi^*\frac{\partial S}{\partial x_i} - d\frac{\partial}{\partial x_i}\left\{\frac{\rho}{4g}\varphi\varphi^*\frac{\omega_r^2}{d}\right\}$$

$$+ \frac{\rho\omega_r}{2g}\varphi\varphi^* \frac{\partial S}{\partial x_j}\left\{\frac{\partial U_i}{\partial x_j} - \frac{\partial U_j}{\partial x_i}\right\} - c^2\frac{\partial}{\partial x_i}\left\{\frac{\rho}{4g}\varphi\varphi^*\frac{1}{A}\frac{\partial^2 A}{\partial x_j^2}\right\} \qquad (2.20)$$

The first term in the right side of (2.20) is the rotational term which contains the wave energy dissipation and the wave direction. Dingemans, Radder and De Vriend (1987) demonstrated that this rotational term alone is able to generate non-zero depth-averaged current velocities. The second term is the irrotational one. The third term describes the interaction between mass transport due to waves and currents. The last term is the additional effect resulting from the diffraction of waves. When neglecting the wave diffraction effect, (2.20) coincides with the equation derived by Crapper(1984). They also formulated the wave induced driving forces by assumming that wave diffraction effects are small enough to be neglected. Substituting (2.20) into (2.6), the momentum equations can finally be reduced to

$$U_j\frac{\partial U_i}{\partial x_j} + R_{ij} = -g\delta_{ij}\frac{\partial \bar{\eta}}{\partial x_j} + \frac{D}{\rho d\omega_r}\frac{\partial S}{\partial x_i}$$

$$-\frac{\partial}{\partial x_i}\left\{\frac{E}{2\rho d}\right\} + \frac{E}{\rho d\omega_r}\frac{\partial S}{\partial x_i}\left\{\frac{\partial U_j}{\partial x_i} - \frac{\partial U_i}{\partial x_j}\right\} \qquad (2.21)$$

where $R_{ij} = \tau_{ij} + f_i U_i$. The equation of mass conservation is then written as

$$\frac{\partial}{\partial x_j}\left\{\rho U_j d + \frac{E}{\omega_r}\frac{\partial S}{\partial x_j}\right\} = 0 \qquad (2.22)$$

The cross-differentiation of the momentum equation (2.21)together with

substitution of mass conservation (2.22) yields

$$\{U_j + \frac{E}{\rho d\omega_r}\frac{\partial \delta}{\partial x_j}\}\frac{\partial}{\partial x_j}(\frac{\Omega}{d}) + \{\frac{\partial R_{ij}}{\partial x_i} - \frac{\partial R_{ji}}{\partial x_j}\} +$$

$$\{\frac{\partial \delta}{\partial x_i}\frac{\partial}{\partial x_j} - \frac{\partial \delta}{\partial x_j}\frac{\partial}{\partial x_i}\}(\frac{D}{\rho d\omega_r}) = 0 \qquad (2.23)$$

where $\Omega = \partial U_j / \partial x_i - \partial U_i / \partial x_j$. In the absence of the first term, i.e. neglecting the convective terms, (2.23) describes the balancing state between the frictional forces and the driving forces, which generates the rip currents.

The driving forces in (2.23) can be described by the wave energy dissipation D, the wave phase function δ, and the relative angular frequency ω_r. This means that the driving forces subject to both the wave energy decay and difraction refraction in the nearshore zone. Wave refraction due to seaward currents makes wave direction more oblique, which then generates the feeder currents (wave induced currents running parallel to the shoreline). Two opposite feeder currents merge at a location where the rip current is generated. The wave ray direction can be calculated using the conservation of wave number equation, which is described in Section 2.4.2 by employing a geometrical calculation. In the steady state, the wave number conservation is equivalent to the irrotational condition of wave number, which is written as

$$\frac{\partial k_j}{\partial x_i} = \frac{\partial k_i}{\partial x_j} \qquad (2.24)$$

Wave action, rather than wave energy flux, is conserved in the wave-current combined system, which is written as

$$\frac{\partial}{\partial x_j}\left\{\frac{E}{\omega_r}(U_j + c_j)\right\} + \frac{D}{\omega_r} = 0 \qquad (2.25.a)$$

which can be transformed to

$$\frac{\partial}{\partial x_j}\{E(U_j + c_j)\} - \frac{E}{\omega_r}(U_j + c_j)\frac{\partial \omega_r}{\partial x_j} + D = 0 \qquad (2.26)$$

According to Christoffersen and Jonsson (1980) the second term in (2.26) can be written by

$$-\frac{E}{\omega_r}(U_j + c_j)\frac{\partial \omega_r}{\partial x_j} = S_{ij}\frac{\partial U_i}{\partial x_j} \qquad (2.27)$$

It is clearly shown that the right hand side of (2.27) represents the work done by radiation stresses on the gradient of velocities. The expression of (2.27) is not used in this study, because, as shown in the momentum equation, the gradient of radiation stresses has been modified in relation to the driving forces.

2.4 Field Equations of Rip Current

2.4.1 Perturbation scheme

Before ordering the equations using the perturbation method, non-dimensionalization of the equations first be required. The water depth d_B at the breaking point was selected as the representative length to facilitate the non-dimensionalization process. This process is given below:

$$(x,\ y,\ \bar{\eta},\ d) = d_B(x^*,\ y^*,\ \bar{\eta}^*,\ d^*) \tag{2.28.a}$$

$$(U,\ V,\ c) = (gd_B)^{1/2}(U^*,\ V^*,\ c^*) \tag{2.28.b}$$

$$(\omega,\ \omega_r) = (g/d_B)^{1/2}(\omega^*,\ \omega_r^*) \tag{2.28.c}$$

$$(k,\ k_x,\ k_y) = d_B^{-1}(k^*,\ k_x^*,\ k_y^*) \tag{2.28.d}$$

where the asteric represents the dimensionless quantities.

Inserting equations of (2.28) into (2.4), (2.21), (2.25a), and (2.24) and neglecting the contribution of the mass transport due to waves, the equations in the steady state become:

$$\frac{\partial}{\partial x_j^*}(U_j^* d^*) = 0 \tag{2.29}$$

$$U_j^* \frac{\partial U_i^*}{\partial x_j^*} - \frac{N}{S} d^{*3/2} \frac{\partial^2}{\partial x_j^{*2}} U_i^* - \frac{5Nm}{2} d^{*1/2} \delta_{ij} \frac{\partial U_i^*}{\partial x_j^*} + f_{ij}^* U_i^* +$$

$$\delta_{ij} \frac{\partial \bar{\eta}^*}{\partial x_j^*} = \frac{D^*}{\rho d^* \omega_r^*} \frac{\partial S^*}{\partial x_i^*} - \frac{\partial}{\partial x_i^*} \frac{E^*}{\rho 2 d^*} \tag{2.30}$$

$$\frac{\partial}{\partial x_j^*} \left\{ \frac{E^*}{\omega_r^*} (U_j^* + c_j^*) \right\} + \frac{D^*}{\omega_r^*} = 0 \tag{2.31}$$

$$\frac{\partial k_j^*}{\partial x_i^*} = \frac{\partial k_i^*}{\partial x_j^*} \tag{2.32}$$

The bottom slope, s ,is selected as a parameter of perturbation in ordering the equations, and the expansion procedures are listed below. The asteric has been dropped for convenience.

$$d = s\{d_0 + s\zeta_1 + s^2\zeta_2 + \ldots\} \tag{2.33.a}$$

$$c = s^{1/2}\{c_0 + sc_1 + s^2c_2 + \ldots\} \tag{2.33.b}$$

$$U = s^{1/2}\{sU_1 + s^2U_2 + \ldots\} \tag{2.33.c}$$

$$V = s^{1/2}\{sV_1 + s^2V_2 + \ldots\} \tag{2.33.d}$$

$$a = s\{a_0 + sa_1 + s^2a_2 + \ldots\} \tag{2.33.e}$$

$$k = \{k_{0x} + sk_{1x} + s^2k_{2x} + \ldots\}i + \{sk_{1y} + s^2k_{2y} + \ldots\}j \tag{2.33.f}$$

$$\omega_r = s^{1/2}\{k_{0x}c_0 + s(k_{1x}c_0 + k_{0x}c_1) + \ldots\} \tag{2.33.g}$$

$$\delta = \{\delta_0 + s\delta_1 + s^2\delta_2 + \ldots\} \tag{2.33.h}$$

where

$$d_0 = (x+\zeta_0),\ c_0 = (x+\zeta_0)^{1/2},\ a_0 = \gamma(x+\zeta_0), \tag{2.33.i}$$

and γ is the ratio of wave amplitude to the local depth, and ζ has relation to $\bar{\eta}$ as $\bar{\eta} = s\zeta$.

2.4.2 Geometrical calculation and conservation of the wave number

The normally incident waves refract due to their interaction with rip currents. This means that the wave number direction will intersect the beach obliquely, therefore based on Figure 2.1 the wave number can be represented as

$$\boldsymbol{k} = -|k|\cos\theta\ \boldsymbol{i} - |k|\sin\theta\ \boldsymbol{j} \tag{2.34}$$

where $|k|$ is the norm of vector $\boldsymbol{k}$. Equation (2.34) can be expanded with respect to the perturbation parameter s , such that

$$\boldsymbol{k} = -(k_{0x} + sk_{1x})\boldsymbol{i} - (sk_{1y})\boldsymbol{j} \tag{2.35}$$

The wave group velocity, assuming nearly equal to the wave celerity in the surf zone, was assumed to be in the same direction with the wave number vectors, consequently, it can be expressed as

$$\boldsymbol{c} = -\{c_0 + s(c_1 - U_1) + \ldots\}\boldsymbol{i} - \{s(-V_1) + \ldots.\}\boldsymbol{j} \tag{2.36}$$

Using (2.34), (2.35), and (2.36), $\cos\theta$ can be expressed as:

$$\cos\theta = \frac{-(k_{0x} + sk_{1x})}{|k|} = \frac{-(c_0 + s(c_1 - U_1))}{|c|} \tag{2.37.a}$$

By the same way, $\sin\theta$ is:

$$\sin\theta = \frac{-k_{1y}}{|k|} = \frac{V_1}{|c|} \qquad (2.37.b)$$

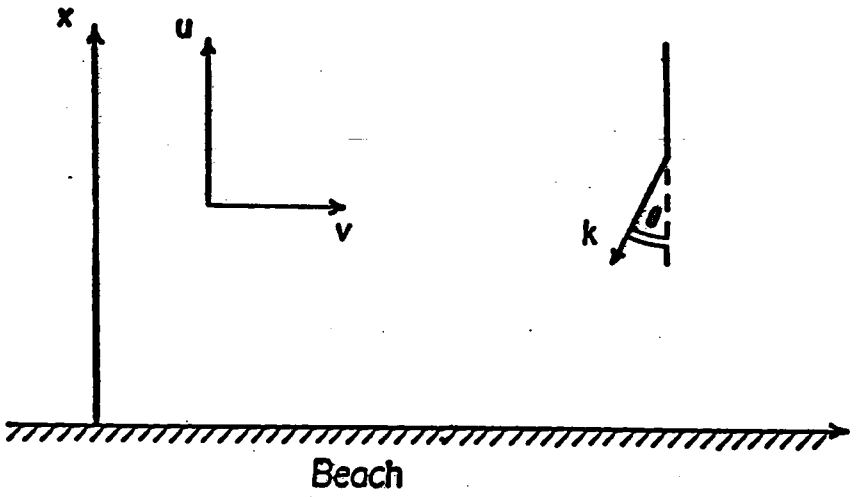

Figure 2.1 The coordinate system and geometry for the nearshore current vectors U, V and wave number k.

From (2.37), the wave numbers are given as:

$$O(s^0): \quad k_{0x} = \frac{|k|}{|c|} c_0 \qquad (2.38.a)$$

$$O(s^1): \quad k_{1x} = \frac{|k|}{|c|}(c_1 - U_1) = \frac{k_{0x}}{c_0}(c_1 - U_1) \qquad (2.38.b)$$

$$O(s^1): \quad k_{1y} = -\frac{|k|}{|c|}V_1 = -\frac{k_{0x}}{c_0}V_1 \tag{2.38.c}$$

The conservation equation of the wave number can be formulated for each order using the relations (2.37) and (2.38), as well as the condition of $\partial \omega_{0r} / \partial x = 0$,as:

$$O(s^0): \quad \frac{\partial k_{0x}}{\partial y} = 0 \tag{2.39.a}$$

$$O(s^1): \quad \frac{\partial k_{1x}}{\partial y} = \frac{\partial k_{1y}}{\partial x} \tag{2.39.b}$$

or

$$O(s^1): \quad c_{1y} = U_{1y} - mV_{1\bar{x}} + \frac{m}{\bar{x}}V_1 \tag{2.39.c}$$

where m is the slope of mean water level $(1+\zeta_{0x})$, $\bar{x}=m(x+x_s)$ is actually equal to d_0, and x_s is the maximum run-up position.

2.4.3 Zeroth-order field equation

The leading terms of the governing equations produced by the perturbation expansion are listed below for each region, the surf zone and the shoaling zone, respectively.

In the surf zone, the zeroth order momentum equation is given as

$$\rho d_0 \frac{\partial \zeta_0}{\partial x} = \frac{D_0}{\omega_{0r}} \frac{\partial \delta_0}{\partial x} - d_0 \frac{\partial}{\partial x}\left(\frac{E_0}{2d_0}\right) \tag{2.40}$$

and the wave action conservation equation is deduced from (2.31).

$$-\frac{\partial}{\partial x}(E_0 c_0) + D_0 = 0 \tag{2.41}$$

In the shoaling zone, the momentum equation is given by

$$\rho d_0 \frac{\partial \zeta_0}{\partial x} = - d_0 \frac{\partial}{\partial x}\left(\frac{E_0}{2d_0}\right) \tag{2.42}$$

and the wave action conservation is given by

$$\frac{\partial}{\partial x}(E_0 c_0) = 0 \tag{2.43}$$

Mass conservation in both regions does not exist since the mass transport by wave is neglected, furthermore the wave number conservation equation does not appear because k_{0x} is only a function of x, see (2.39.a).

In order to solve the above equations, the wave amplitude, a_0, in the surf zone is assumed to be proportional to the local depth,of the leading order, as is usually employed in the breaker model, as

$$a_0 = \gamma d_0 \tag{2.44}$$

It should, however, be emphasized that this assumption is not applied to the first order amplitude a_1, because a_1 is an unknown value interdependent to the other unknown functions such as U_1, V_1, C_1, and ζ_1 in the first order equations.

Wave energy dissipation is hypothesized as

$$D = \frac{5\rho\gamma^2}{4}\left[m d_0^{3/2} + s\left\{ \frac{3m}{2} d_0^{1/2}\zeta_1 + d_0^{3/2}\zeta_{1x} \right\} + \cdots\cdots \right] \tag{2.45}$$

where $D_0=(5\rho\gamma^2 m/4)d_0$ and $m=(1+\zeta_{0x})$.

The solution for the wave set-up is obtained from (2.40), (2.44) and (2.45) as

$$\zeta_0(x) = -\frac{3\gamma^2/2}{1+3\gamma^2/2} + x_s' \tag{2.46}$$

where x_s' is an integration constant. The zeroth order wave amplitude in the shoaling zone is obtained from (2.43) and written as

$$a_0 = B_0^{1/2}\, d_0^{1/4} \tag{2.47}$$

where B_0 is an integration constant. By substituting (2.47) into (2.42) yields the wave set-down expression as

$$\zeta_0(x) = -\frac{1}{4}B_0\, d_0^{3/2} + K_1 \tag{2.48}$$

where K_1 is an integration constant.

The boundary condition of (2.48), $\zeta_0=0$ at infinite distance $d_0\to\infty$, gives $K_1=0$, so that (2.48) becomes

$$\zeta_0(x) = -\frac{1}{4}B_0\, d_0^{3/2} \tag{2.49}$$

The matching condition at the breaking point is given by

$$\zeta_0(x)\big|_{\text{surf zone}(x=x_B)} = \zeta_0(x)\big|_{\text{shoaling zone}(x=x_B)} \tag{2.50}$$

Substituting (2.46) and (2.49) into (2.50),we get

$$x_s = \frac{x_B}{(1+ 3\gamma^2/2)}\left[\frac{3\gamma^2}{2} - \frac{\gamma_B^2(1 + 3\gamma^2/2)}{4(1 - 3\gamma_B^2/8)}\right] \tag{2.51}$$

where $\gamma_B^2 = B_0 x_B^{-5/2}$. The wave set-up is finally given by

$$\zeta_0(x) = -\frac{3\gamma^2/2}{(1 + 3\gamma^2/2)}x + \frac{x_B}{(1+ 3\gamma^2/2)}\left[\frac{3\gamma^2}{2} - \frac{\gamma_B^2(1 + 3\gamma^2/2)}{4(1 - 3\gamma_B^2/8)}\right] \tag{2.52}$$

The position of maximum run-up can be calculated by using (2.52) through the definition of $d_0 = \bar{x} = m(x+x_s)$, where $m=1/(1+ 3\gamma^2/2)$, as

$$x_s = \left\{3\gamma^2/2 - \frac{\gamma_B^2(1 + 3\gamma^2/2)}{4(1 - 3\gamma_B^2/8)}\right\}x_B \tag{2.53}$$

2.4.4 First order field equations

1) Field equation in the surf zone

Unlike the zeroth-order, the first order mass conservation equation is required to define the stream function. In (2.4) the mass transport due to waves has been formulated, nevertheless, in the present analysis it will not be considered. This means that the depth-integrated currents of the first order are merely generated by the gradient of radiation stress which has been formulated as the driving forces induced by wave. Of course the presence of the mass transport by waves is of importance in the governing equations especially for the circulation in the vertical plane.

The mass conservation equation is given from (2.29) by considering (2.33) as:

$$\frac{\partial}{\partial \bar{x}}\{U_1\bar{x}\} + \frac{\partial}{\partial y}\{V_1\bar{x}\} = 0 \tag{2.54}$$

The definition of the stream function can be made from (2.54) as:

$$U_1\bar{x} = \hat{\Psi}_y \quad \text{and} \quad V_1\bar{x} = -m\hat{\Psi}_{\bar{x}} \tag{2.55}$$

Using (2.55), the governing equations (2.30)-(2.32) can be transformed to the four equations below.

The momentum equation is given by:

$$\frac{c_1}{\bar{x}^{1/2}} + \left\{\frac{(2\kappa + \nu m^2/2)}{\bar{x}^{3/2}}\right\}\hat{\Psi}_y + \nu\bar{x}^{1/2}\frac{\partial}{\partial y}\left\{\hat{\Psi}_{yy} + m^2\hat{\Psi}_{\bar{x}\bar{x}} - \frac{2m^2}{\bar{x}}\hat{\Psi}_{\bar{x}}\right\} +$$

$$\frac{5}{2}\frac{\nu m^2}{\bar{x}^{1/2}}\hat{\Psi}_{\bar{x}y} = \frac{4(1+\gamma^2)}{5\gamma^2}\zeta_{1\bar{x}} + \frac{2}{5\gamma}a_{1\bar{x}} + \frac{1}{2\bar{x}}\zeta_1 \tag{2.56}$$

$$-\left\{\frac{(1-\kappa)m}{\bar{x}^{3/2}}\right\}\hat{\Psi}_{\bar{x}} - \nu m\bar{x}^{1/2}\frac{\partial}{\partial \bar{x}}\left\{\hat{\Psi}_{yy} + m^2\hat{\Psi}_{\bar{x}\bar{x}} - \frac{2m^2}{\bar{x}}\hat{\Psi}_{\bar{x}}\right\} - \frac{5m^3\nu}{2\bar{x}^{1/2}}\hat{\Psi}_{\bar{x}\bar{x}}$$

$$+ \frac{9m^3\nu}{2\bar{x}^{3/2}}\hat{\Psi}_{\bar{x}} = \frac{4(1 - \gamma^2/4)}{5\gamma^2}\zeta_{1y} + \frac{2}{5\gamma m}a_{1y} \tag{2.57}$$

the wave action conservation is given by:

$$\frac{\partial}{\partial \bar{x}}\left\{\bar{x}^{3/2}(\zeta_1 - \frac{4}{5\gamma}a_1)\right\} = \frac{3}{5}(\bar{x}c_1 - \hat{\Psi}_y) - \frac{2}{5}\bar{x}^2\frac{\partial}{\partial \bar{x}}(c_1 - \frac{1}{\bar{x}}\hat{\Psi}_y) \tag{2.58}$$

and the wave number conservation equation is finally written from (2.39.c) as:

$$\bar{x} c_{1y} = \hat{\Psi}_{yy} + m^2 \hat{\Psi}_{\bar{x}\bar{x}} - \frac{2m^2}{\bar{x}} \hat{\Psi}_{\bar{x}} \tag{2.59}$$

where $\kappa = 4K/5\gamma^2 sm$, $K = (2/\pi)\gamma K_*$ and $\nu = 4N/5\gamma^2 m$. In the above four equations there are four unknowns $\hat{\Psi}$, ζ_1, a_1, and c_1 to be solved. The principal discrepancy between this study and of Dalrymple and Lozano's (1978) is in the approximation of wave refraction. Dalrymple and Lozano assumed the wave refraction angle to be very small. By equating $c_1 = (1/2\bar{x}^{1/2})\zeta_1$ and neglecting $\hat{\Psi}_{\bar{x}\bar{x}}$ and $(1/\bar{x})\hat{\Psi}_{\bar{x}}$, (2.59) can be reduced to their equation:

$$\zeta_1 = \frac{2}{\bar{x}^{1/2}} \hat{\Psi}_y \tag{2.60}$$

This approximation obviously assumes no refraction of the waves caused by the interaction of waves and currents. For this reason the wave-current interaction model developed by Dalrymple and Lozano does not yield a steady circulation in the nearshore zone. Another approximation is made to the so-called wave dispersion relation, $c_0 + \varepsilon c_1 + \ldots = (h + \bar{\eta}_0 + \varepsilon\eta_1 + \ldots)^{1/2}$ to evaluate c_1. This equation is therefore combined with the set of governing equations, while the number of unknowns remain the same. It is necessary, of course, to find a simple relation between c_1 and ζ_1 in order to reduce higher order differentiation terms. This simple relation can be derived from the set of established governing equations. In order to approximate the relation along with four equations are employed, (2.56) can be used by

considering the most effective terms, as:

$$c_1 = \frac{q}{\bar{x}^{1/2}} \zeta_1 \tag{2.61}$$

If the other non-leading terms are neglected, q will equal 1/2 which is equivalent to that of Dalrymple and Lozano's approximation. Even though based on this approximation, the value of q may be somewhat larger than 1/2.

Substituting (2.57), (2.59) and (2.61) into (2.58) after making differentiation with respect to y in order to eliminate α_{1y}, (2.58) is reduced to:

$$\alpha\frac{\partial}{\partial \bar{x}}(\bar{x}^{3/2}\zeta_{1y}) - \frac{5q\gamma^2}{4}(\kappa + \frac{11m^2\nu}{2})\bar{x}^{1/2}\zeta_{1y} =$$

$$\frac{\gamma^2}{4}\frac{\partial}{\partial \bar{x}}(\bar{x}\hat{\Psi}_{yy}) + \frac{3\gamma^2}{8}(1 - \frac{10\kappa}{3} + 10m^2\nu)\hat{\Psi}_{yy}$$

$$- \frac{5\gamma^2}{2}(1 - \kappa + \frac{m^2\nu}{2})(\frac{m^2}{\bar{x}})\hat{\Psi}_{\bar{x}} + \frac{25m^2\gamma^2\nu}{8}\bar{x}\hat{\Psi}_{\bar{x}yy} - \frac{5m^2\gamma^2\nu}{4}\bar{x}^3 c_{1\bar{x}\bar{x}y} \tag{2.62}$$

α_{1x}, α_{1y}, and ζ_1 in (2.58) are written by using (2.56), (2.57), (2.59) and (2.61), then (2.58) is reduced to the form:

$$\beta\frac{\partial}{\partial \bar{x}}(\bar{x}^{3/2}\zeta_{1y}) - \frac{5\gamma^2}{4}(1 + 2q - \frac{9qm^2\nu}{4})\bar{x}^{1/2}\zeta_{1y} =$$

$$\frac{\gamma^2}{4}\frac{\partial}{\partial \bar{x}}(\bar{x}\hat{\Psi}_{yy}) - \frac{7\gamma^2}{8}(1 + \frac{20\kappa}{7} - \frac{65m^2\nu}{14})\hat{\Psi}_{yy}$$

$$- \frac{15\gamma^2}{8}(1 - \kappa + \frac{m^2\nu}{2})\frac{m^2}{\bar{x}}\hat{\psi}_{\bar{x}} + \frac{25m^2\gamma^2\nu}{8}\bar{x}\hat{\psi}_{\bar{x}yy} + \frac{5\gamma^2\nu}{4}\bar{x}^3 c_{1yyy} \qquad (2.63)$$

where $\alpha = \{1+(3/8+q/4+65qm^2\nu/8)\gamma^2\}$ and $\beta = \{1+(13/8+q/4+15qm^2\nu/8)\gamma^2\}$. Eliminating the term of $\bar{x}^{3/2}\zeta_{1\bar{x}y}$ from (2.62) and (2.63), the equation for $\bar{x}^{1/2}\zeta_{1y}$ can be written as:

$$\{\frac{5q\gamma^2}{4\alpha}(\kappa + \frac{11m^2\nu}{2}) - \frac{5\gamma^2}{4\beta}(1 + 2q - \frac{9qm^2\nu}{4})\}\bar{x}^{1/2}\zeta_{1y} =$$

$$\frac{\gamma^2}{4}(\frac{1}{\beta} - \frac{1}{\alpha})\frac{\partial}{\partial\bar{x}}(\bar{x}\hat{\psi}_{yy})$$

$$- \{\frac{7}{8\beta}(1 + \frac{20\kappa}{7} - \frac{65m^2\nu}{14}) + \frac{3}{8\alpha}(1 - \frac{10\kappa}{3} + 10m^2\nu)\}\gamma^2\hat{\psi}_{yy}$$

$$- (\frac{15}{8\beta} - \frac{5}{2\alpha})(1 - \kappa + \frac{m^2\nu}{2})(\frac{m^2\gamma^2}{\bar{x}})\hat{\psi}_{\bar{x}}$$

$$+ \frac{25m^2\gamma^2\nu}{8}(\frac{1}{\beta} - \frac{1}{\alpha})\bar{x}\hat{\psi}_{\bar{x}yy} + \frac{5\gamma^2\nu}{4}(\frac{c_{1yyy}}{\beta} + \frac{m^2 c_{1\bar{x}\bar{x}y}}{\alpha}) \qquad (2.64)$$

By cross-differentiating the momentum equations (2.56) and (2.57), the following equation can be obtained as:

$$\bar{x}\frac{\partial}{\partial\bar{x}}(\bar{x}^{1/2}\zeta_{1y}) = -(2\kappa + \frac{m^2\nu}{2})\hat{\psi}_{yy} + (1 - \kappa - \frac{3m^2\nu}{4})m^2\hat{\psi}_{\bar{x}\bar{x}}$$

$$- \frac{3}{2}(1 - \kappa - \frac{7m^2\nu}{6})\frac{m^2}{\bar{x}}\hat{\psi}_{\bar{x}} + (1 + \frac{11m^2\nu}{2})\bar{x}c_{1y}$$

$$+ \frac{15m^2\nu}{2}\bar{x}^2 c_{1\bar{x}y} + \nu\bar{x}^3(c_{1yyy} + m^2 c_{1\bar{x}\bar{x}y}) \qquad (2.65)$$

Eliminating the term of ζ_{1y} with (2.64) and (2.65), the first order

field equation of rip current can be obtained with respect to the stream function $\hat{\Psi}$. This details of this procedure are as follows. The left hand side of (2.65) is separated into two terms, $\bar{x}^{3/2}\zeta_{1y\bar{x}}$ and $(1/2)\bar{x}^{1/2}\zeta_{1y}$. The former term is replaced by (2.64), and the latter by (2.61). The wave number conservation equation (2.59) is applied to the term c_1 to obtained the partial differential equation with respect to $\hat{\Psi}$. Nevertheless, the resulting equation remains as a fourth-order partial differential equation due to the contribution of the coefficient of lateral mixing terms. To simplify the analysis without sacrificing the generality of the present theory, the lateral mixing terms are omitted. The first order field equation of rip currents can finally be obtained as:

$$m^2\hat{P}\hat{\Psi}_{\bar{x}\bar{x}} - \hat{Q}\bar{x}^2\hat{\Psi}_{\bar{x}\bar{x}yy} - m^2\frac{\hat{R}}{\bar{x}}\hat{\Psi}_{\bar{x}} - \hat{S}\bar{x}\hat{\Psi}_{\bar{x}yy} + \hat{T}\hat{\Psi}_{yy} = 0 \qquad (2.66.a)$$

where

$$\hat{P} = \{\{1 + 2q(1 - \frac{\beta\kappa}{2\alpha})\} + \frac{3}{2}(\frac{4\beta}{3\alpha} - 1)\}q(1 - \kappa)$$

$$+ (q - \frac{1}{2})\{1 + 2q(1 - \frac{\beta\kappa}{2\alpha})\} \qquad (2.66.b)$$

$$\hat{Q} = \frac{1}{5}(\frac{\beta}{\alpha} - 1) \qquad (2.66.c)$$

$$\hat{R} = \frac{3}{2}\{\{1 + 2q(1 - \frac{\beta\kappa}{2\alpha})\} + \frac{3}{2}(\frac{4\beta}{3\alpha} - 1)\}q(1-\kappa)$$

$$+ 2(q - \frac{1}{2})\{1 + 2q(1 - \frac{\beta\kappa}{2\alpha})\} \qquad (2.66.d)$$

$$\hat{S} = q\{\frac{3}{5}(\frac{2}{3} + \frac{\beta}{\alpha}) + 2\kappa(1 - \frac{\beta}{2\alpha})\} \qquad (2.66.e)$$

$$\hat{T} = \{1 + 2q(1 - \frac{\beta\kappa}{2\alpha})\}\{q(1 - 2\kappa) - \frac{1}{2}\}$$

$$+ q\{\frac{1}{4}(1 + \frac{\beta}{\alpha}) + \kappa(1 - \frac{\beta}{2\alpha})\} \qquad (2.66.f)$$

2) Field equation in the shoaling zone

In the shoaling zone the governing equations differ from the surf zone equations principally in the wave energy dissipation term and in the formulation of the bottom friction stresses. In this zone, the driving forces are presented in the irrotational form, which may be incapable of generating currents of the first order. The remaining terms in the cross-differentiated momentum equations originate from the friction terms. Consequently, the momentum equations in the shoaling zone play an important role in the decay of currents produced in the surf zone.

For the governing equations in the shoaling zone, the mass conservation equation is first considered. As was previously indicated in (2.55), the stream function can be defined as:

$$U_1\bar{x} = \hat{\Psi}_y \quad \text{and} \quad V_1\bar{x} = -\tilde{m}\hat{\Psi}_{\bar{x}} \qquad (2.67)$$

where $\tilde{m} = (1 - 3\gamma_B^2/8)$.

The momentum equations are given by:

$$-\frac{2\kappa}{s^{3/2}\bar{x}}U_1 = \tilde{m}\left[1 - \frac{1}{4}B_0\bar{x}^{-5/2}\right]\frac{\partial\zeta_1}{\partial\bar{x}} + \frac{1}{2}\tilde{m}B_0^{1/2}\frac{\partial}{\partial\bar{x}}(a_1\bar{x}^{-5/4}) \qquad (2.68)$$

$$-\frac{\kappa}{s^{3/2}\bar{x}}V_1 = \left[1-\frac{1}{4}B_0\bar{x}^{-5/2}\right]\frac{\partial \zeta_1}{\partial y} + \frac{1}{2}B_0^{1/2}\frac{\partial}{\partial y}(a_1\bar{x}^{-5/4}) \tag{2.69}$$

The wave action conservation equation is written as:

$$\tilde{m}\frac{\partial}{\partial \bar{x}}\left(\frac{1}{\bar{x}^{1/2}}U_1\right) + \frac{\partial}{\partial y}\left(\frac{1}{\bar{x}^{1/2}}V_1\right) + \frac{\tilde{m}}{\bar{x}^{1/2}}\frac{\partial U_1}{\partial \bar{x}}$$

$$-\tilde{m}\frac{\partial}{\partial \bar{x}}\left[\bar{x}^{1/2}c_1 + \frac{2}{B_0^{1/2}}\bar{x}^{1/4}a_1\right] = 0 \tag{2.70}$$

While the equation of wave number conservation remains the same as (2.59).

In the shoaling zone the cross-differentiation of the momentum equations (2.68) and (2.69) results in the form:

$$\tilde{m}\hat{\Psi}_{\bar{x}\bar{x}} + 2\hat{\Psi}_{yy} - \frac{2\tilde{m}}{\bar{x}}\hat{\Psi}_{\bar{x}} = 0 \tag{2.71}$$

2.5 Solutions of Field Equations of Rip Currents

2.5.1 General solutions

The solutions to (2.66) for the surf and (2.71) for the shoaling zone, can be obtained by means of the method of separation of variables. The stream function Ψ to be solved can be expressed by:

$$\hat{\Psi}(\bar{x},y) = \Xi(\bar{x})Y(y) \tag{2.72}$$

where $\Xi(\bar{x})$ and Y (y) are functions of only $\bar{x}$ and y, respectively. As will

be shown later, the obtained solution in the longshore direction, y, is periodic, while the solutions in the seaward direction, $\bar{x}$, are expressed by hypergeometric functions for the surf zone and the modified Bessel functions for the shoaling zone.

1) Solutions in the surf zone

Substituting (2.72) in (2.66), the equation can be separated into two equation with respect to $\Xi(\bar{x})$ and $Y(y)$, which are respectively expressed as:

$$\left[1 + \frac{\lambda^2\hat{Q}}{m^2\hat{P}}\bar{x}^2\right]\Xi_{\bar{x}\bar{x}} + \left[\frac{\lambda^2\hat{S}}{m^2\hat{P}}\bar{x}^2 - \frac{\hat{R}}{\hat{P}}\right]\frac{1}{\bar{x}}\Xi_{\bar{x}} - \frac{\lambda^2\hat{T}}{m^2\hat{P}}\Xi = 0 \qquad (2.73)$$

$$Y_{yy} + \lambda^2 Y = 0 \qquad (2.74)$$

where λ is the separation constant which corresponds to the number of rip current. Replacing $\bar{x}$ in (2.73) by $\hat{x}$, where

$$\hat{x} = 1 + \frac{\lambda^2\hat{Q}}{m^2\hat{P}}\bar{x}^2 \qquad (2.75)$$

(2.73) becomes

$$\hat{x}(1-\hat{x})\Xi_{\hat{x}\hat{x}} + \left[\frac{1}{2}\left(\frac{\hat{R}}{\hat{P}}+\frac{\hat{S}}{\hat{Q}}\right)-\frac{1}{2}\left(1+\frac{\hat{S}}{\hat{Q}}\right)\hat{x}\right]\Xi_{\hat{x}} + \frac{\hat{T}}{4\hat{Q}}\Xi = 0 \qquad (2.76)$$

Equation (2.76) is a kind of the so-called hypergeometric differential

equations whose usual form is given as:

$$\hat{x}(1-\hat{x})\Xi_{\hat{x}\hat{x}} + \left[\hat{c}-(\hat{a}+\hat{b}+1)\hat{x}\right]\Xi_{\hat{x}} - \hat{a}\hat{b}\Xi = 0 \qquad (2.77)$$

Comparing (2.76) with (2.77), the coefficients of the equation can be given by:

$$\hat{a} + \hat{b} = \frac{1}{2}\left(\frac{\hat{S}}{\hat{Q}} - 1\right) \qquad (2.78.a)$$

$$\hat{a}\hat{b} = -\frac{1}{4}\frac{\hat{T}}{\hat{Q}} \qquad (2.78.b)$$

$$\hat{a} = \frac{1}{4}\left[\left(\frac{\hat{S}}{\hat{Q}} - 1\right) + \left\{\left(\frac{\hat{S}}{\hat{Q}} - 1\right)^2 + \frac{4\hat{T}}{\hat{Q}}\right\}^{1/2}\right] \qquad (2.78.c)$$

$$\hat{b} = \frac{1}{4}\left[\left(\frac{\hat{S}}{\hat{Q}} - 1\right) - \left\{\left(\frac{\hat{S}}{\hat{Q}} - 1\right)^2 + \frac{4\hat{T}}{\hat{Q}}\right\}^{1/2}\right] \qquad (2.78.d)$$

$$\hat{c} = \frac{1}{2}\left(\frac{\hat{S}}{\hat{Q}} + \frac{\hat{R}}{\hat{P}}\right) \qquad (2.78.e)$$

The behaviour of the solution $\Xi(\hat{x})$ in the surf zone, whether it has a maximum point or not, can be examined by replacing $\hat{x}$ in (2.77) by $\hat{\xi}$, where,

$$\hat{\xi} = \frac{1}{\hat{x}} \qquad (2.79)$$

By this change of variable, (2.77) becomes

$$\hat{\xi}^2(1-\hat{\xi})\Xi_{\hat{\xi}\hat{\xi}} - \left\{(\hat{a}+\hat{b}-1)\hat{\xi} + (2-\hat{c})\hat{\xi}^2\right\}\Xi_{\hat{\xi}} + \hat{a}\hat{b}\Xi = 0 \qquad (2.80)$$

The general solution of this equation can be expressed by the Gaussian hypergeometric function in the form

$$\Xi(\hat{\xi}) = A_1 \hat{\xi}^{\hat{a}} \hat{F}(\hat{a},\ 1+\hat{a}-\hat{c};\ 1+\hat{a}-\hat{b};\ \hat{\xi})$$

$$+ A_2\ \hat{\xi}^{\hat{b}} \hat{F}(\hat{b},\ 1+\hat{b}-\hat{c};\ 1+\hat{b}-\hat{a};\ \hat{\xi}) \qquad (2.81)$$

To solve the the so-called regular rip current spacing as an eigenvalue problem of the equation, the condition that the existence of a maximum point for $\Xi(\overline{x})$ in the surf zone is necessary. In order to clarify the behaviour of solution, (2.81) is rewritten by Kummers transformation, i.e. $\hat{F}(\hat{a},\hat{b};\hat{c};\hat{\xi}) = (1-\hat{\xi})^{\hat{c}-\hat{b}-\hat{a}} \hat{F}(\hat{c}-\hat{a},\hat{c}-\hat{b};\hat{c};\hat{\xi})$, in the form

$$\Xi_{surf}(\hat{\xi}) = A_1\ \hat{\xi}^{\hat{a}}(1-\hat{\xi})^{\hat{c}-\hat{a}-\hat{b}}\ \hat{F}(1-\hat{b},\ \hat{c}-\hat{b};\ 1+\hat{a}-\hat{b};\ \hat{\xi})$$

$$+ A_2\ \hat{\xi}^{\hat{b}}(1-\hat{\xi})^{\hat{c}\ -\hat{a}-\hat{b}} \hat{F}(1-\hat{a},\ \hat{c}-\hat{a};\ 1+\hat{b}-\hat{a};\ \hat{\xi}) \qquad (2.82)$$

where A_1 and A_2 are constants to be determined and the suffix "surf" indicates the surf zone solution. If $\hat{F}$ has a finite value, the behaviour of $\Xi(\overline{x})$ can be seen through:

$$\Xi(\hat{\xi})=0 \quad \text{if } (\hat{c}-\hat{a}-\hat{b})>0 \qquad \text{when } \hat{\xi}=1 \qquad (2.83.a)$$

$$\Xi(\hat{\xi})=0 \quad \text{if } \hat{a} \text{ and/or } \hat{b}>0 \text{ when } \hat{\xi}=0 \qquad (2.83.b)$$

and it is also confirmed by numerical calculation that $\Xi(\hat{\xi})$ has at least

one maximum point within $0<\hat{\xi}<1$.

2) Solution in the shoaling zone

The solution in the shoaling zone can be obtained by solving (2.71) using the method of separation of variables. Defining the following transformation of variable $\bar{x}$ and unknown function $\Xi(\bar{x})$ as

$$\tilde{x} = \sqrt{2}\bar{x}\frac{\lambda}{m} \tag{2.84.a}$$

$$\tilde{\varphi} = \frac{1}{\bar{x}^{3/2}}\Xi(\tilde{x}) \tag{2.84.b}$$

The basic equation of (2.71) with respect to Ξ is reduced to

$$\tilde{\varphi}_{\tilde{x}\tilde{x}} + \frac{1}{\tilde{x}}\tilde{\varphi}_{\tilde{x}} - (1 + \frac{\tilde{\nu}^2}{\tilde{x}^2})\tilde{\varphi} = 0 \tag{2.85}$$

where $\tilde{\nu} = \pm 3/2$. The solution of this differential equation can be obtained by the modified Bessel functions of the first and second kinds $\hat{I}(\hat{x})$ and $\hat{K}(\hat{x})$ in the form

$$\tilde{\varphi}(\tilde{x}) = \tilde{C}_1\hat{I}_{\tilde{\nu}}(\tilde{x}) + \tilde{C}_2\hat{K}_{\tilde{\nu}}(\tilde{x}) \tag{2.86}$$

This solution can be rewritten by using the relations in (2.84), as

$$\Xi_{shoal}(\bar{x}) = \tilde{C}_1\bar{x}^{3/2}\hat{I}_{3/2}(\bar{x}\frac{\lambda}{m}\sqrt{2}) + \tilde{C}_2\bar{x}^{3/2}\hat{K}_{3/2}(\bar{x}\frac{\lambda}{m}\sqrt{2}) \tag{2.87}$$

where $\tilde{C}_1$ and $\tilde{C}_2$ are the integration constants to be determined, and the suffix "shoal" represents the shoaling zone.

2.5.2 Boundary conditions

For any mode, the existence of rip current cells requires that the function $\Xi(\bar{x})$ and its derivative $\Xi_{\bar{x}}$ should be bounded at $\bar{x} = 0$ and $\bar{x} \to \infty$, such that:

$$\Xi_{surf} = 0 \quad \text{and} \quad \Xi_{surf\bar{x}} = 0 \quad \text{at} \quad \bar{x}=0 \quad \text{and} \quad \bar{x} \to \infty \tag{2.88.a}$$

$$\Xi_{shoal} = 0 \quad \text{and} \quad \Xi_{shoal\bar{x}} = 0 \quad \text{at} \quad \bar{x} \to \infty \tag{2.88.b}$$

It is important for Ξ_{surf} to be bounded at both the run-up line and infinity, i.e., one maximum point which is called as the zeroth mode, one maximum and one minimum point as the first mode and so on, inside the surf zone, see Figure 2.2.

These conditions are required in order to obtain real and positive eigenvalues of the field equations in the surf zone and shoaling zone. The eigenvalues can be determined by the matching condition at the breaking point, that is:

$$\lim_{\bar{x} \to \bar{x}_B} \frac{\Xi_{surf\bar{x}}}{\Xi_{surf}} = \frac{\Xi_{shoal\bar{x}}}{\Xi_{shoal}} \tag{2.89}$$

The solution satisfying the boundary condition (2.88.a) is:

$$\Xi_{surf} = A_{surf}\hat{\xi}^{\hat{a}}(1-\hat{\xi})^{\hat{c}-\hat{b}-\hat{a}}\, \hat{F}(1-\hat{b},\ \hat{c}-\hat{b};\ 1+\hat{a}-\hat{b};\ \hat{\xi}) \tag{2.90}$$

where A_{surf} is written instead of A_1 in (2.81). A_2 is found to be zero since δ is always less than 0.5 for $0.0<\kappa<1.0$, and by this value of δ no eigenvalues obtained.

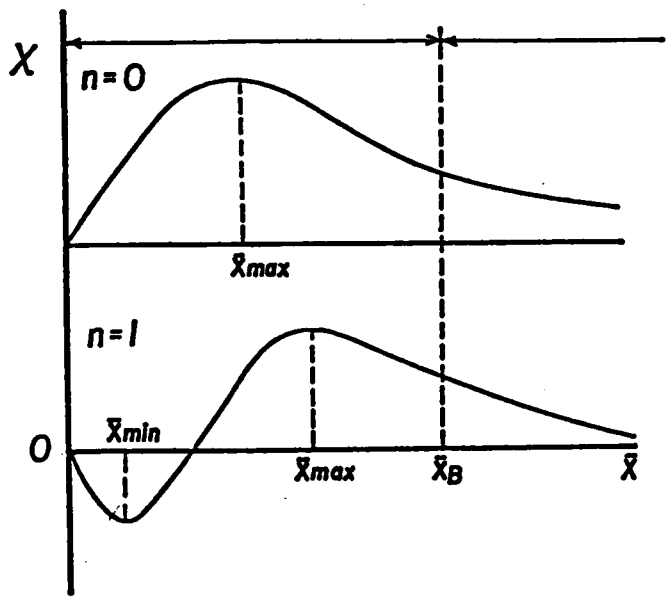

Figure 2.2 Characteristics of the stream function in the surf and shoaling zone to be matched at the breaking point. Where n=0 and n=1 represent the lowest and the first modes, respectively.

In the same way under the condition of (2.88b), the solution (2.87) is describe as:

$$\Xi_{shoal} = A_{shoal}(1 + x\lambda\sqrt{2})\exp(-x\lambda\sqrt{2}) \tag{2.91}$$

where $A_{shoal} = (\tilde{C}_2 \tilde{m}^2 / 2\lambda^2) \sqrt{\pi/2}$, and $\tilde{C}_1$ is zero to make the function bounded.

The real and positive eigenvalues which satisfying the matching condition (2.89) can be determined if the stream functions in both the regions are decrease monotonically in the offshore direction. Substituting (2.90) and (2.91) into (2.89) the characteristic equation is given in the form:

$$\frac{1}{(1 + x_B \lambda \sqrt{2})} \hat{F}(1-\hat{b},\ \hat{c}-\hat{b};\ 1+\hat{a}-\hat{b};\ \hat{\xi}_B)$$

$$- \frac{\hat{a}\hat{Q}}{\hat{P}} \frac{\hat{\xi}_B}{(1-\hat{\xi}_B)} \hat{F}(-\hat{b},\ \hat{c}-\hat{b};\ 1+\hat{a}-\hat{b};\ \hat{\xi}_B) \quad = 0 \qquad (2.92)$$

By numerical calculation of this characteristic equation, reasonable eigenvalues can be determined. The resonable eigenvalue is defined as the mathematical solution which is in the range of field and laboratory data .

2.6 Determination of The Integration Constant of Stream Function

The integration constant of the stream function A_{surf} in (2.90) can be determined by the steady state wave energy flux budget in the shoaling and surf zones. The wave energy dissipation rate immediately after breaking is different from that in the inner region as is reflected by the different wave elevation decay rates. Therefore, the ratio of wave amplitude to local depth should be taken into consideration in wave energy budgeting. This difference in the rate of wave energy dissipation is responsible for the structure of the nearshore current. Therefore, the wave energy flux contribution to the generation of the nearshore currents initates at the breaking point. The changes in wave energy flux occurring in the region just before to just after the breaking point can be expressed by:

$$\left[Ec_g\right]_{x_B+0} = \left[Ec_g\right]_{x_B-0} \tag{2.93}$$

The left and right hand sides of (2.93) indicate the wave energy fluxes just before and after the breaking point, which are given respectively by:

$$\left[Ec_g\right]_{x_B+0} = \frac{1}{4}\rho g H_o^2 n c_o = \frac{1}{4}\rho g\left\{H^2 nc\right\}_{x_B+0} \tag{2.94.a}$$

$$\left[Ec_g\right]_{x_B-0} = \frac{1}{4}\rho g\left\{H^2(nc - U)\right\}_{x_B-0} \tag{2.94.b}$$

where wave energy dissipation just before the breaking point due to bottom friction is neglected, and $n=c_g/c\sim 1$ is assumed. Substituting (2.94.a) and (2.94.b) into (2.93) results in

$$\{H^2c\}_{x_B+0} = \{H^2(c-U)\}_{x_B-0} \qquad (2.95.a)$$

the dimensionless form of this equation is:

$$\{H^{*2}c^*\}_{x_B+0} = \{H^{*2}(c^*-U^*)\}_{x_B-0} \qquad (2.95.b)$$

The right hand side of (2.95.b) can be expanded by using the bottom slope, s, as a perturbation parameter, while the left hand side will be expressed by the breaker index γ_B, as:

$$\gamma_B^2 = \gamma^2\left[1+s\bar{x}_B^{-1}\left\{\frac{a_{1B}}{\gamma} + \frac{1}{2}\bar{x}_B^{1/2}(c_{1B}-U_{1B})\right\} + \ldots\right] \qquad (2.96)$$

where the asterics "*" have been omitted for convenience. Kimura, Goto and Seyama's (1988) recent experimental work suggests the condition $\gamma_B > \gamma$. Using this fact, the first order approximation of (2.96) is reduced to:

$$\left[\frac{a_1}{\gamma} + \frac{1}{2}\bar{x}^{1/2}(c_1 - U_1)\right]_{x_B-0} = \frac{1}{s}\left(\frac{\gamma_B}{\gamma} - 1\right)\bar{x}_B \qquad (2.97)$$

where a_1 can be given by the alongshore momentum equation, and (c_1-U_1) can be estimated by the wave number conservation equation. Using the maximum value of a_1 and (c_1-U_1) they are finally formulated as:

$$\frac{a_1}{\gamma} = \frac{2m^2}{q\lambda\gamma^2}\bar{x}^{-1/2}\left\{\left(1-\frac{\gamma^2}{4}\right)\frac{\lambda^2}{m^2}\bar{\Xi} - \frac{q\gamma^2}{2}(1-\kappa)\frac{1}{\bar{x}}\bar{\Xi}_{\bar{x}}\right.$$

$$-(1-\frac{\gamma^2}{4})(\Xi_{\bar{x}\bar{x}} - \frac{2}{\bar{x}}\Xi_{\bar{x}})\} \tag{2.98}$$

$$\bar{x}(c_1-U_1) = \frac{m^2}{\lambda \bar{x}^{1/2}}(\Xi_{\bar{x}\bar{x}} - \frac{2}{\bar{x}}\Xi_{\bar{x}}) \tag{2.99}$$

Substitution of (2.98) and (2.99) into (2.97) yields:

$$\left[(1-\frac{\gamma^2}{4})\frac{\lambda^2}{m^2}\Xi - \frac{q\gamma^2}{2}(1-\kappa)\frac{1}{\bar{x}}\Xi_{\bar{x}} - \{1-\frac{1}{4}(1+q)\gamma^2\}(\Xi_{\bar{x}\bar{x}} - \frac{2}{\bar{x}}\Xi_{\bar{x}})\right]$$

$$= \frac{q\gamma^2\lambda}{2m^2}\bar{x}_B^{3/2}\left[\frac{1}{s}(\frac{\gamma_B}{\gamma} - 1)\right] \tag{2.100}$$

The integration constant A_{surf} finally can be derived from (2.100) by using (2.90) and written as:

$$A_{surf} = \frac{(q\gamma^2/2s\lambda)(\gamma_B/\gamma - 1)\ (m/\lambda)^{3/2}(\hat{P}/\hat{Q})^{3/4}\hat{\xi}_B^{-3/4}(1-\hat{\xi}_B)^{3/4}}{\{\tilde{A}(\hat{\xi}_B)\hat{f}(1-\delta,\hat{\xi}_B) + \tilde{B}(\hat{\xi}_B)\hat{f}(-\delta,\ \hat{\xi}_B)\}} \tag{2.101.a}$$

where

$$\tilde{A}(\hat{\xi}_B) = \left[(1-\frac{\gamma^2}{4}) + 4\frac{\hat{Q}}{\hat{P}}\hat{a}\delta\{1-(1+q)\frac{\gamma^2}{4}\}\hat{\xi}_B\right] \tag{2.101.b}$$

$$\tilde{B}(\hat{\xi}_B) = 4\hat{a}\frac{\hat{Q}}{\hat{P}}\left[\frac{\gamma^2}{4}\{q(1-\kappa)+(1+q)(\hat{a}+\delta+\frac{3}{2})\} - (\hat{a}+\delta+\frac{3}{2})\right.$$

$$\left. + \{1-(1+q)\frac{\gamma^2}{4}\}\hat{c}\hat{\xi}_B\right] \tag{2.101.c}$$

$$\hat{f}(1-\delta,\hat{\xi}_B) = \hat{\xi}_B^{\hat{a}}(1-\hat{\xi}_B)^{\hat{c}-\delta-\hat{a}}\hat{F}(1-\delta,\ \hat{c}-\delta;\ 1+\hat{a}-\delta;\ \hat{\xi}_B) \tag{2.101.d}$$

$$\hat{f}(-\delta,\ \hat{\xi}_B) = \hat{\xi}_B^{1+\hat{a}}(1-\hat{\xi}_B)^{\hat{c}-\delta-\hat{a}-1}\hat{F}(-\delta,\ \hat{c}-\delta;\ 1+\hat{a}-\delta;\ \hat{\xi}_B) \quad (2.101.e)$$

2.7 Theoretical Results of the Horizontal Circulation

2.7.1 Rip current spacing

A theory of the steady nearshore horizontal circulation cells induced by normally incident waves on a plane beach is proposed. Theoretical results predict two main characteristics of rip currents, the alongshore spacing and velocity distribution. The results are then disscused in terms of laboratory and field data. Furthermore, the rip current spacing is compared with the theoretical curve of Dalrymple and Lozano (1978) and the empirical curve of Sasaki (1977).

In comparing the results of this study with those of Dalrymple and Lozano, the parameter κ, which has been previously defined, is transformed to the Dalrymple and Lozano's parameter A_D. The same procedure was performed in transforming κ into the surf similarity parameter of Battjes at the breaking point. This procedure was necessary in order to make a comparison with the empirical curve of Sasaki (1977). The parameter A_D is defined in terms of the notations presently adopted as:

$$A_D = \frac{m(2\gamma)^2}{8\tilde{f}} \quad (2.102)$$

where $m = (1 + 3\gamma^2/2)^{-1}$, $\tilde{f} = (2/\pi)\gamma K_*/s = K/s$, and $K_* = 1.41(\gamma/kk_e)^{-2/3}$. Modifying (2.102) to determine the relation between A_D and κ gives:

$$A_D = \frac{2}{5\kappa} \tag{2.103}$$

The eigenvalues $\tilde{\alpha} = \lambda x_B$ are obtained from (2.92) as a function of κ. Using (2.103) $\tilde{\alpha}$ can then be expressed in terms of A_D. The separation constant λ is defined in terms of the rip current spacing Y_r as:

$$\lambda = \frac{2\pi}{Y_r} \tag{2.104}$$

Therefore, the dimensionless rip current spacing is finally written as:

$$\frac{Y_r}{x_B} = \frac{2\pi}{\tilde{\alpha}} \tag{2.105}$$

Because the eigenvalue $\tilde{\alpha}$ is a function of A_D, the dimensionless rip current spacing Y_r/x_B is also function of A_D. The dimensionless rip current spacing is shown in Figure 2.3 in terms of the parameter A_D, where theoretical curve (1) is of the present study, (2) is of Dalrymple and Lozano. For comparison, the field data of Balsillie, Bowen, and Dalrymple are shown together with the theoretical curve of Dalrymple and Lozano's in the figure.

In Figure 2.3, the dimensionless rip current spacing, Y_r/x_B, for curve (1), rapidly increases as A_D becomes less than 1, while Y_r/x_B for curve (2), decreases as A_D goes to 0. This difference can be explained by the empirical curve of Sasaki (1977). The field data of Balsillie (1975) and Dalrymple (1978) correspond to the curve (2), while the data of Bowen (1969) tends to agree with the curve (1). As was reported by Dalrymple and Lozano, 59% of Balsillie data shown in Figure 2.3 were spilling breakers. Furthermore 36% of the data were spilling/plunging transition breakers, and only one was surging breaker. Most of the Balsillie data tended to accumulate around

a dimensionless rip current spacing of 1, particularly if $A_D \sim 1$. This feature may correspond to the empirically curve by Sasaki (1977).

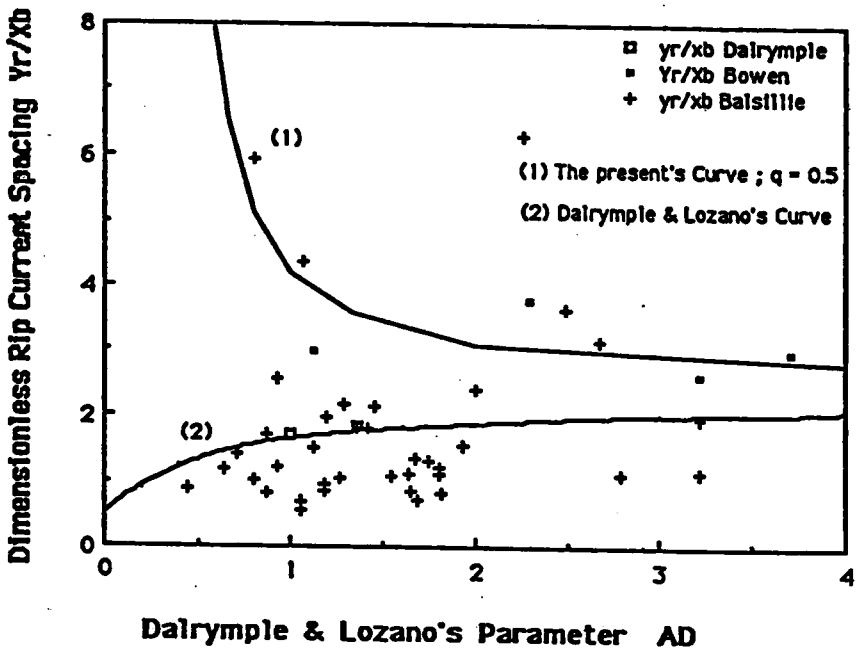

Figure 2.3 The theoretical curves of dimensionless rip current spacing: (1) is the present study, (2) is Dalrymple & Lozano (1978), and Sasaki's empirical curve, including the rearranged field data of rip current spacings.

Furthermore, laboratory data of Horikawa and Mizuguchi (1976) and of Tsuchiya, Kawata, Shibano, Dadang and Shishikura (1986) are plotted around 1, as shown in Figure 2.4. This deviation from the theory may be explained

as an influence of the littoral boundaries in the laboratory basin, which will be further discussed in the next section.

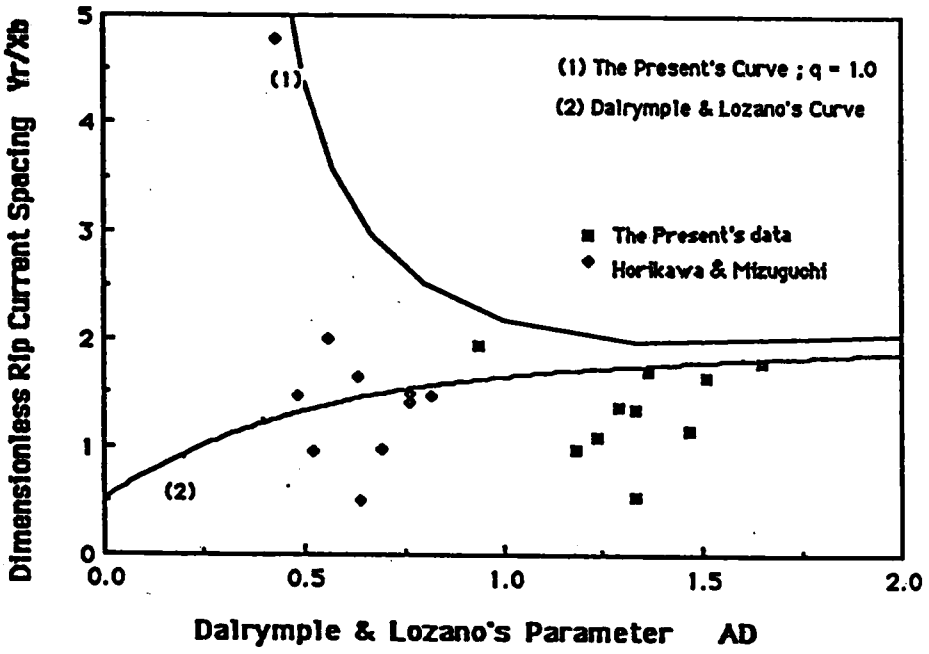

Figure 2.4 Comparison of the theoretical dimensionless rip current spacings of this study and Dalrymple & Lozano, with the experimental data for a planar beach whose slope is s=0.05.

To compare Sasaki's (1977) empirical curve of rip current spacing, the relationship between the parameter A_D and the surf similarity parameter ξ_B is evaluated. Modifying (2.102), we get:

$$\gamma_B = \sqrt{2A_D K/ms} \tag{2.106}$$

where γ_B is the so-called breaker index which is defined as the ratio of wave amplitude to the water depth at breaking point. For example, its empirical expression by Goda (1973) is:

$$\frac{H_B}{h_B}\frac{h_B}{L_0} = A\left[1-\exp\left\{-1.5\frac{\pi h_B}{L_0}(1 + 15s^{4/3})\right\}\right] \tag{2.107}$$

where $A = 0.17$, $H_B/L_0 = (s/\xi_B)^2$, and $a_B = H_B/2 = \gamma_B h_B$. After some manipulation, the relation between ξ_B and γ_B is then obtain as:

$$\gamma_B = -\frac{0.75\pi(1 + 15s^{4/3})(s/\xi_B)^2}{\ln\left\{1-(1/A)(s/\xi_B)^2\right\}} \tag{2.108}$$

The relationship between ξ_B and γ_B is illustrated in Figure 2.5 for variations in the beach slope, s .

The dimensionless rip current spacing $Y_r/x_B = f(A_D)$ where $A_D = \gamma_B^2 ms/2K$, such that it can be reduced to

$$Y_r/x_B = f(\gamma_B) \tag{2.109.a}$$

where $\gamma_B = \sqrt{2A_D K/ms}$ and $\gamma_B = f(\xi_B, s)$ as shown in Figure 2.5. By using the inverse relation of $\xi_B = g(\gamma_B, s)$, (2.109.a) becomes

$$Y_r/x_B = f(\xi_B, K, s) \tag{2.109.b}$$

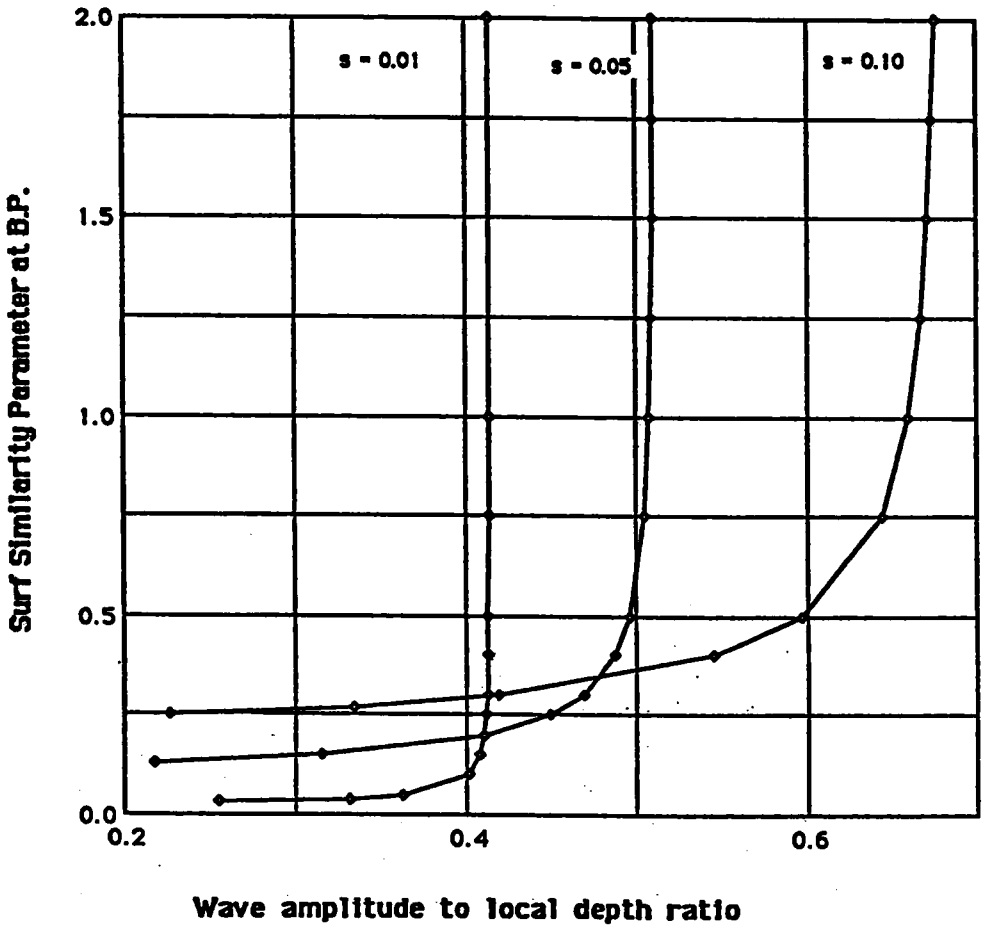

Figure 2.5 Relationship between the surf similarity parameter, ξ_B, evaluated at the breaking point and breaker index, γ_B, with changes in the beach slope s.

Sasaki (1977) formulated (2.109b) empirically for ranging values of the surf similarity parameter at the breaking point ξ_B as:

$$Y_r/x_B = 165\xi_B^2 \quad ;\text{for} \quad \xi_B<0.2; \quad \text{Infragravity wave region}$$

$$Y_r/x_B = 3\sim5 \quad ;\text{for} \quad 0.2<\xi_B<0.6; \quad \text{Instability region}$$

$$Y_r/x_B = 2\pi(n=0) \quad ;\text{for} \quad 0.6<\xi_B; \quad \text{Edge wave region}$$

$$= \pi(n=1)$$

$$= 2\pi/3(n=2) \tag{2.110}$$

where n is the mode of the edge waves. In addition to (2.110), Sasaki (1977) also formulated the upper limit of all the plotted data in the region of infragravity wave, as:

$$\left(\frac{Y_r}{x_B}\right)_{(\text{upper limit})} = \frac{3.4}{\xi_B^{1/2}} \tag{2.111}$$

In Figure 2.6, a comparison is made between the theoretical dimensionless rip current spacing by the present theory and field data in terms of the surf similarity parameter at the breaking point for the case of $q = 1/2$. For $q=1$ the same comparison is shown in Figure 2.7; q is the parameter defined by (2.61).

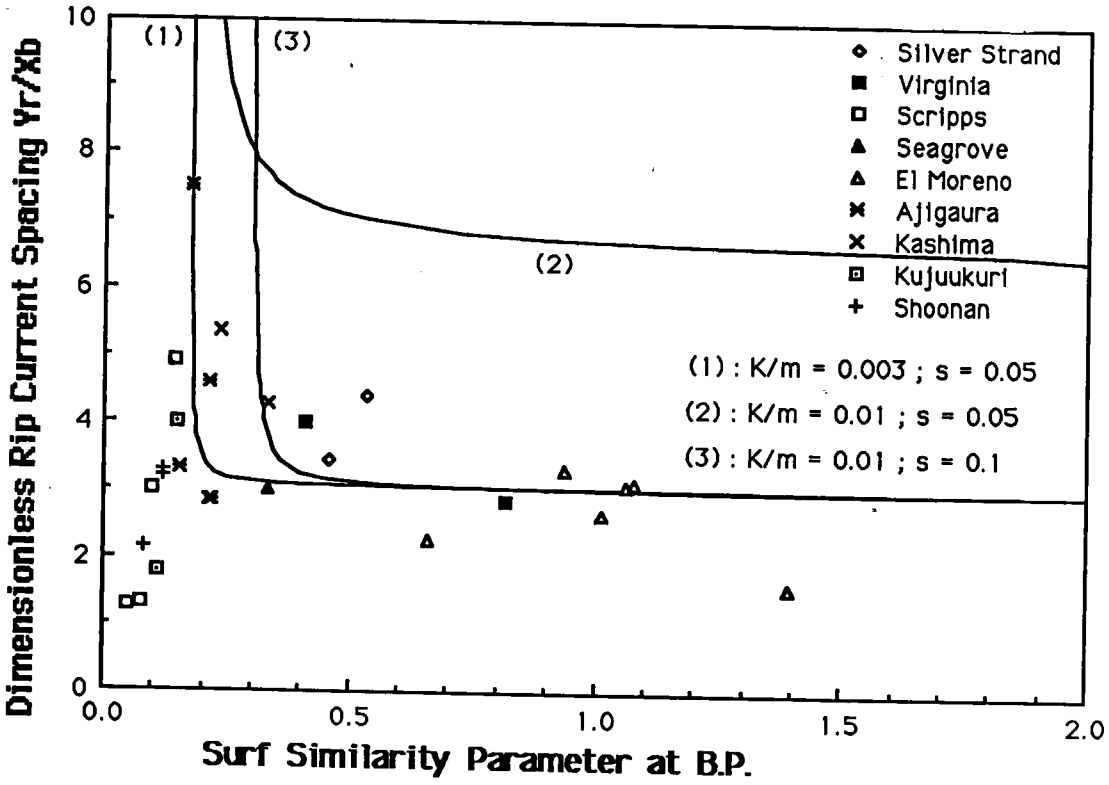

Figure 2.6 Comparison between the present theoretical curves of dimensionless rip current spacing for the case of q=1/2 and the surf similarity parameter evaluated at the breaking point, with field data.

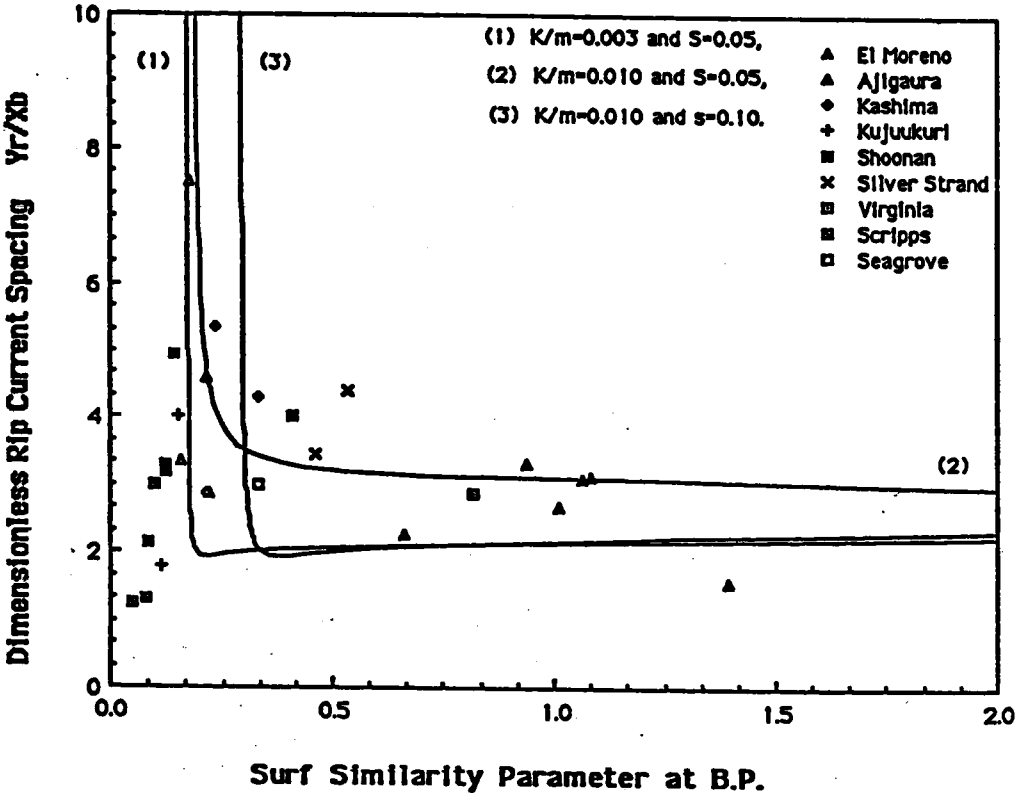

Figure 2.7 Comparison between the present theoretical curves of dimensionless rip current spacing for the case of q=1 and the surf similarity parameter evaluated at the breaking point, with field data.

Based on the comparisons shown in Figures 2.6 and 2.7, the present theoretical curves tend to agree with the field data in the region of surf similarity parameter $0.2 < \xi_B$. For a constant beach slope $s = 1/20$, as the friction coefficient K becomes smaller the rip current spacing becomes smaller. This feature is shown by curves (1) and (2) in Figure 2.6, where for curves (1) and (2) $K/m = 0.003$, $s = 1/20$ and $K/m = 0.01$, $s = 1/20$. The inverse trend exist for the same friction coefficient K, when the bottom slope becomes milder the rip current spacing increases. This feature is shown in curves (2) and (3) of Figure 2.6, where for curve(3) $K/m = 0.01$ and $s = 1/10$. A similar tendency can be observed in case of $q = 1$, as shown in Figure 2.7, but the rip current spacing is relatively small compared with the case where $q = 1/2$.

In Figure 2.8 a comparison is made between the present theoretical curve for the rip current spacing and the Sasaki's empirical curve for the case of $s = 1/20$ and $K/m = 0.003$. In the region where $\xi_B < 0.2$, the present theoretical curve shows a sudden increase, which tends to follow Sasaki's empirical curve in the infragravity wave region. In the region $0.2 < \xi_B < 0.6$, the dimensionless rip current spacing ranges between 2 and 6, depending on the value of s, K and q. A similar tendency in the range of $0.2 < \xi_B < 0.6$ can be observed for $0.6 < \xi_B$. As already mentioned, q may take a value between 1/2 and 1 depending on the nonlinearity of the circulation system as well as the dispersion relation of waves in the surf zone. Therefore, further consideration is needed before q can be more accurately determined.

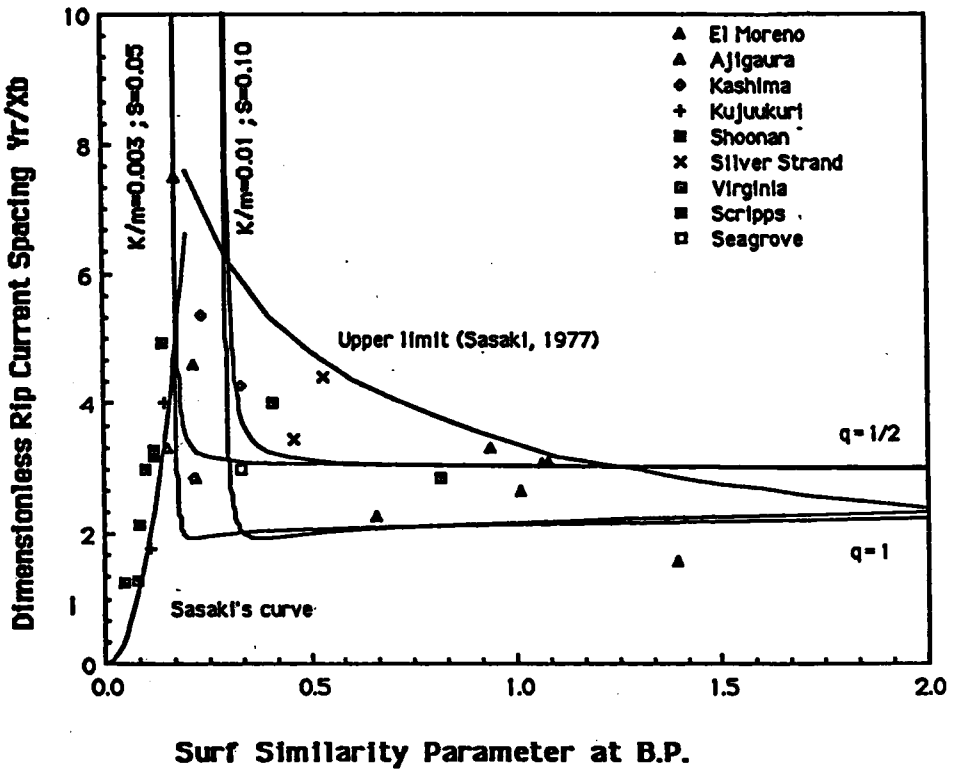

Figure 2.8 Comparison between the present theoretical curves of dimensionless rip current spacing for the cases of q=1/2 and q=1, with Sasaki's empirical curves in the regions of infragravity waves, instability, and edge waves and their upper limit together with field data.

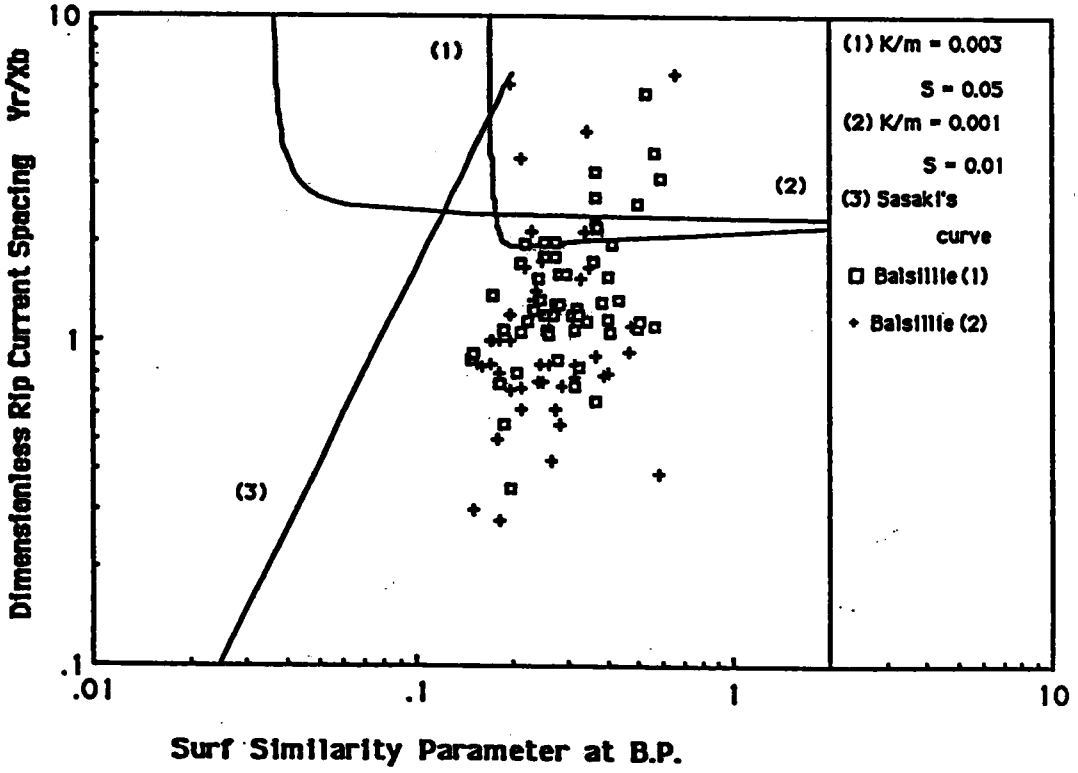

Figure 2.9 Comparison between the present theoretical curves of dimensionless rip current spacing for the cases of q=1, with the data of Balsillie in terms of surf similarity parameter at the breaking point, together with Sasaki's empirical relationship of rip current spacing in the regions of infragravity waves.

In Figure 2.9 field data collected by Balsillie (1975) of rip current spacing are shown expressed in terms of the surf similarity parameter evaluated at breaking point. Balsillie reported the breaking conditions of his field study as spilling and spilling/plunging transition. His data plots below the present curves and parallel to the empirical curve of Sasaki in the region of infragravity waves where the similarity parameter is less than 0.2.

2.7.2 Discharge and velocity distribution of the rip current

From the stream function of rip currents obtained in this study, the rip current velocity distribution can be calculated. Inserting the eigenvalue which was obtained theoretically into the stream function, (2.72), the distribution of the rip current discharge is given by:

$$dU_1 = s\bar{x}U_1 = s\hat{\Psi}_y = s\lambda A_{surf}\Xi(x)\cos\lambda y \tag{2.112}$$

Recalling the perturbation expansion of (2.33.c),the rip current velocity is expressed in the form

$$U = s^{1/2}(sU_1 + s^2U_2 + \ldots) \tag{2.113}$$

Up to the first-order approximation, the depth-integrated rip current discharge is given as:

$$dU = s^{5/2}\ \lambda\ A_{surf}\Xi(x)\cos\lambda y \tag{2.114}$$

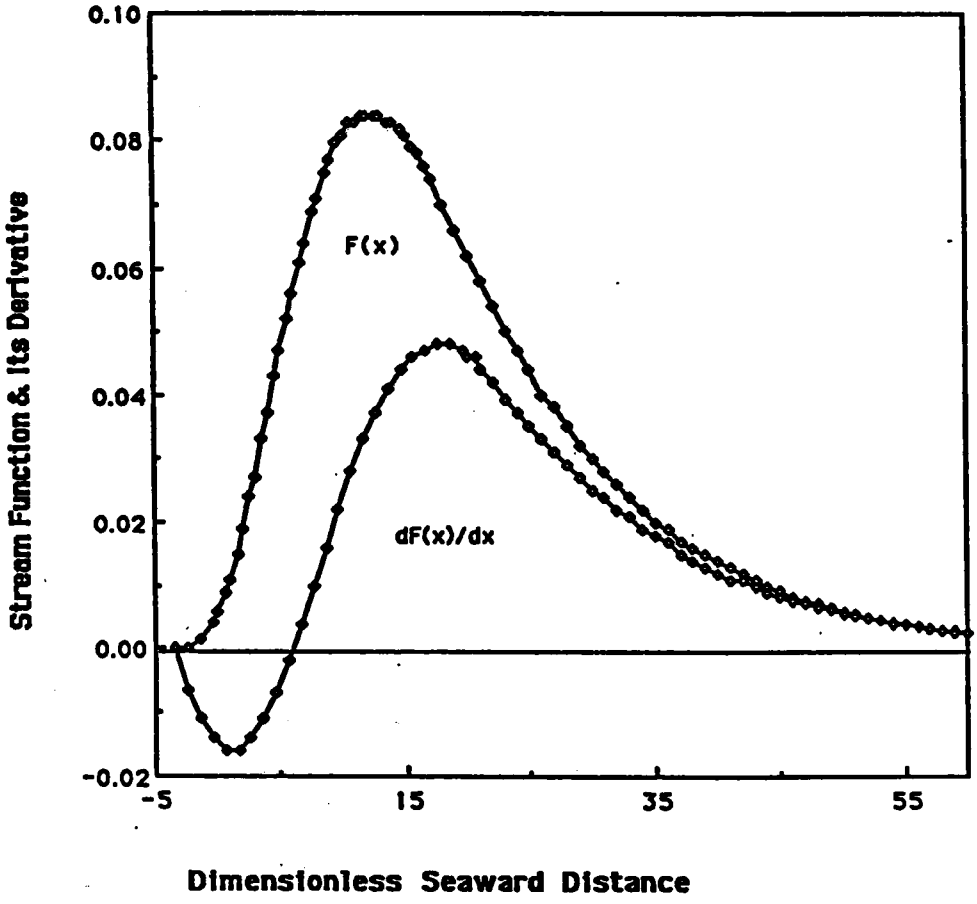

Figure 2.10 Offshore distribution of the dimensionless stream fuction and its derivative which is the rip current discharge. The beach slope is 1/20 and the breaking point is located at x = 20, A_{surf} = 1, and the dimensionless rip current spacing is equal to 4.40.

Mulitiplying the discharge (2.114) by the inverse of local water depth, the rip current velocity can be calculated. Figure 2.10 shows an example of the offshore distributions, in which $A_{surf}=1$ and the beach slope is s = 1/20, the breaking point x = 20, and dimensionless rip current spacing of 4.40 are assumed.

Table 2.1 Dimensionless wave conditions for a numerical calculation in 2-D horizontal nearshore circulation at the laboratory scale.

To (sec)	*Ho/Lo*	*s*	γ_B
0.80	0.025	1/20	0.46
0.97	0.006	1/20	0.49

Table 2.2 Dimensionless wave conditions for a numerical calculation in 2-D horizontal nearshore circulation at the field scale.

To (sec)	*Ho/Lo*	*s*	γ_B
10	0.019	1/30	0.41

Table 2.3 Maximum rip current discharge in terms of the dimensionless rip current spacings for the case of the beach slope is 1/20 and the breaking depth are shown.

γ_B	h_B(cm)	Y_r/x_B	dU(cm2/sec)
0.46	3.73	2.18	66.47
0.46	3.73	2.97	49.91
0.46	3.73	4.39	48.66
0.49	1.65	2.16	30.95
0.49	1.65	2.94	23.22
0.49	1.65	4.35	22.66

Numerical examples of the rip current velocity distribution are shown, under the wave conditions of laboratory and field, by numerically calculating the rip current velocity distributions using waves conditions listed in Table 2.1 and 2.2. The calculated maximum rip current velocities are summarized in Table 2.3 and assumed beach slope of 1/20. In the laboratory scale, the calculated rip current velocities are reasonable in comparison with experiments.

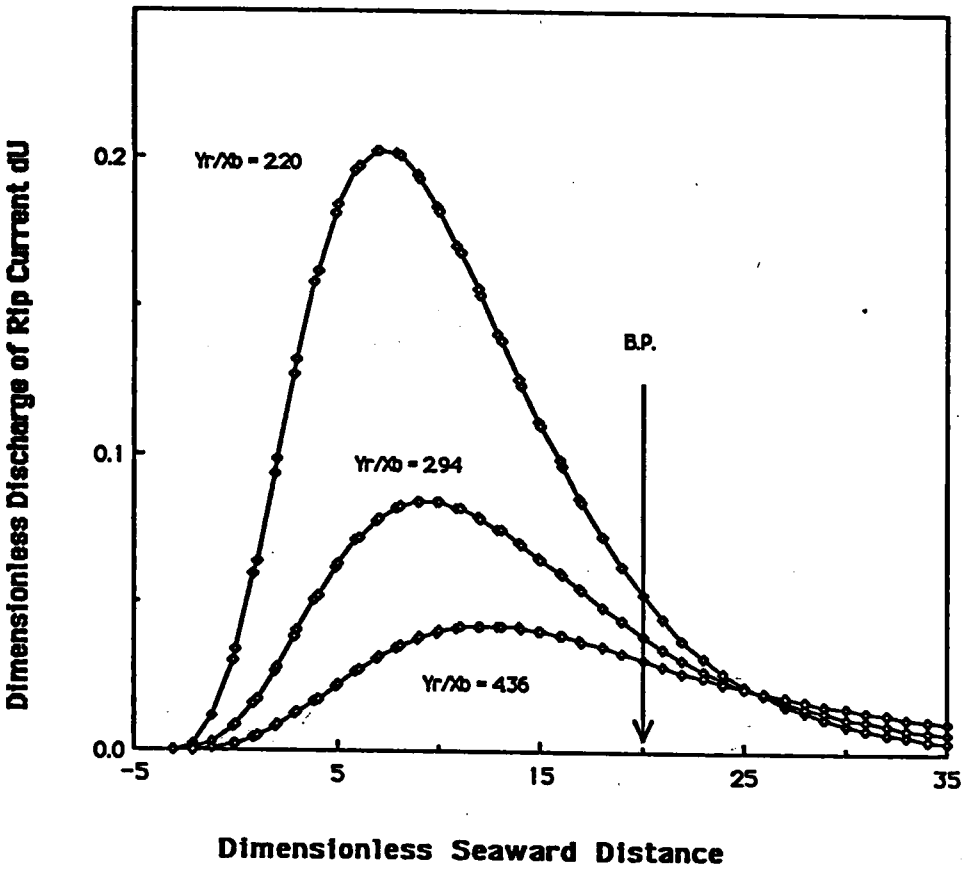

Figure 2.11 Changes in offshore distributions of rip current discharge with different dimensionless rip current spacings, 2.20, 2.94 and 4.36.

Figure 2.11 shows the offshore distributions of rip current discharge along the center of the rip current using different dimensionless rip current spacings of 2.20, 2.94 and 4.36. This figure shows that when the

rip spacing becomes larger the rip current discharge decreases, and the circulation pattern is expanded offshore.

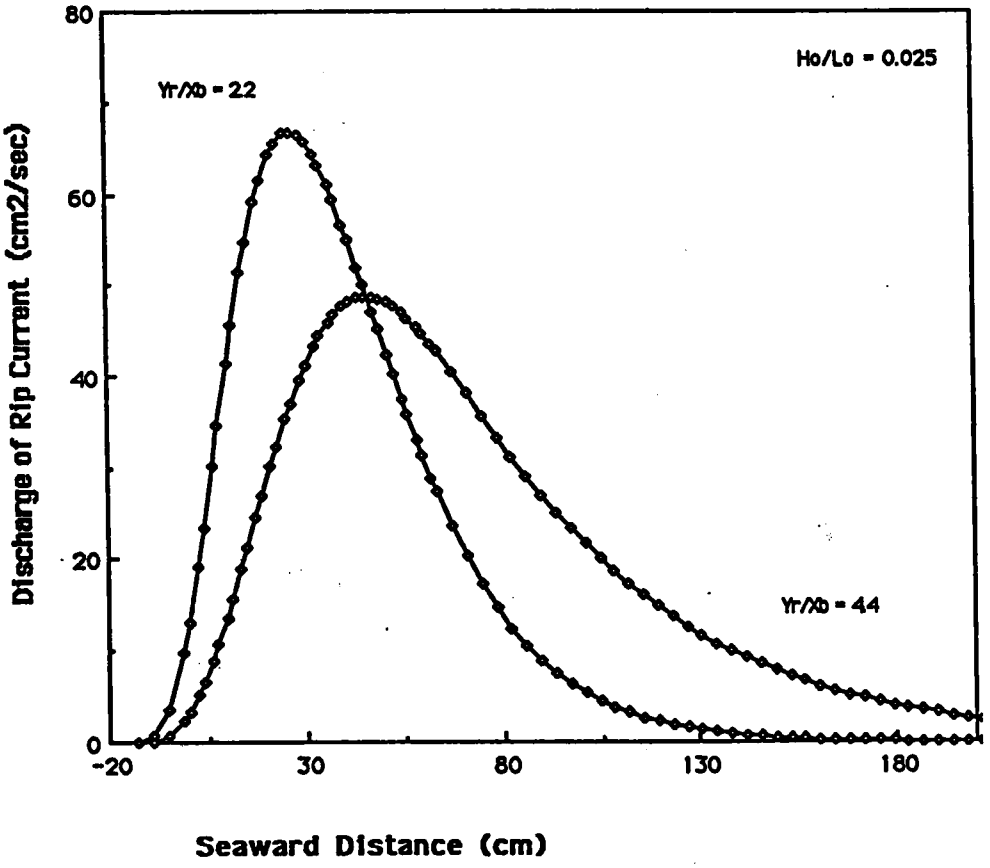

Figure 2.12 Offshore distributions of rip current discharge along the rip center with changing dimensionless rip current spacings (laboratory scale: the beach slope is 1/20, the deep water steepness is 0.025 and the breaking point is located at 74.6 cm).

The offshore distributions of rip current discharge along the rip center are shown for fixed values of deep water waves steepness, and variable dimensionless rip current spacing in Figure 2.12, where the following conditions are assumed: beach slope = 1/20, deep water wave steepness = 0.025, and the breaking point distance = 74.6. From the figure it is noted that the circulation extends further offshore as dimensionless rip current spacing increases.

Figure 2.13 shows the changes in the offshore distributions for different deep water steepness, where the beach slope is fixed at 1/20, the breaking points are varied as shown in the figure. Steeper incident wave generates a wider surf zone width, thus resulting in stronger rip currents. These characteristics of rip currents can be understood more clearly in Figures 2.14 and 2.15, which show the typical results of theoretical circulation patterns at the scale of laboratory and field, respectively.

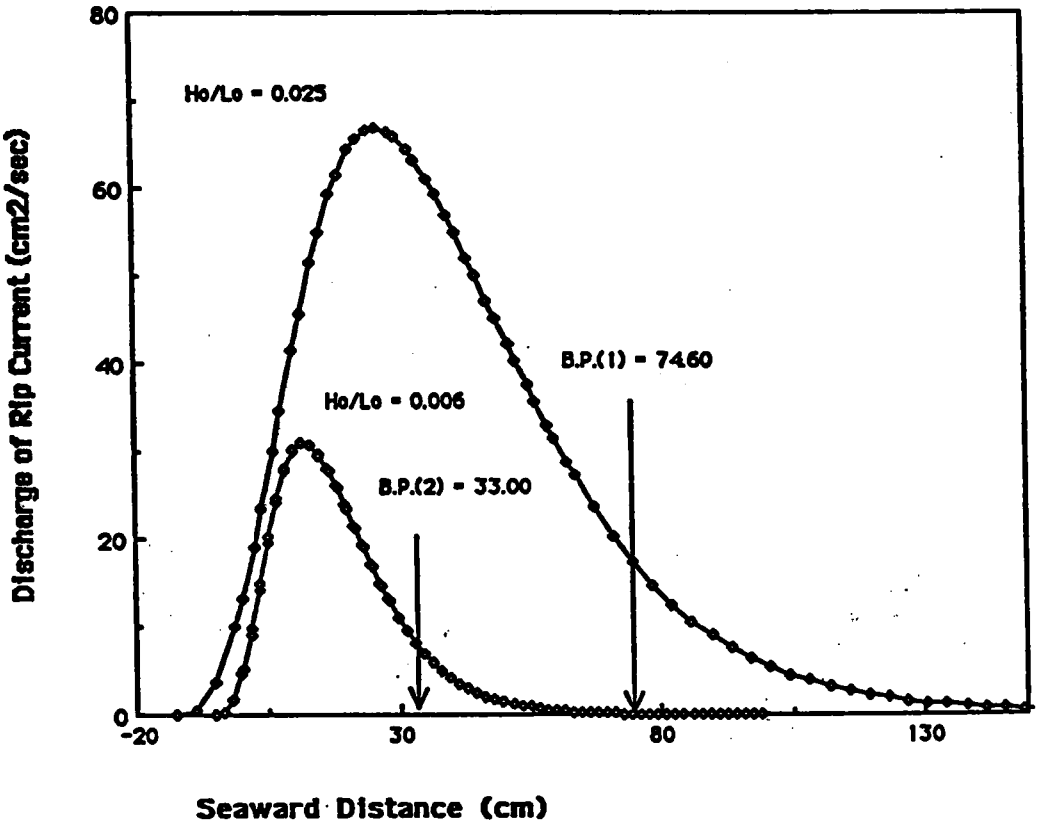

Figure 2.13 Offshore distribution of rip current discharge with different wave steepnesses, where the beach slope is fixed at 1/20 and the variation in the the breaking point location (33 cm and 74.6 cm).

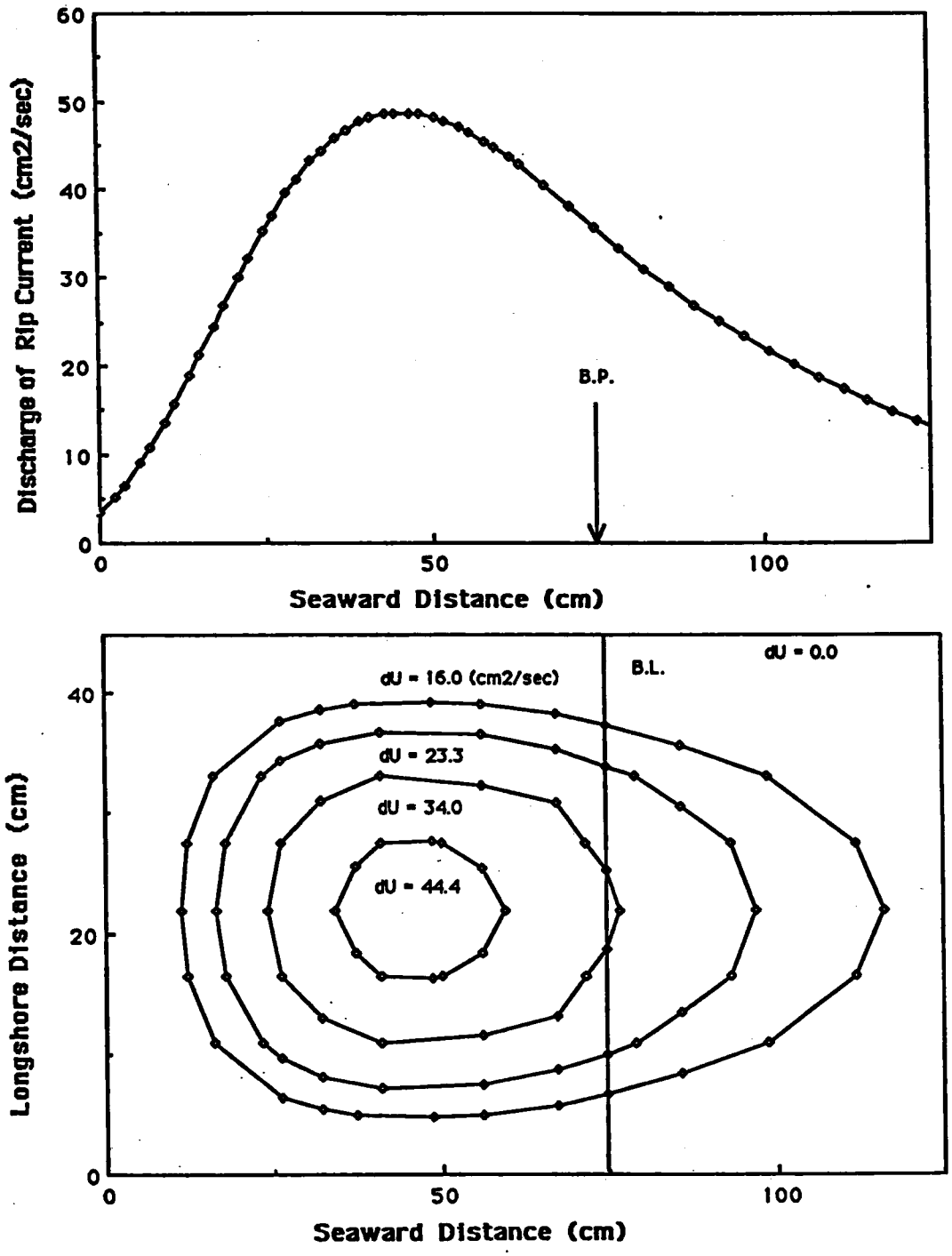

Figure 2.14 Theoretical result of the horizontal circulation pattern at the laboratory scale, where the beach slope : 1/20 the deep water wave steepness: 0.025, and the dimensionless rip current spacing : 4.40 are used.

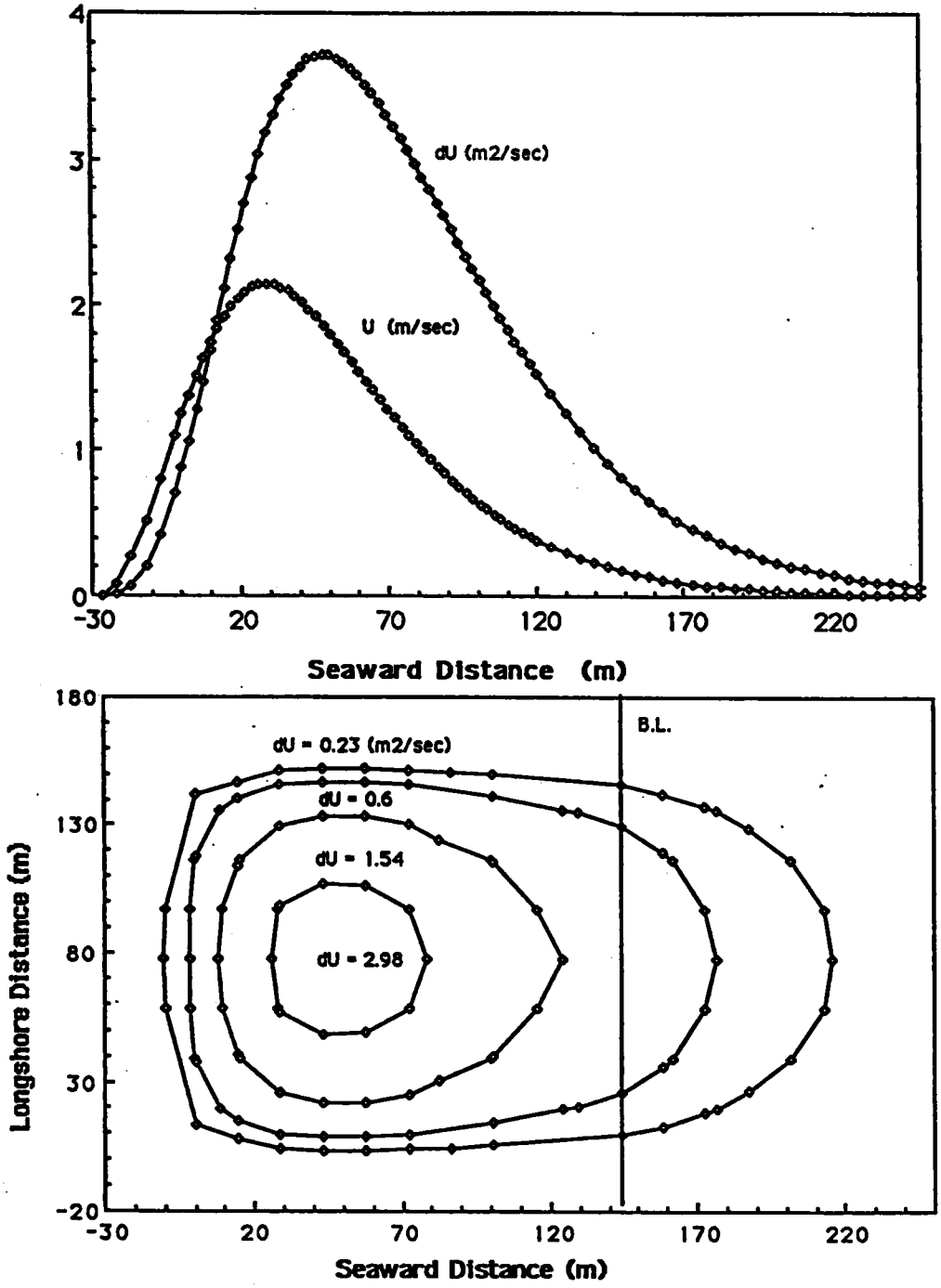

Figure 2.15 Theoretical result of the horizontal circulation pattern at the field scale, where the beach slope: 1/30, the deep water wave steepness: 0.019, the dimensionless rip current spacing: 2 and bottom friction coefficient: K=0.002 are used.

2.8 Experimental Investigation on Rip Current Formation on a Planar Beach with Littoral Reflective Boundary Conditions

2.8.1 Introduction

The interaction between existing currents and incoming waves is sufficient to generate rip currents. This type of rip current is known as "self excited". Wave refraction due to currents causes wave orthogonals converge on the locations where rip currents are generated, and diverge in the locations where shoreward currents exist. Maximum wave heights occure at the rip current locations, and the minimum elevations occure at the shoreward current locations, consequently, causing an alongshore variation of breaker line. As is shown in Table 2.4, Bowen and Inman (1969) observed an opposite relation for rip current which are generated by the interaction between the existing edge waves and the incoming waves. They observed that rip currents generate at the antinode of the edge which had the inverse phase of incident wave. However, the rip current did not generate at the next longshore antinode which had a same phase as the incident waves. The variation of the alongshore breaker line is then characterized by alternately appearing large and a small antinodes. A longhsore current (feeder current) generates near the shoreline, whose direction is from larger wave elevations to low ones. This current flows seaward in the form of rip current at the low breaker regions. Consequently, the breaker line in this region moves seaward resulting in an asymmetric breaker line.

Matsunaga, Takebara and Kuritani (1988) showed in their experimental results that the circulation cell was excited by both synchronous and subharmonic edge waves generated in the laboratory basin with planar beach and littoral reflective boundaries. Their experiment was conducted in the

absence of breaker and under the condition of the zero-gradient of radiation stresses. Their results show that the rip current spacings excited by the synchronous edge wave are the same as the incident wave lengths, and half the wave length for the subharmonic cases. Furthermore all rip currents were generated at the maximum antinode of edge wave, i.e., the maximum run-up point. They concluded that the circulation excited under the above mentioned conditions was not dependent on the radiation stress gradient, but on the generation of vorticity from the periodic oscillation boundaries at the shoreline. In the author's opinion, the experimental results indicate that for the smaller bifurcation modes than the incident wave length is in a higher mode of instability, influenced by the boundaries. This includes littoral reflective boundaries which will be discussed in this chapter for the experiment of rip current spacing in the surf zone (inducing breaker effects). This experimental result is considered as a possible mode of circulation in the shoaling zone in this study.

In the present experiment two topics are investigated. An attempt is made first to confirm the existence of the self-exciting mechanism for rip current generation. This mechanism can be considered as one of the bifurcation solutions caused by the destabilization of the incoming wave front due to the interaction of existing currents and incoming waves. Secondly, the influence of littoral reflective boundaries on the rip current spacing are investigated and the derived theory for rip current formation is compared with the experiment. This topic is of importance in estimating the discrepancy between rip current spacing obtained in the field and laboratory.

Table 2.4 Classification of rip current formation by previous experimental investigators.

Driving Forces	Investigators
Edge wave and incident wave interaction	Bowen and Inman (1969) Horikawa and Mizuguchi (1975)
Existing currents and incident wave interaction	Horikawa and Mizuguchi (1975) Ozaki and Sasaki (1976) Tsuchiya, Kawata, Shibano, Dadang and Shishikura (1986)
Cross waves interaction	Horikawa and Maruyama (1976)
Topography and incident wave interaction	Wada and Mizuguchi (1982)
Edge wave and vortex forma tion along run-up line	Matsunaga and Kaneko (1981) Matsunaga et.al (1988)

2.8.2 Experimental set-up and measuring method

The experiment was carried out at the Ujigawa Hydraulics Laboratory, Disaster Prevention Research Institute, Kyoto University. The model beach facility was located in a fan-shaped (half circle) wave basin, 35 m in

diameter, and covered by the wind sheltering tent as shown in Figure 2.16.

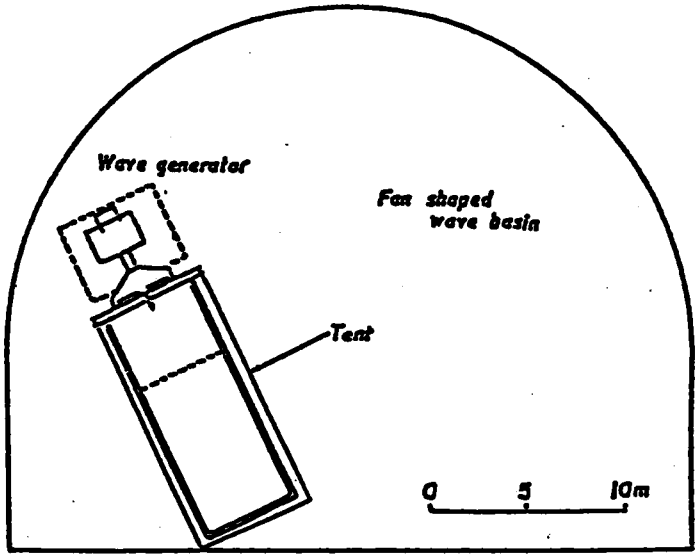

Figure 2.16 3-D fan-shaped wave basin arrangement used in the present investigation.

The beach was made of smooth mortar, 12 m long and 5 m wide with a slope of 1/20, see Figure 2.17. The wave generator was a piston type. To observed the nearshore circulation pattern, rip current visualization technique was employed. A motor-driven fixed-camera system was installed above the model beach facility to photograph the top view of the entire experimental area.

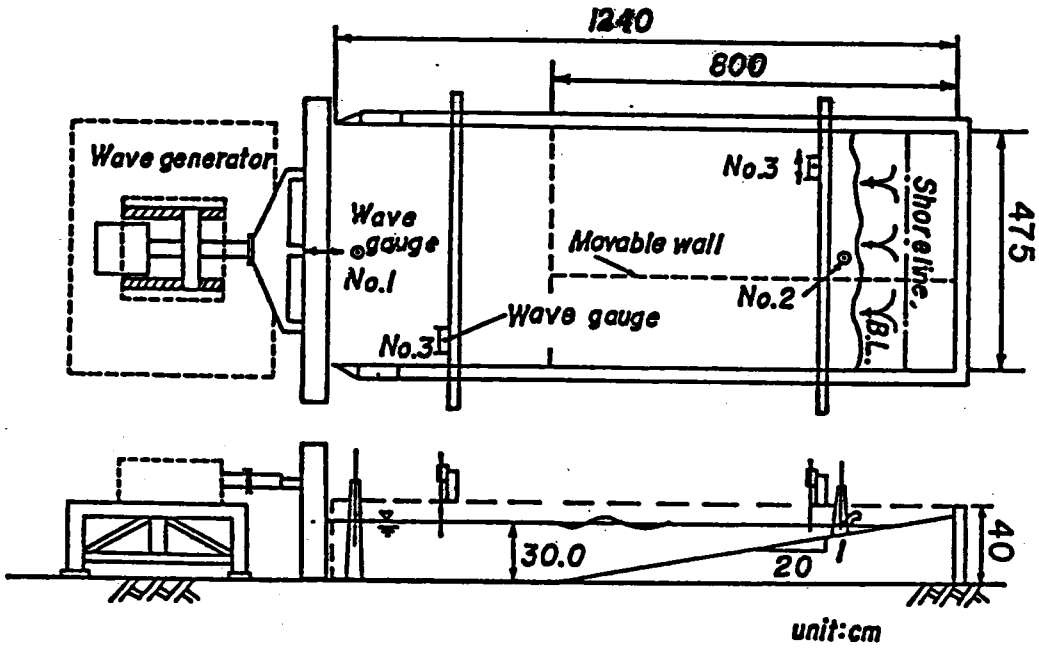

Figure 2.17 Schematic diagram of the experimental arrangement of rip current formation with littoral reflective boundaries.

A dye injection system was set up along the still water of shoreline, and controlled by a cock system. In combining the camera-dye injection systems, successive photographs of dye trajectory and wave crestline, are observed. The wave height distribution in the nearshore zone was

measured by capacitance type wave gauges mounted on a carriage controlled by micro computer. The experimental conditions and data for the wave height and wave periode are listed in table 2.5.

Table 2.5 Experimental conditions of rip current formation on a planar beach with littoral reflective boundaries.

Run No.	$ho(cm)$	$Ho'(cm)$	$T(sec)$	$h_B(cm)$	$Y_r(cm)$
1-1	30.24	5.40	0.994	6.65	237
1-2	30.29	3.75	1.045	4.60	152
1-3	30.06	2.70	0.994	3.20	88
2-1	30.02	6.18	0.798	7.25	166
2-2	30.02	4.47	0.798	5.45	147
2-3	29.75	3.09	0.798	3.80	74
3-1	30.06	5.55	0.600	9.65	102
3-2	29.93	4.44	0.599	3.45	134
4-1	30.16	5.70	0.666	6.25	137.5
4-2	0.019	4.35	0.666	4.75	162.5

Before making rip current measurements, the alongshore uniformity of

the incoming wave height was examined and adjusted to normal incidence by placing small amounts of gravel onto the bed near the wave generator. Therefore, the uniformity of incident wave height and the condition of normal incidence are fully confirmed.

2.8.3 Experimental results of the horizontal nearshore circulation

1) Observations of rip current formation

The observations of rip current formation process in this experiment are mentioned as follows. Following the third or forth incoming wave reaching the shoreline, weak rip current initiated. Prior to the 3rd or 4th wave the breaker line remains parallel to the shoreline. As the rip current grows the injected dye is transported and diffused seaward. The excited feeder and rip currents in the nearshore zone are illuminated by this dye patch. The first maximum run-up mark is almost parallel to the still water shoreline, however, after third to forth wave, the run-up mark becomes zigzag alongshore. Rip currents are generated at the minimum run-up height. The rip currents accelerate in the seaward to the mid position of the surf zone, then decelerate. A rip current resembles a tree stemming from the shore and branching out into a rip head near the breaking point, consequently, a non-uniform breaker line is formed.

2) Wave height variation alongshore and rip current formation processes

To confirm the uniformity of incident wave height, photographs of the leading wave's crest line are analyzed. The maximum alongshore crest line variation does not exceed 4% of the deep water wavelength as shown in Figure 2.18. After the third or forth wave, it is observed that the run-up height and the breaker line become zigzag, but they are in phase. At this stage,

the uniformity of wave height has already been broken down and the radiation stress gradients vary alonghsore, which acts as the driving forces of nearshore currents. This indicates the importance of the wave-current interaction in the generation mechanism of nearshore circulation. The large wave heights are observed at the location where rip currents are generated. It is also observed that breaker line moves offshore where the rip current and incident waves collide. This phenomenon can be explained by the energy flux conservation in the wave-current system.

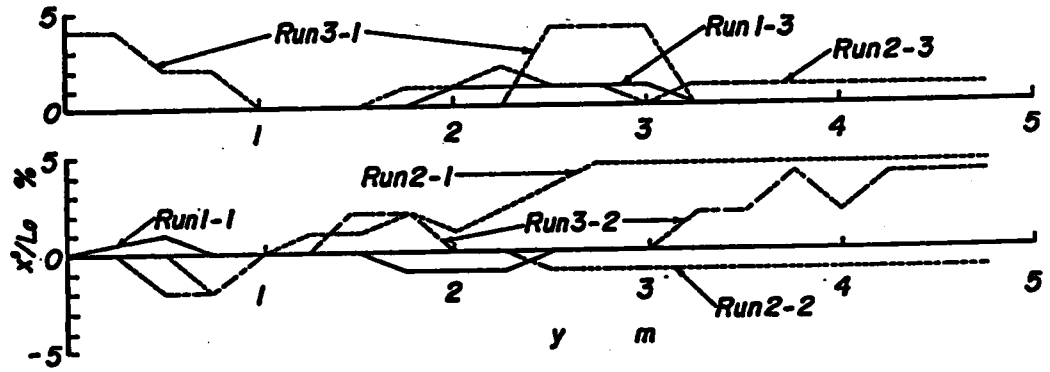

Figure 2.18 Variation of crest of leading waves at the point of 4 cm in depth.

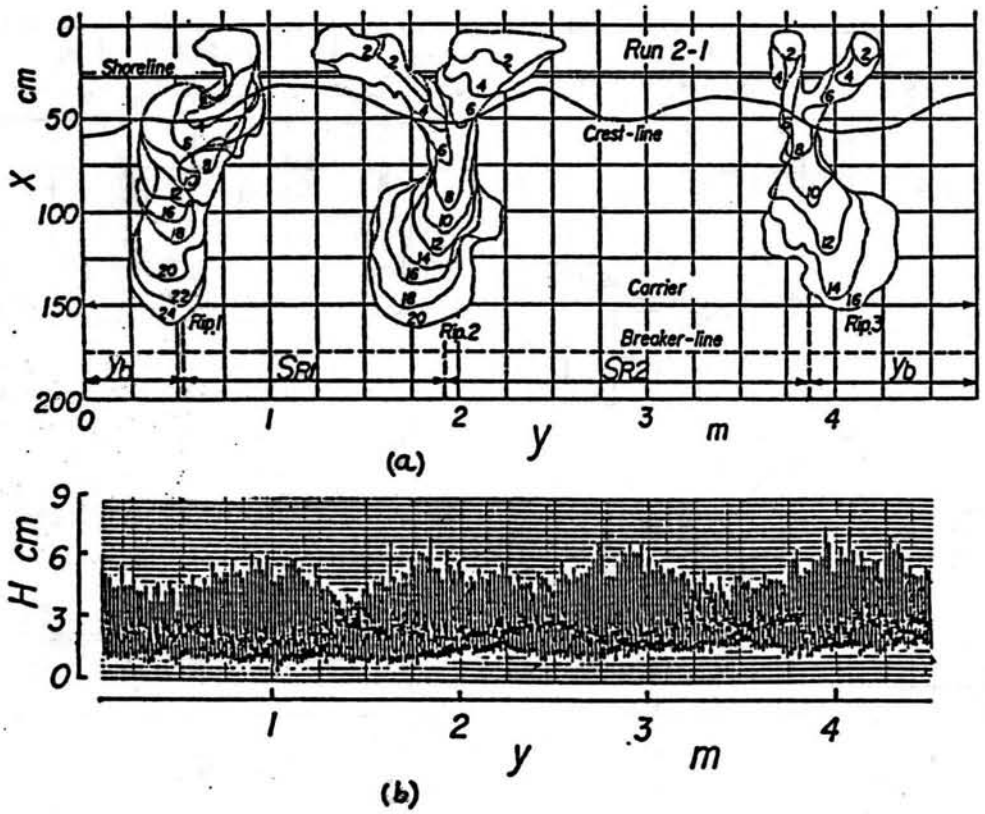

Figure 2.19 Rip current formation processes and alongshore distribution of wave heights, observed in Run 2-1.

(a) Evolution of dye patch measured by the interval of 2s.

(b) Alongshore distribution of wave height just before breaking.

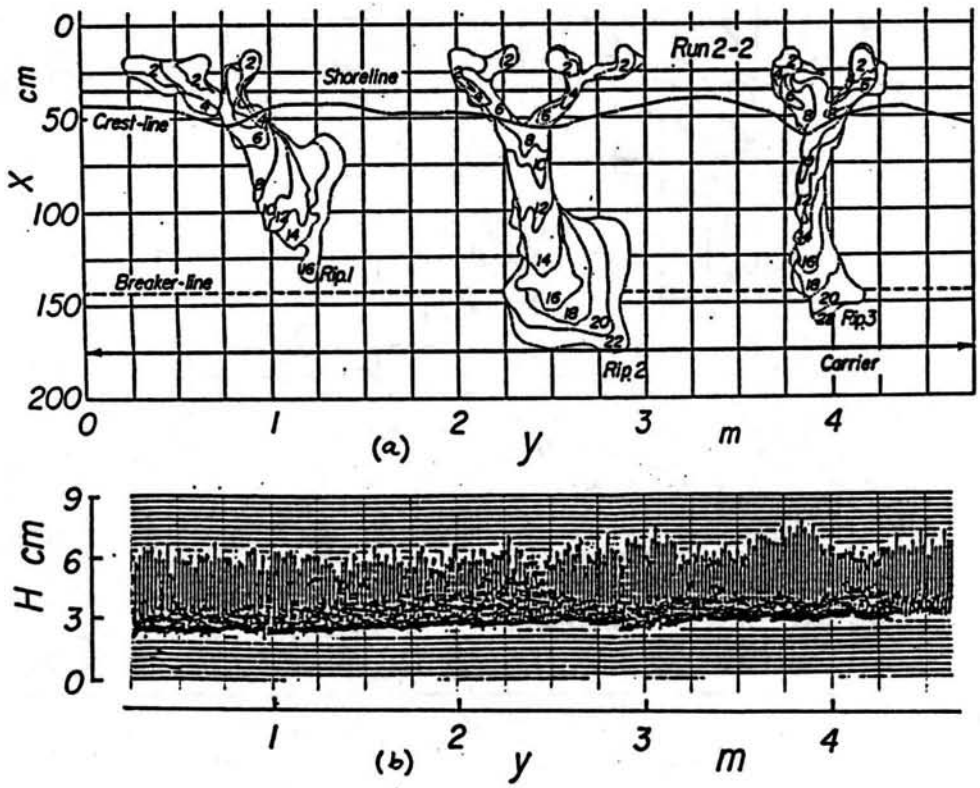

Figure 2.20 Rip current formation processes and alongshore distribution of wave heights, observed in Run 2-2.

(a) Evolution of dye patch measured by the interval of 1s.

(b) Alongshore distribution of wave height just before breaking.

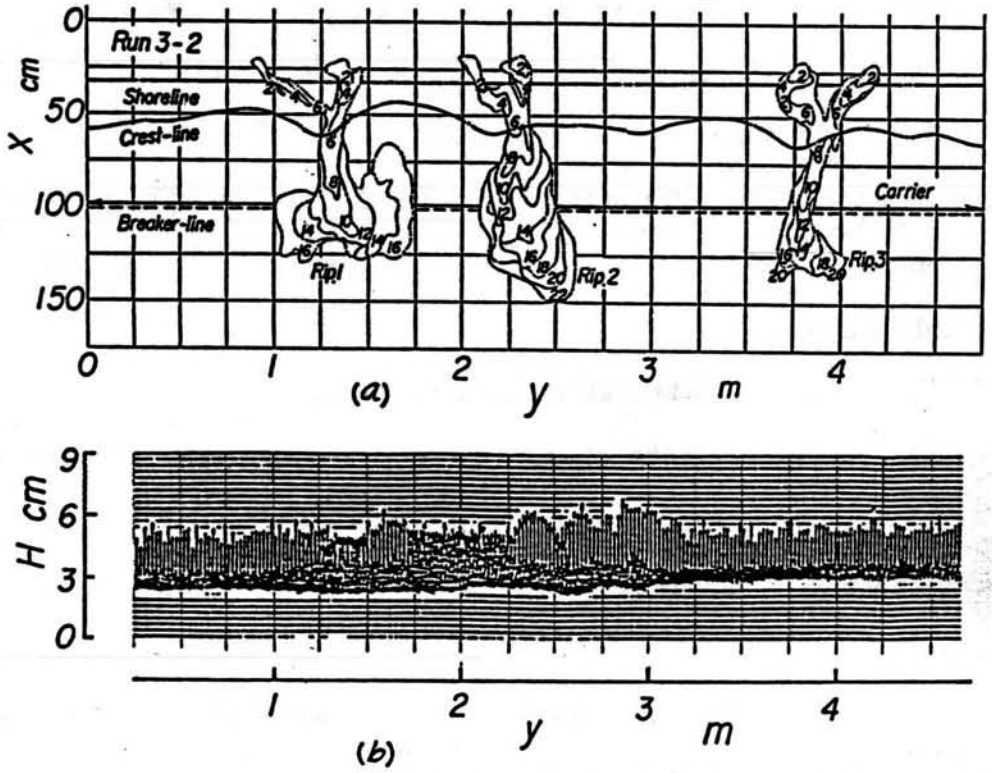

Figure 2.21 Rip current formation processes and alongshore distribution of wave heights, observed in Run 3-2.

(a) Evolution of dye patch measured by the interval of 1s.

(b) Alongshore distribution of wave height just before breaking.

Rip current formation processes and alongshore distribution of wave heights in the steady state are shown in Figures 2.19-2.21. Wave heights are measured just before breaking by wave gauge mounted on the carriage moving alonghshore with constant speed from one side wall to the other. Run 2-1 (Figure 2.19) shows that the three observed rip heads (rip 1, rip 2, rip 3 in the figure) are generated at the locations of large wave heights. In the figure of run 2-2 and run 3-2 (figures 2.20 and 2.21), three rip currents are also observed, and two of these are generated in the large wave height region.

3) Influence of the littoral reflective boundaries

Laboratory experiments of rip current are usually influenced by the litoral reflective boundaries which are actually side walls. Side walls in the basin act as the reflective boundaries for a long period flow, such as nearshore circulation.

Supposing the width of basin is l and the number of rip current n, the relationships between l to rip current spacing Y_r are given, for A-mode and B-mode, where their definition are illustrated in Figure 2.22(b), respectively by:

$$l = (n-1)Y_r + 2y_b; \quad \text{for } A \text{ mode} \tag{2.115.a}$$

$$l = (n-1)Y_r; \quad \text{for } B \text{ mode} \tag{2.115.b}$$

where y_b is the distance between boundary and the nearest rip current.

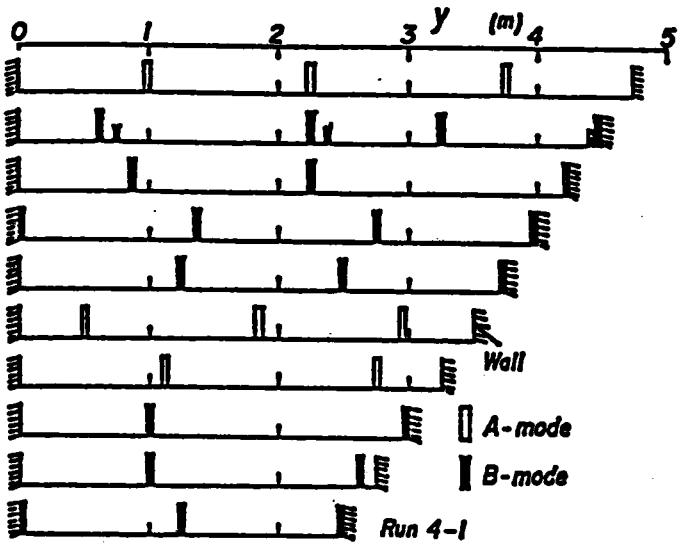

(a)

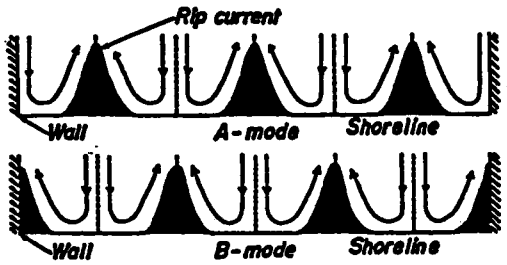

(b)

Figure 2.22 The width of beach span l and observed rip current spacings, two modes, A and B modes of rip current formation with longshore boundaries.

(a) Position of rip currents and their modes.

(b) The definition of two modes, A and B mode.

For both the surf and shoaling zones, the stream function in the

longshore direction, y, is given by:

$$Y_{yy} + \lambda^2 Y = 0 \tag{2.116}$$

to which the general solution is given as:

$$Y(y) = \tilde{\alpha}_1 \sin\lambda y + \tilde{\alpha}_2 \cos\lambda y \tag{2.117}$$

where $\tilde{\alpha}_1$ and $\tilde{\alpha}_2$ are integration constants, and λ is the separation constant which corresponds to the number of rip current. Due to the presence of littoral boundaries at both ends $y=0$ and $y=l$ the reflection boundary condition is applied as:

$$\frac{d\,Y(y)}{dy}\Big|_{y=0} = 0 \text{ and } \frac{d\,Y(y)}{dy}\Big|_{y=l} = 0 \tag{2.118}$$

from which we get:

$$\alpha_1 . 1 = 0 \qquad \text{at } y = 0 \tag{2.119.a}$$

$$\alpha_2 \sin\lambda l = 0 \qquad \text{at } y = l \tag{2.119.b}$$

finally λ can be determined as

$$\lambda = \frac{2\pi n}{l} \quad \text{where } n = 1,2,3,\ldots \tag{2.120}$$

As was previously mentioned in the theory of rip currents, the periodic solution is obtained which gives the other boundary condition, given as:

$$Y(y)|_{y=y_b} = Y(y)|_{y=y_b+nY_r} \tag{2.121}$$

from which the rip current spacing Y_r is determined as:

$$Y_r = \frac{2\pi}{\lambda} \tag{2.122}$$

which is the same by substituting (2.115.b) into (2.120) to find the expression of rip current spacing for B-mode. Substituting (2.115.a) into (2.120), Y_r for A-mode can be expressed as:

$$Y_r = \frac{2\pi}{\lambda}(1-2\frac{y_b}{l}) \tag{2.123}$$

Equation (2.123) implies that for $l \rightarrow \infty$ (no littoral boundary i.e., open coast), Y_r takes the same form as previously determined by the present theory of rip current. Therefore, as the longshore span of beach l becomes longer or the number of rips n becomes larger the influence of the littoral boundary on the rip current spacing becomes smaller. Furthermore, Y_r depends also on y_b, e.g., if y_b becomes smaller Y_r becomes larger, and if $y_b = 0$, Y_r will represent the intrinsic length of spacing. This tendency described by (2.123) agrees with the experimental result illustrated in Figure 2.23, where the curves indicate the theoretical ones.

The experiment was conducted by changing l from 4.8 m to 2.4 m as described by Figure 2.22(a), and fixing the wave steepness Ho/Lo = 0.082, and beach slope, 1/20. The observed rip current spacings are significantly influenced by the width of the beach span, l . The obtained data are plotted in Figure 2.23.

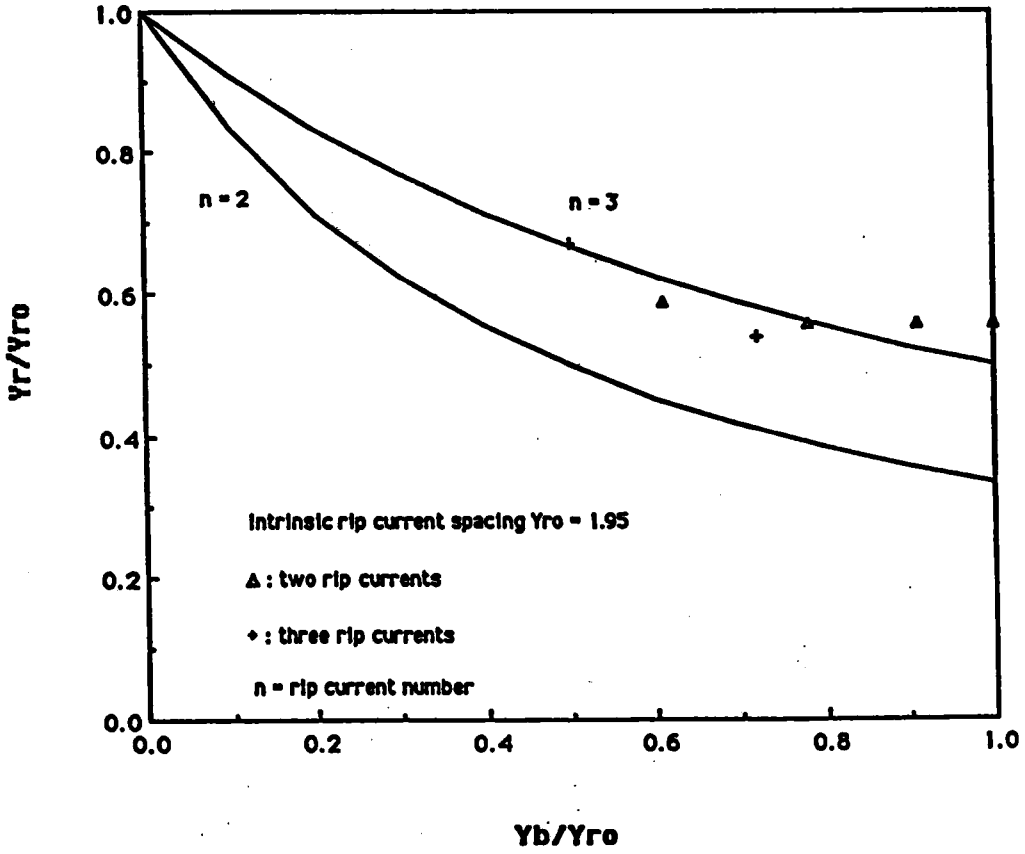

Figure 2.23 Changes in dimensionless rip current spacings with the dimensionless distance between boundary and the nearest rip current center relative to the intrinsic rip current spacing. The data indicate the experimental results of two and three rip currents.

2.9 Conlusions

In this study a new mathematical model for the steady state horizontal nearshore circulation was developed, in which wave-current interaction was taken into consideration. The basic equations consists of the depth-integrated equations for conservation of mass, momentum and wave action, as well as the conservation of wave number in the wave-current system. The wave-current interaction includes not only wave refraction due to currents but the work done by radiation stresses against the mean current. In the formulation, and the latter was considered to be inclusive in the conservation of wave action which was used to calculate the decay of wave amplitude in the surf zone. Based on this wave-current interaction, a field equation of 2-D horizontal nearshore circulation, such as rip currents, was derived mathematically and the solution of rip current spacing was obtained as an eigenvalue problem through a perturbation scheme.

2.9.1 Formulation and solution of governing equations.

The nearshore circulations were generated by the rotational driving forces in the momentum equations which were originally expressed as the gradient of radiation stresses, and balanced with the bottom friction. This circulation was theoretically formed due to the inclusion of the wave-current interaction term in the formulation of the driving forces, in which the MSE was employed. The calculation of wave amplitude decay was first determined using the equation of wave action conservation. Moreover, the wave dispersion relation, which was justified from the momentum conservation equation, was utilized to reduce the higher order of

differentiation. Consequently, by substituting the relation of mean water level and stream function into the cross-differentisted momentum equations, the solvable differential equation for stream function was obtained.

Owing to the difference of wave characteristics, in the surf zone and the shoaling zone, the field equations of rip currents were formulated. The field equations to be solved were linearized by a perturbation method where the bottom slope, s, was chosen as the ordering parameter. Furthermore, the method of seperation of variables was used to solved the partial differential equations. In the zeroth-order, the solution to the ordinary differential equation (ODE) for wave set-up in the surf zone and wave set-down in the shoaling zone were also obtained. In the first order, the linearized field equations of rip currents were obtained, whose solutions are the rip current spacings and velocity distributions. The solutions were characterized by the boundary conditions at infinity, at the breaking and the run-up position.

In the surf zone, the solution to the proposed field equation of rip currents was represented by the Gaussian hypergeometric function, while in the shoaling zone, the solution was found to be a a modified Bessel function of the first and second kind. It was also confirmed that the stream function has at least one maximum point in the surf zone, and is a monotonically reducing function in the shoaling zone. Using the characteristic equation, which was extracted from the matching condition at the breaking point, the eigenvalues of the field equations were obtained, and the solutions were derived. To determine the integration constant in the solution of the stream function, the wave energy flux balance between just and after the breaking points were used.

2.9.2 Rip current spacing

The theoretical curves of rip current spacing obtained by the present theory agreed well with Sasaki's field data presented in terms of Battjes's surf similarity parameter. The curves showed a sudden increase in the range of small surf similarity parameter, which agreed with the empirical curve by Sasaki in the region of so-called infragravity waves. And in the range of larger values, the curve tended to a constant value, dependent on the bottom slope and bottom friction. Using the Dalrymple and Lozano's parameter instead of the surf similarity parameter, the curve of the present theory showed a sudden increase in the range of low values, while Dalrymple and Lozano's curve showed a decrease. Comparing the theoretical curve with the field observation of rip current spacing by Balsillie, especially those obtained during the spilling and spilling-plunging transition breakers, the data in the vicinity of the surf similarity parameter of 0.3, were plotted below the present curves. Sasaki's empirically curve runs parallel to but slightly shifted from this experimental data.

2.9.3 Circulation pattern

The rip current spacing was found to characterize the rip current velocity profile and circulation pattern. The rip current velocity along the rip center decreases as the rip current spacing increases, and the circulation pattern extendes seaward. Rip currents circulation patterns were calculated for both in the laboratory and field scales. Furthermore the discharge and velocity distribution in a rip current were obtained for both scales. The magnitude of rip current velocity was found to reasonably compare for both laboratory and field observations. This suggested that the determined integration constant of the stream function was appropriate.

2.9.4 Littoral reflective boundary effects on rip current spacing

Rip current spacings obtained by laboratory experiments in this study, were about half of these calculated by the present theory. This discrepancy may be caused by the existence of the littoral reflective boundaries which restricted rip current formation in the basin. This influence was also investigated theoretically and experimentally. In rip current experiments whichare performed with littoral reflective boundaries, it was determined that two rip current formation modes exists. The rip current spacing of A mode were specified by the distance from the littoral boundaries to the nearest rip center. This theoretical study showed that the rip current spacing decreases with boundary the distance, which was in agreement with the experimental values.

REFERENCES

Balsillie, J.H., 1975, Surf observations and longshore current prediction, Technical Memorandum no. 58, CERC, 39p.

Basco, D.R., 1982, Surf zone currents Volume I, Miscellaneous Report No. 82-7 (I), U.S. Army, Virginia.

Basco, D.R., 1983, Surf zone currents, Coastal Engineering, Vol.7, pp. 331-355.

Battjes, J.A., 1974, Surf similarity, Proc. 14th Conf. on Coastal Eng., pp. 466-480.

Beer, T., 1983, Environmental oceanography, Pergamon Press, New York, pp. 20-36.

Bowen, A.J.,1969, Rip currents, I, Theoretical investigation, Jour.

Geophys. Res., Vol. 74, pp.5479-5490.

Bowen, A.J. and D.L. Inman, 1969, Rip currents,II, Laboratory and field observations, Jour. Geophys. Res., Vol. 74, pp. 5479-5490.

Christoffersen, J.B. and I.G. Jonsson, 1980, A note on wave action conservation in a dissipative current motion, Applied Ocean Research, 2, 4, pp. 179-182.

Crapper, G.D., 1984, Introduction to water waves, John Wiley & Sons, New York, pp. 93-106.

Dalrymple, R.A., and C.J. Lozano, 1978, Wave-current interaction model for rip currents, Jour. Geophys. Res., Vol. 83, C12, pp. 6063-6071.

Dingemans, M.W., A.C. Radder and H.J. De Vriend, 1987, Computation of the driving forces of wave induced currents, Coastal Engineering, Vol. 11, pp. 539-563.

Dolata, J.B., and W. Rosenthal, 1984, Wave set-up and wave-induced currents in coastal zones, Jour. Geophys. Res., Vol. 82, C2, pp. 1973-1982.

Hansen, J.B. and I.A. Svendsen, 1979, Regular waves in shoaling water - experimental data, Inst. Hydrodyn. Hydraulic Eng., Series paper 21, Tech.University of Denmark, Lyngby.

Horikawa, K., and Y. Maruyama, 1976, On the generation of rip current in laboratory, Proc. 23rd Japanese Conf. on Coastal Eng., pp. 464-469. (in Japanese)

Horikawa, K., and M. Mizuguchi, 1975, Experiment on nearshore currents on a plane beach, Proc. 22nd Japanese Conf. on Coastal Eng., pp. 141-153. (in Japanese)

Humi, M., and W. Miller, 1988, Second course in ordinary differential equations for scientist and engineers, Springer-Verlag, New York, pp.60-88.

Iwata, N., 1976, Rip current spacing, Jour. of the Oceanographical Society of Japan, 32, pp. 1-10.

Kimura, A., K. Goto and A. Seyama, 1988, On the wave height variation of irregular waves in shallow water, Proc. 35th Japanese Conf. on Coastal Eng., pp. 168-172. (in Japanese)

Kirby, J.T., 1984, A note on linear surface wave current interaction over slowly varying topography, J.G.R., 89, C1, pp. 745-747.

Liu, P.L.F., 1983, Wave-current interaction on a slowly varying topography, Jour. of Geophys. Res., 88, C7, pp. 4421-4426.

Liu, P.L.F., and R.A. Dalrymple, 1978, Bottom frictional stresses and longshore currents due to waves with large angles of incidence, Jour. of Marine research, 36, 2, pp.357-375.

Le Blond, P.H., and C.L. Tang, 1974, On energy coupling between wave and currents, Jour. Geophys. Res., Vol. 79, 6, pp. 811-816.

Longuet-Higgins, M.S., 1972, Waves on beaches and resulting sediment transport, Public. No.28 of the Math. Res. Center, the Univ. Wisconsin, New York, pp.203-248.

Matsunaga, N., and A. Kaneko, 1981, Standing edge wave induced rip currents and sand pattern formation, Proc. 28th Japanese Conf. on Coastal Eng., pp. 305-309. (in Japanese)

Matsunaga, N., and Y. Takebara, Y. Kuritani, 1988, On the rip current model of Bowen, Annual meeting abstrac of Civil Eng. Conf., pp. 22-23. (in Japanese)

Mei, C.C., and P. L-F Liu, 1977, Effects of topography on the circulation in and near the surf zone - linear theory, Estuarine and Coastal Marine Science, 5, pp. 25-37.

Mizuguchi, M., 1976, Eigenvalue problems for rip current spacing, Proc.

JSCE, 248, pp. 83-88. (in Japanese)

Mizuguchi, M., 1977, On the mechanism of nearshore circulation, Proc. 24th Japanese Conf. on Coastal Eng., pp. 591-595. (in Japanese)

Nielsen, P., 1977, Turbulent mixing and shear stresses in the surf zone, Inst. Hydrodyn. and Hydraulic Eng., Tech. Univ. Denmark, Prog. Rep. 42, pp. 3-10.

Noda, E.K., 1974, Wave-induced nearshore circulation, Jour. of Geophys. Res., 79, 27, pp. 50-59.

Phillips, O.M., 1977, The dynamics of the upper ocean, second edition, Cambride University Press, pp. 23-81.

Sasaki, M. and A. Ozaki, 1979, Rip currents of free jet type and regular circulation type, Proc. JSCE, 288, pp. 95-106. (in Japanese)

Sasaki, T., 1977, Field Investigations of nearshore currents on gently sloping bottom, PhD Disertation, NERC, Tokyo University, Japan.

Shepard, F.P., and Inman, D.L., 1951, Nearshore circulation, Proc. 1st Conf. on Coastal Eng., pp. 4097-4106.

Sonu, C.J., 1972, Field observation of nearshore circulation and meandering currents, Jour. Geophys. Res., Vol. 77, 18, pp. 3232-3247.

Tam, C.K.W., 1973, Dynamic of Rip currents, Jour. of Geophys. Res., 78, 12, pp. 1937-1943.

Tsuchiya, Y., Y. Kawata, T. Shibano, A.S. Dadang and T. Shishikura, 1986, Proc. 33rd Japanese Conf. on Coastal Eng., pp. 36-40.(in Japanese)

Tsuchiya, Y.,and A.S. Dadang, 1989, Studies on the formation of rip currents in a plane beach, Annual Dis. Prev. Res. Ins., Kyoto University, No. 32 B-2. (in Press in Japanese)

Tsuchiya, Y., T. Yasuda, and K. Tokuda, 1979, Rip current theory (1), Proc. 26th Japanese Conf. on Coastal Eng., pp. 459-499. (in

Japanese)

Tsuchiya, Y., T. Yasuda, and A. Katayama, 1980, Rip current theory (2), Proc. 27th Japanese Conf. on Coastal Eng., pp. 158-162. (in Japanese)

Tsuchiya, Y. and T. Yasuda, 1983, Rip current theory (3), Proc. 30th Japanese Conf. on Coastal Eng., pp. 465-469. (in Japanese)

CHAPTER 3. VERTICAL NEARSHORE CIRCULATION IN THE SURF ZONE

3.1 Introduction

The nearshore circulation is one of the most important topics in the study of coastal hydrodynamics, which has recently received much attention. As mentioned in Chapter 2, nearshore currents are composed of horizontal and vertical circulations. They are individually identified as rip currents, longshore currents, and undertow. These currents are defined as the mean flow components in the complex flow field in the surf zone. Two additional dominant flow field components are wave and turbulence motion. Most nearshore circulation models have been developed assuming the depth-averaged current fields. This model describes the 2-D horizontal nearshore circulation as was discussed in Chapter 2. The vertical circulation occuring in the surf zone consists of both the shoreward mass transport due to breaking wave and the offshore-directed bottom current (undertow). By combining the 2-D vertical and horizontal models, it may be possible to construct a 3-D model of the nearshore circulation system.

The first qualitative work and theoretical analysis of the undertow was done by Dyhr-Nielsen and Sørensen(1970), who proposed many physical ideas. Svendsen (1984 a, b) developed a theoretical model using the first order approximation technique in describing breaking waves. Buhr-Hansen and Svendsen (1984) considered the effect of the bottom boundary layer in the undertow. This model was examined by using Stive and Wind's experimental data (1985). It was shown that the undertow is suppressed by the shear stress at the trough level, the static pressure induced by set-up, and the constraint of zero net flow. Tsuchiya, Yamashita and Uemoto (1986)

modified Svendsen's undertow model by redefining the boundary conditions at the trough level and bottom. Furthermore they suggested that the eddy viscosity coefficient must be theoretically determined by means of the dynamics of turbulence in the surf zone. Madsen and Svendsen (1979) developed a theory of vertically integrated conservation equations for breaking waves in the surf zone by introducing the concept of time and depth averaging of mass, momentum and energy between the bottom and mean water level M.W.L. From their treatment an idea came to mind to define the total depth by the surface and inner layers, thus allowing a theoretical treatment of the breaking waves in the surface layer.

In the present study, a simplified two layer model is proposed, in which the surface layer is introduced to describe breaking wave dynamics and to obtain the time-averaged boundary conditions for dynamics in the inner layer. The interface between these two layers is set by M.W.L. The breaking waves generate turbulence and the turbulent kinetic energy conservation is considered in the model for the inner layer. Therefore, the boundary conditions for the k-ε equations in the inner layer are defined by modelling the dynamics of surface layer. Mass, momentum, and energy conservation laws are formulated by employing Madsen and Svendsen's model. The motion in the inner layer is decomposed into time-averaged mean flow and turbulence. The governing equations of mean flow motion are expressed in terms of the vorticity and stream function, which are derived from the mass and momentum conservation equations. The k-ε equations are employed as the governing equation for turbulent motion. The coordinate transformation (conformal mapping) method developed by Wanstrath, Whitaker and Reid (1976), was used to numerically calculate the 2-D vertical circulation pattern in arbitrary depth. Computation coding and calibration

of the numerical model are performed by a comparison with the experimental data of Stive and Wind (1985).

3.2 Governing Equations of Vertical Nearshore Circulation in the Surf Zone

In this section, the governing equations of fluid motion in the surf zone are discussed. Fluid motion in the surf zone is rotational and multi-modal, in which nonlinear interaction between different modes of rotating fluid elements exist. Therefore the powerful potential theory is not applicable to this region. Svendsen (1984) divided the surf zone into two regions, the outer, and inner regions, as shown in Figure 3.1. The inner region is usually defined as the region over which the quasi-steady bore propagates, and the outer region as the zone between the breaking point and the inner region. In the outer region, rotational motion which originated from wave breaking and irrotational motion associated with wave motion co-exist.

The vertically two-dimensional modelling of the mean flow motion in the inner layer will be presented in this section.

3.2.1 Mean-flow equations

The mass and momentum equations of incompressible fluid are:

$$\frac{\partial u_i}{\partial x_i} = 0 \tag{3.1}$$

$$\frac{\partial u_i}{\partial t} + u_j \frac{\partial u_i}{\partial x_j} = \frac{1}{\rho} \frac{\partial \sigma_{ij}}{\partial x_j} \tag{3.2}$$

where u_i are the x_i-components of the velocity, ρ the fluid density, and

σ_{ij} the stress tensors given by

$$\sigma_{ij} = -p\delta_{ij} + 2\mu s_{ij} \tag{3.3}$$

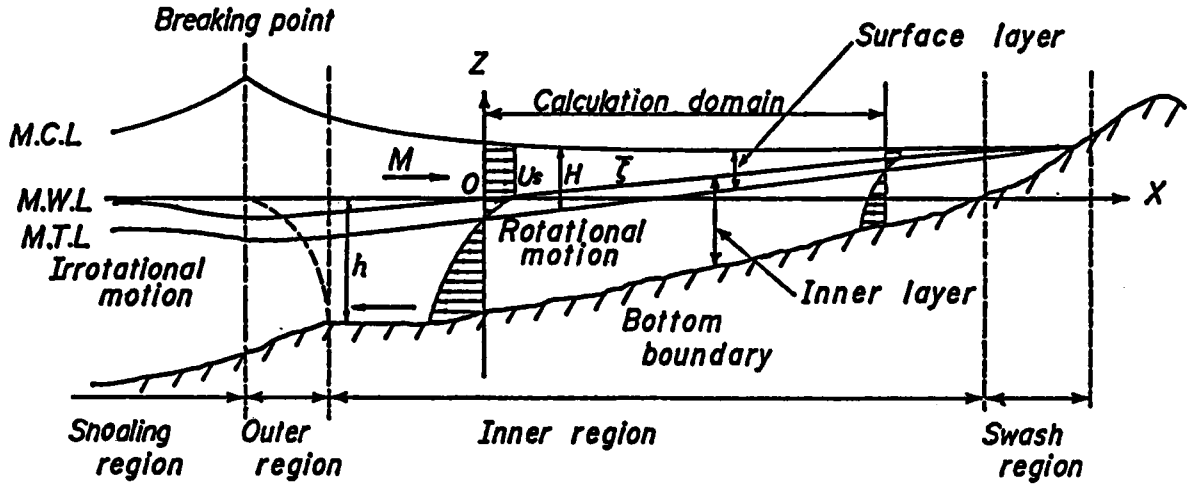

Figure 3.1 Schematic explanation of the 2-D vertical circulation model and and the coordinate system.

In (3.3), p is the total pressure, δ_{ij} the Kronecker's delta, and μ the

viscosity of the fluid. The rate of strains of fluid element, s_{ij}, are defined by

$$s_{ij} = \frac{1}{2}\left(\frac{\partial u_i}{\partial x_j} + \frac{\partial u_j}{\partial x_i}\right) \tag{3.4}$$

The velocities u_i are decomposed into three modes, i.e. the mean flow $\bar{u}_i$, waves u_{wi} and fluctuations u'_i. Other quantities, σ_{ij}, p, s_{ij} are also decomposed in the same manner, as:

$$u_i = \bar{u}_i + u_{wi} + u'_i, \quad \sigma_{ij} = \bar{\sigma}_{ij} + \sigma_{wij} + \sigma'_{ij},$$

$$p_{ij} = \bar{p}_{ij} + p_{wij} + p'_{ij}, \; s_{ij} = \bar{s}_{ij} + s_{wij} + s'_{ij} \tag{3.5}$$

The characteristic time-scales of the three components are assumed to be quite different, therefore no correlation between them is considered. By assuming the time-scale of the fluctuations T_f to be much smaller than the others, the decomposition into means (overbar) and waves becomes possible, as:

$$\langle u_i \rangle \sim \bar{u}_i + u_{wi}, \; \langle \sigma_{ij} \rangle \sim \bar{\sigma}_{ij} + \sigma_{wij}, \; \langle p \rangle \sim \bar{p} + p_w, \; \langle s_{ij} \rangle \sim \bar{s}_{ij} + s_{wij} \tag{3.6}$$

where bracket $\langle\ \rangle$ indicates time-averaging operation over T_f. In the same manner as T_f, the time-averaging over the wave period T_w is defined. Applying these operations to (3.1) and (3.2), the basic equations for the mean flow are obtained.

$$\frac{\partial \bar{u}_i}{\partial x_i} = 0 \tag{3.7}$$

$$\frac{\partial}{\partial x_j}(\bar{u}_i \bar{u}_j + \overline{u_{wi} u_{wj}} + \overline{u'_i u'_j}) = \frac{1}{\rho}\frac{\partial \bar{\sigma}_{ij}}{\partial x_i} \tag{3.8}$$

To solve (3.7) and (3.8) mathematically, a turbulence closure model is needed. When the Boussinesq's eddy-viscosity assumption is used to describe the Reynolds stresses $\overline{u'_i u'_j}$ by means of velocity gradients, the closure problem becomes a matter of how to determine the eddy viscosity ν_t, which is defined by:

$$\overline{u'_i u'_j} = -\nu_t\left(\frac{\partial \bar{u}_i}{\partial x_j} + \frac{\partial \bar{u}_j}{\partial x_i}\right) + \frac{2}{3}k\delta_{ij} \tag{3.9.a}$$

$$\nu_t = C_\mu \frac{k^2}{\varepsilon} \tag{3.9.b}$$

$$k = \frac{1}{2}\overline{u'_i u'_i} \tag{3.9.c}$$

where k and ε are the turbulent kinetic energy and turbulent dissipation quantities, respectively, and C_μ is an empirical constant which is taken as 0.09, for the turbulence field where the local isotrophy assumption is valid. This closure problem is called the k-ε model. In the present study, this model is employed to determine the value of ν_t inside the inner layer.

3.2.2 k-ε Model

1) k-equation

To derive the kinetic energy equation for steady mean flow, the time

dependent momentum equations are first averaged over the time T_f as

$$\frac{\partial}{\partial t}(\overline{u}_i + u_{wi}) + (\overline{u}_j + u_{wj})\frac{\partial}{\partial x_j}(\overline{u}_i + u_{wi}) = \frac{\partial}{\partial x_j}\left(\frac{T_{ij}}{\rho}\right) \tag{3.10}$$

where the stress tensors T_{ij} are

$$T_{ij} = -(\overline{p} + p_w)\delta_{ij} + 2\mu(\overline{s}_{ij} + s_{wij}) - \rho\overline{(u'_i u'_j)} \tag{3.11}$$

The mean-flow energy equations are then obtained by multiplying (3.11) by $(\overline{u}_i + u_{wi})$, resulting in

$$\rho\frac{\partial}{\partial t}\left\{\frac{1}{2}(\overline{u}_i + u_{wi})^2\right\} + \rho(\overline{u}_j + u_{wj})\frac{\partial}{\partial x_j}\left\{\frac{1}{2}(\overline{u}_i + u_{wi})^2\right\}$$

$$= \frac{\partial}{\partial x_j}T_{ij}(\overline{u}_i + u_{wi}) - T_{ij}\frac{\partial}{\partial x_j}(\overline{u}_i + u_{wi}) \tag{3.12}$$

Because T_{ij} are symmetric tensors, the products $T_{ij}\partial(\overline{u}_i + u_{wi})/\partial x_j$ are equal to the products of T_{ij} and the symmetric parts $(\overline{s}_{ij} + s_{wij})$. Therefore, (3.12) becomes

$$\frac{\partial}{\partial t}\left\{\frac{1}{2}(\overline{u}_i + u_{wi})^2\right\} + (\overline{u}_j + u_{wj})\frac{\partial}{\partial x_j}\left\{\frac{1}{2}(\overline{u}_i + u_{wi})^2\right\}$$

$$= \frac{\partial}{\partial x_j}\left\{-\frac{1}{\rho}(\overline{p} + p_w)(\overline{u}_j + u_{wj}) + 2\nu(\overline{u}_i + u_{wi})(\overline{s}_{ij} + s_{wij})\right.$$

$$\left. - \overline{u'_i u'_j}(\overline{u}_i + u_{wi})\right\}$$

$$+ 2\nu(\overline{s}_{ij} + s_{wij})^2 + \overline{u'_i u'_j}(\overline{s}_{ij} + s_{wij}) \tag{3.13}$$

where ν is the kinematic viscosity. Averaging over the wave period T_w, the kinetic energy equation for the steady mean flow is obtained, as

$$\frac{\partial}{\partial x_j}\{\overline{u}_j(\frac{\overline{p}}{\rho} + Q + \overline{q^*}) + u_{wj}(\overline{\frac{p_w}{\rho} + q^* + \overline{u}_i u_{wi}})\}$$

$$- \frac{\partial}{\partial x_j}\{2\nu(\overline{u}_i\overline{s}_{ij}+\overline{u_{wi}s_{wij}}) - \overline{u^*_i u^*_j}\overline{u}_i\}$$

$$- 2\nu(\overline{s}_{ij}^2 + \overline{s}_{wij}^2) + \overline{u^*_i u^*_j}\overline{s}_{ij} \qquad (3.14)$$

where,

$$Q = \frac{1}{2}(\overline{u}_i\overline{u}_i), \quad q^* = \frac{1}{2}(u_{wi}u_{wi}) \qquad (3.15)$$

On the other hand, multiplying (3.2) by u_i and time-averaging over T_f yields the energy equation in the form

$$\frac{\partial}{\partial t}[\frac{1}{2}\{(\overline{u}_i + u_{wi})^2 + u^*_i u^*_i\}]$$

$$+ (\overline{u}_j + u_{wj})\frac{\partial}{\partial x_j}\{\frac{1}{2}(\overline{u}_i + u_{wi})^2 + \frac{1}{2}(u^*_i u^*_i)\}$$

$$+ u^*_j\frac{\partial}{\partial x_j}\{(\overline{u}_i + u_{wi})u^*_i\} + \frac{\partial}{\partial x_j}(\frac{1}{2}u^*_i u^*_i u^*_j)$$

$$= \frac{1}{\rho}\frac{\partial}{\partial x_j}\{(\sigma_{ij} + \sigma_{wij})(u_i + u_{wi}) + \sigma^*_{ij}u^*_i\}$$

$$- \frac{1}{\rho}\{(\sigma_{ij} + \sigma_{wij})(s_{ij} + s_{wij}) + \sigma^*_{ij}s^*_{ij}\} \qquad (3.16)$$

By subtracting (3.14) from (3.16), the time-dependent turbulent kinetic energy equation is obtained. The steady state turbulent kinetic energy

equation is then obtained by time averaging over the wave period T_w. The final form of the equation is

$$\bar{u}_j \frac{\partial k}{\partial x_j} = -\frac{\partial}{\partial x_j}\{\overline{u'_j\left(\frac{1}{2}u'_i u'_i + \frac{p'}{\rho}\right)} - \overline{2\nu u'_i s'_{ij}}\}$$

$$-\overline{u'_i u'_j}\bar{s}_{ij} - \overline{2\nu s'_{ij} s'_{ij}} \qquad (3.17)$$

The first term on the right-hand side of (3.17) is a diffusive transport term due to : i) the transport of turbulent kinetic energy TKE by turbulent velocity fluctuations, ii)work done by the pressure-gradient and iii) TKE transported by viscous stresses. The last two terms define two kinds work done in deformation. One is the production of k, which can be interpreted as the interaction of Reynolds stresses and mean-velocity gradients. The other is the dissipation of k by viscous action, which transfers k into heat. The rate of change of k in steady state, convective transport, is thus balanced by the diffusive transport and deformation works.

However, (3.17) is of no use without a turbulent closure model because unknown correlations appear in the diffusion and dissipation terms. The effort to solve this problem is by Hanjalic and Launder(1972) who proposed a closure aproximation to triple velocity correlation in high turbulence Reynolds number, in relation to this approximation Rodi(1984) reviewed the eddy-diffusivity concept in which the turbulent heat or mass transport is assumed to be related to the gradient of the transported quantity. By using this, the diffusion flux of k can be assumed to be proportional to the gradient of k, as

$$-\overline{u'_j\left(\frac{1}{2}u'_i u'_i + \frac{p'}{\rho}\right)} = \frac{\nu_t}{\sigma_k}\frac{\partial k}{\partial x_j} \tag{3.18}$$

where σ_k is an empirical constant which is usually taken as 1.0. Substituting (3.4) and (3.18) into (3.17) yields

$$\bar{u}_j\frac{\partial k}{\partial x_j} = \frac{\partial}{x_j}\left\{\left(\frac{\nu_t}{\sigma_k} + \nu\right)\frac{\partial k}{\partial x_j}\right\} + \text{Prod} - \varepsilon \tag{3.19.a}$$

where,

$$\text{Prod} = \nu_t\left(\frac{\partial \bar{u}_i}{\partial x_j} + \frac{\partial \bar{u}_j}{\partial x_i}\right)\frac{\partial \bar{u}_i}{\partial x_j} \tag{3.19.b}$$

$$\varepsilon = \nu\left(\frac{\partial u_i'}{\partial x_j}\right)^2 \tag{3.19.c}$$

Note that (3.19) agrees with the standard k-equation derived under condition of only two flow components, mean flow and turbulence.

2) ε-equation

The equation for the dissipation of turbulent kinetic energy is derived from the equation of motion. Subtracting (3.10) from (3.2) by using (3.6) yields the equation for velocity fluctuations, as

$$\frac{\partial u'_i}{\partial t} + (\bar{u}_j + u_{wj})\frac{\partial u'_i}{\partial x_j} + u'_j\frac{\partial}{\partial x_j}(\bar{u}_i + u_{wi}) + u'_j\frac{\partial u'_i}{\partial x_j}$$

$$= \nu\frac{\partial^2 u'_i}{\partial x_j^2} - \frac{1}{\rho}\frac{\partial p'}{\partial x_i} + \frac{\partial}{\partial x_j}\langle u'_i u'_j\rangle \tag{3.20}$$

By differentiating (3.20) by x_l, then multiplying by $2\nu\,\partial u'_i/\partial x_l$, and time-averaging over the wave period T_w, finally the equation for the

dissipation of turbulent kinetic energy is obtained as:

$$\bar{u}_j \frac{\partial \varepsilon}{\partial x_j} = -2\nu \frac{\partial \bar{u}_i}{\partial x_j}\left(\overline{\frac{\partial u'_l}{\partial x_i}\frac{\partial u'_l}{\partial x_j}} + \overline{\frac{\partial u'_i}{\partial x_l}\frac{\partial u'_j}{\partial x_l}}\right)$$

$$- 2\nu \overline{\frac{\partial u'_i}{\partial x_j}\frac{\partial u'_i}{\partial x_l}\frac{\partial u'_j}{\partial x_l}} - 2\left(\nu \overline{\frac{\partial^2 u'_i}{\partial x_j \partial x_l}}\right)^2$$

$$- \frac{\partial}{\partial x_j}\left\{-\nu \overline{u'_j\left(\frac{\partial u'_i}{\partial x_l}\right)^2} + \frac{2\nu}{\rho}\overline{\frac{\partial u'_j}{\partial x_l}\frac{\partial p'}{\partial x_l}} - \nu \frac{\partial \varepsilon}{\partial x_j}\right\}$$

$$- 2\nu \overline{u'_j \frac{\partial u'_i}{\partial x_l}\frac{\partial^2 \bar{u}_i}{\partial x_l \partial x_j}} \qquad (3.21)$$

The left-hand side of the equation is a convective term. On the right-hand side, the first term describes the generation of energy from mean motion, the second and third terms describe the generation of ε by vortex-stretching and its destruction by viscous effect, and the last two terms describe the transport of ε by diffusion.

The diffusion, generation and destruction terms require further model assumptions. These models were summarized by Svensson (1978). The first term on the right-hand side is modeled as

$$- 2\nu \frac{\partial \bar{u}_i}{\partial x_j}\overline{\frac{\partial u'_l}{\partial x_i}\frac{\partial u'_l}{\partial x_j}} = 0 \qquad (3.22)$$

$$- 2\nu \frac{\partial \bar{u}_i}{\partial x_j}\overline{\frac{\partial u'_i}{\partial x_l}\frac{\partial u'_j}{\partial x_l}} = -C_{1\varepsilon}\frac{\overline{u'_i u'_j}\varepsilon}{k}\frac{\partial \bar{u}_i}{\partial x_j}$$

$$= C_{1\varepsilon}\frac{\varepsilon}{k}\nu_t\left(\frac{\partial \bar{u}_i}{\partial x_j} + \frac{\partial \bar{u}_j}{\partial x_i}\right)\frac{\partial \bar{u}_i}{\partial x_j} \qquad (3.23)$$

where $C_{1\varepsilon}$ is an empirical constant which is taken to be 1.44. Equation (3.22) is verified by the continuity equation when $i=j$, or by the assumption that dissipative motions are isotropic when $i \neq j$. (3.23) was suggested by Daly and Harlow (1970) who assumed that the dissipation correlation $2\nu \partial u'_i / \partial x_l \cdot \partial u'_j / \partial x_l$ are related to the dissipation of kinetic energy ε. The generation and destruction terms are modeled together by dimensional analysis,as:

$$- \{2\nu \overline{\frac{\partial u'_i}{\partial x_j}\frac{\partial u'_i}{\partial x_l}\frac{\partial u'_j}{\partial x_l}} + 2(\nu \overline{\frac{\partial^2 u'_i}{\partial x_l \partial x_j}})^2\} = - C_{2\varepsilon}\frac{\varepsilon^2}{k} \tag{3.24}$$

where $C_{2\varepsilon}$ is an empirical coefficient which is taken to be 1.92. The diffusion term is formulated with the gradient model as:

$$- \frac{\partial}{\partial x_j}\{\nu \overline{u'_j (\frac{\partial u'_i}{\partial x_l})^2} - \nu \frac{\partial \varepsilon}{\partial x_j}\} = - \frac{\partial}{\partial x_j}\{\overline{u'_j \varepsilon'} - \nu \frac{\partial \varepsilon}{\partial x_j}\}$$

$$= \frac{\partial}{\partial x_j}\{(\frac{\nu_t}{\sigma_\varepsilon} + \nu)\frac{\partial \varepsilon}{\partial x_j}\} \tag{3.25}$$

where σ_ε is an empirical coefficient which is taken to be 1.3. It is assumed that the term containing pressure fluctuations is negligible in the diffusion terms (Hanjalic and Launder ,1972). The last term is also assumed to be negligible (Hanjalic and Launder ,1976).

Finally, the equation for the dissipation of turbulent kinetic energy (3.21) becomes

$$\bar{u}_j \frac{\partial \varepsilon}{\partial x_j} = \frac{\partial}{\partial x_j}\{(\frac{\nu_t}{\sigma_\varepsilon} + \nu)\frac{\partial \varepsilon}{\partial x_j})$$

$$+ \frac{\varepsilon}{k}\{C_{1\varepsilon}\nu_t(\frac{\partial \bar{u}_i}{\partial x_j} + \frac{\partial \bar{u}_j}{\partial x_i})\frac{\partial \bar{u}_i}{\partial x_j} - C_{2\varepsilon}\varepsilon\} \tag{3.26}$$

3.2.3 Governing equation of the 2-DV circulation model in the inner layer

Using the coordinates and variables shown in Figure 3.1 the governing equations for the two-dimensional model of the surf zone circulation are derived. The inner layer is defined as the region extending from the bottom to the mean water level $\bar{\zeta}$. While the surface layer extends from the mean trough level to the mean crest level (Figure 3.1). The free surface displacement ζ, is defined by

$$\zeta = \bar{\zeta} + \zeta_w + \zeta' \tag{3.27}$$

From the equations derived in the previous section, the governing equations of the 2-DV circulation model in the inner layer are derived below.

1) **Mean-flow equations**

By using (3.3) and (3.4), the equations for steady mean flow, (3.7) and (3.8), are rewritten, as:

$$\frac{\partial \bar{u}}{\partial x} + \frac{\partial \bar{w}}{\partial z} = 0 \tag{3.28}$$

$$\frac{\partial}{\partial x}(\bar{u}\bar{u} + \overline{u_w u_w} + \overline{u'u'}) + \frac{\partial}{\partial z}(\bar{u}\bar{w} + \overline{u_w w_w} + \overline{u'w'})$$

$$= -\frac{1}{\rho}\frac{\partial \bar{p}}{\partial x} + \nu\nabla^2\bar{u} \tag{3.29.a}$$

$$\frac{\partial}{\partial x}(\bar{u}\bar{w} + \overline{u_w w_w} + \overline{u'w'}) + \frac{\partial}{\partial z}(\bar{w}\bar{w} + \overline{w_w w_w} + \overline{w'w'})$$

$$= - g - \frac{1}{\rho}\frac{\partial \overline{p}}{\partial z} + \nu \nabla^2 \overline{w} \qquad (3.29.b)$$

where g is the gravitational acceleration, and u, w are velocities in the x and z directions. By differentiating (3.29.a) and (3.29.b) with respect to z and x, and subtracting the results, the pressure term $\overline{p}$ is eliminated resulting in

$$\frac{\partial^2}{\partial x \partial z}(\overline{u}\overline{u} + \overline{u_w u_w} + \overline{u' u'}) + \left(\frac{\partial^2}{\partial z^2} - \frac{\partial^2}{\partial x^2}\right)(\overline{u}\overline{w} + \overline{u_w w_w} + \overline{u' w'})$$

$$- \frac{\partial^2}{\partial x \partial z}(\overline{w}\overline{w} + \overline{w_w w_w} + \overline{w' w'}) = \nu \nabla^2 \left(\frac{\partial \overline{u}}{\partial z} - \frac{\partial \overline{w}}{\partial x}\right) \qquad (3.30)$$

As for the velocities associated with waves, small amplitude wave theory is assumed to be applicable, hence u_w and w_w are described as:

$$u_w = \frac{H}{2}\sigma \frac{\cosh k_w(h+z)}{\sinh k_w h} \cos(k_w x - \sigma t) \qquad (3.31.a)$$

$$w_w = \frac{H}{2}\sigma \frac{\sinh k_w(h+z)}{\sinh k_w h} \sin(k_w x - \sigma t) \qquad (3.31.b)$$

where σ is the angular frequency, k_w the wave number, and H the wave height. When small amplitude wave theory is assumed the momentum fluxes of the total wave component, $u_w u_w$, $u_w w_w$ and $w_w w_w$, become zero in (3.30).

The stream function ψ and vorticity Ω are now defined as:

$$\frac{\partial \psi}{\partial z} = \overline{u}, \quad \frac{\partial \psi}{\partial x} = - \overline{w} \qquad (3.32)$$

$$\Omega = \frac{\partial \overline{u}}{\partial z} - \frac{\partial \overline{w}}{\partial x} \tag{3.33}$$

In terms of the stream function and vorticity defined above, the governing equations (3.28) and (3.29) are rewritten as:

$$\nabla^2 \psi = \Omega \tag{3.34}$$

$$\left(\frac{\partial \psi}{\partial z}\right)\left(\frac{\partial \Omega}{\partial x}\right) - \left(\frac{\partial \psi}{\partial x}\right)\left(\frac{\partial \Omega}{\partial z}\right) - \frac{\partial^2}{\partial x \partial z}\left(4\nu_t \frac{\partial^2 \psi}{\partial x \partial z}\right)$$

$$+ \left(\frac{\partial^2}{\partial x^2} - \frac{\partial^2}{\partial z^2}\right)\left\{\nu_t\left(\frac{\partial^2 \psi}{\partial z^2} - \frac{\partial^2 \psi}{\partial x^2}\right)\right\} = \nu \nabla^2 \Omega \tag{3.35}$$

Since the turbulent eddy viscocity dominates, the molecular viscous terms in the right-hand side of (3.35) is negligible, therefore, (3.35) becomes

$$\left(\frac{\partial \psi}{\partial z}\right)\left(\frac{\partial \Omega}{\partial x}\right) - \left(\frac{\partial \psi}{\partial x}\right)\left(\frac{\partial \Omega}{\partial z}\right) - \frac{\partial^2}{\partial x \partial z}\left(4\nu_t \frac{\partial^2 \psi}{\partial x \partial z}\right)$$

$$+ \left(\frac{\partial^2}{\partial x^2} - \frac{\partial^2}{\partial z^2}\right)\left\{\nu_t\left(\frac{\partial^2 \psi}{\partial z^2} - \frac{\partial^2 \psi}{\partial x^2}\right)\right\} = 0 \tag{3.36}$$

2) k-ε equations

The k-equation (3.19) is rewritten in the x-z plane as:

$$\overline{u}\frac{\partial k}{\partial x} + \overline{w}\frac{\partial k}{\partial z} = \frac{\partial}{\partial x}\left\{\left(\frac{\nu_t}{\sigma_k} + \nu\right)\frac{\partial k}{\partial x}\right\} + \frac{\partial}{\partial z}\left\{\left(\frac{\nu_t}{\sigma_k} + \nu\right)\frac{\partial k}{\partial z}\right\}$$

$$+ \text{Prod} - \varepsilon \tag{3.37.a}$$

where,

$$\text{Prod} = \nu_t \{2(\frac{\partial \overline{u}}{\partial x})^2 + 2(\frac{\partial \overline{w}}{\partial z})^2 + (\frac{\partial \overline{u}}{\partial z} + \frac{\partial \overline{w}}{\partial x})^2\} \tag{3.37.b}$$

$$\varepsilon = \nu \{(\frac{\partial u'}{\partial x})^2 + (\frac{\partial u'}{\partial z})^2 + (\frac{\partial w'}{\partial x})^2 + (\frac{\partial w'}{\partial z})^2\} \tag{3.37.c}$$

The ε-equation (3.26)is also rewritten as

$$\overline{u}\frac{\partial \varepsilon}{\partial x} + \overline{w}\frac{\partial \varepsilon}{\partial z} = \frac{\partial}{\partial x}\{(\frac{\nu_t}{\sigma_\varepsilon} + \nu)\frac{\partial \varepsilon}{\partial x}\} + \frac{\partial}{\partial z}\{(\frac{\nu_t}{\sigma_\varepsilon} + \nu)\frac{\partial \varepsilon}{\partial z}\}$$

$$+ \frac{\varepsilon}{k}(C_{1\varepsilon}\text{Prod} - C_{2\varepsilon}\varepsilon) \tag{3.38}$$

By ordering each term, it is possible to neglect all viscous terms. The k-equation (3.37.a) and the ε-equation (3.38) then become as:

$$\overline{u}\frac{\partial k}{\partial x} + \overline{w}\frac{\partial k}{\partial z} = \frac{\partial}{\partial x}(\frac{\nu_t}{\sigma_k}\frac{\partial k}{\partial x}) + (\frac{\nu_t}{\sigma_k}\frac{\partial k}{\partial z}) + \text{Prod} - \varepsilon \tag{3.39}$$

$$\overline{u}\frac{\partial \varepsilon}{\partial x} + \overline{w}\frac{\partial \varepsilon}{\partial z} = \frac{\partial}{\partial x}(\frac{\nu_t}{\sigma_\varepsilon}\frac{\partial \varepsilon}{\partial x}) + (\frac{\nu_t}{\sigma_\varepsilon}\frac{\partial \varepsilon}{\partial z}) + \frac{\varepsilon}{k}(C_{1\varepsilon}\text{Prod} - C_{2\varepsilon}\varepsilon) \tag{3.40}$$

3.2.4 Boundary conditions of the 2-DV circulation model

The boundary conditions for the governing equations in the inner layer are discussed here. The surface boundary is the mean water level $\overline{\zeta}$ which is an unknown value in the two layer system. Previous investigations of surf zone wave height and set-up show fairly good predictability of both quantities. Therefore, Svendsen's (1984) model is employed to determine

the wave set-up $\overline{\zeta}$ and breaking wave height variation. Svendsen also presented the mass, momentum, and energy dissipation due to breaking waves in his model by employing the first order approximation of motion, the effect of the surface roller and the wave shape parameter B_0. Consequently, Svendsen's model is needed to determine the wave energy dissipation (production in the k equation), mass flux and shear stress acting on the interface (surface) boundary.

On the other hand, the boundary condition for the stream function ψ, the vorticity Ω, the turbulent kinetic energy k, and it's dissipation ε must be determined. For this problem, Madsen and Svendsen's (1979) formulation of the mass and momentum conservation equations are employed.

1) **Wave set-up and wave height variation**

The momentum equation (3.2) in the x-direction is integrated over depth and then averaged over the wave period T_w as

$$\frac{\partial}{\partial x}\int_{-h}^{\overline{\zeta}} \rho u u dz + \frac{\partial}{\partial x}(S^* + S_w) = -\rho g(h + \overline{\zeta})\frac{\partial \overline{\zeta}}{\partial x} \tag{3.41}$$

where S^* is the depth-integrated Reynolds stress and S_w the radiation stress defined by

$$S^* = \int_{-h}^{\overline{\zeta}} \rho\left(2\nu_t \frac{\partial \overline{u}}{\partial x} - \frac{2}{3}k\right) dz \tag{3.42.a}$$

$$S_w = \overline{\int_{-h}^{\zeta} \rho u_w u_w dz} + \overline{\int_{-h}^{\zeta} p_o dz} - \frac{1}{2}\rho g \overline{\zeta_w \zeta_w} \tag{3.42.b}$$

where p_o is the dynamic pressure given by

$$p_o = \rho g(z - \overline{\zeta}) + p \tag{3.43}$$

In (3.41), the inertia term (self momentum transport of steady mean flow), and the depth-integrated Reynolds stress term are added to the usual momentum balance equation. The latter term described as (3.42.a) is the interaction term with a mean flow distribution and k-equation in the inner layer.

The energy equation is given by

$$\frac{\partial B_*}{\partial x} = D_* \tag{3.44}$$

where B_* is the mean wave energy flux and D_* the wave energy dissipation. The non-dimensional wave energy flux B and energy dissipation D are introduced respectively, as:

$$B = \frac{B_*}{\rho g c H^2} \tag{3.45.a}$$

$$D = D_* \frac{4hT_w}{\rho g c H^3} \tag{3.45.b}$$

where c is the propagation speed of the breaker. In the surf zone, c is approximated by

$$c \sim \sqrt{g(h + \overline{\zeta})} \tag{3.46}$$

Using (3.44) and (3.45), the equation for the wave height variation is given as

$$\frac{H}{H_r} = K_S \Big/ \left(1 - \frac{H_r}{8c_r B_r T_w}\int_{x_r}^{x} \frac{DK_S^3}{h + \bar{\zeta}}dx\right) \tag{3.47}$$

where the subscript r refers to some chosen reference points, and K_S is the shoaling coefficient defined by

$$K_S = \sqrt{c_r B_r / cB} \tag{3.48}$$

By solving (3.41) and (3.47) simultaneously, the wave set-up and breaker wave height variation are obtained. However, in (3.41) and (3.47) three parameters must be estimated, B, S_w and D.

Svendsen (1984) evaluated these parameters assuming that (i) the mean velocity in the roller is equal to the propagation speed c, (ii) the cross sectional area A of the roller is equal to $0.9H^2$, and (iii) wave energy dissipation is analogous to that of hydraulic jump, these are respectively given as:

$$S_w = \rho g\left(\frac{3}{2}B_0 + 0.9\frac{h + \bar{\zeta}}{L}\right)H^2 \tag{3.49.a}$$

$$B = B_0 + 0.45\frac{h + \bar{\zeta}}{L} \tag{3.49.b}$$

$$D = -\left[\left(1 + \frac{\zeta_c}{H}\frac{H}{h + \bar{\zeta}}\right)\left\{1 + \frac{H}{h + \bar{\zeta}}\left(\frac{\zeta_c}{H} - 1\right)\right\}\right]^{-1} \tag{3.49.c}$$

where L is the wave length given as cT_w, ζ_c the crest elevation and B_0 defined by

$$B_0 = \frac{1}{T_w}\int_0^{T_w}\left(\frac{\zeta}{H}\right)^2 dt \sim 0.08 \tag{3.50}$$

2) Boundary conditions for the mean flow equation

a) Surface boundary condition

The boundary conditions for the stream function ψ and the vorticity Ω equations are considered here. To determine the boundary conditions at the surface $\overline{\zeta}$ of the inner layer, the equations of mass and momentum are derived in the surface layer. The kinematic boundary condition at $z = \overline{\zeta}$ is derived from the conservation of mass in the surface layer as

$$\overline{u}(\overline{\zeta})\frac{\partial \overline{\zeta}}{\partial x} - \overline{w}(\overline{\zeta}) = -\overline{\frac{\partial}{\partial x}\int_{\overline{\zeta}}^{\zeta} u dz} \tag{3.51}$$

The dynamic boundary condition at $z = \overline{\zeta}$ is derived from the conservation of momentum in the surface layer. The pressure at $z = \overline{\zeta}$ is obtained by integrating the vertical momentum equation between ζ and $\overline{\zeta}$ and time-averaging over the wave period T_w, as

$$\frac{\overline{p}(\overline{\zeta})}{\rho} = -\overline{w'(\overline{\zeta})w'(\overline{\zeta})} + \overline{u'(\overline{\zeta})w'(\overline{\zeta})}\frac{\partial \overline{\zeta}}{\partial x} - \overline{w}(\overline{\zeta})\overline{\frac{\partial}{\partial x}\int_{\overline{\zeta}}^{\zeta} u dz} \tag{3.52}$$

where the viscous term is neglected. The time-averaged horizontal momentum conservation in the surface layer is derived from the following definition.

$$\overline{\int_{\bar{\zeta}}^{\zeta}(\text{momentum})dz} = \overline{\int_{-h}^{\zeta}(\text{momentum})dz} - \int_{-h}^{\bar{\zeta}}(\text{momentum})dz \tag{3.53}$$

The horizontal momentum equation is given by

$$\frac{\partial}{\partial x}\overline{\int_{\bar{\zeta}}^{\zeta}\left(u^2 + \frac{p}{\rho}\right)dz} = -\frac{\bar{p}(\bar{\zeta})}{\rho}\frac{\partial \bar{\zeta}}{\partial x} - \overline{u'(\bar{\zeta})u'(\bar{\zeta})}\frac{\partial \bar{\zeta}}{\partial x} + \overline{u'(\bar{\zeta})w'(\bar{\zeta})}$$

$$- \bar{u}(\bar{\zeta})\frac{\partial}{\partial x}\overline{\int_{\bar{\zeta}}^{\zeta}udz} \tag{3.54}$$

Substituting the pressure (3.52) into (3.54), the right-hand side of the equation becomes:

$$\text{RHS} = \{\overline{w'(\bar{\zeta})w'(\bar{\zeta})} - \overline{u'(\bar{\zeta})u'(\bar{\zeta})}\}\frac{\partial \bar{\zeta}}{\partial x}$$

$$+ \{\bar{u}(\bar{\zeta}) + \bar{w}(\bar{\zeta})\frac{\partial \bar{\zeta}}{\partial x}\}\frac{\partial M_S}{\partial x}$$

$$- \overline{u'(\bar{\zeta})w'(\bar{\zeta})}\left(\frac{\partial \bar{\zeta}}{\partial x}\right)^2 + \overline{u'(\bar{\zeta})w'(\bar{\zeta})} \tag{3.55}$$

where,

$$M_S = \overline{\int_{\bar{\zeta}}^{\zeta}udz} \tag{3.56}$$

When the orders of $\bar{u}(\bar{\zeta})$ and $\partial\bar{\zeta}/\partial x$ are $0(1)$ and $0(\delta)$, respectively, the orders of the following terms can be estimated in terms of the kinematic boundary condition, (3.51).

$$\overline{w}(\overline{\zeta}) \sim O(\delta), \quad \frac{\partial M_S}{\partial x} \sim O(\delta) \tag{3.57}$$

In the surface layer, strong shear flow is generated by the mass transport shoreward due to the breaker. For this reason, the following order estimation may be reasonable.

$$\overline{u'(\overline{\zeta})w'(\overline{\zeta})} \sim \frac{\partial \overline{u}}{\partial z} \sim O(1) \tag{3.58}$$

This order estimation leads to the brief expression of (3.55), as

$$\text{RHS} = \overline{u'(\overline{\zeta})w'(\overline{\zeta})} + O(\delta) \tag{3.59}$$

On the other hand, LHS of (3.54) can be estimated as follows. The local pressure is given by integrating the vertical momentum equation between z and ζ as

$$\frac{p(z)}{\rho} = g(\zeta - z) + \frac{\partial}{\partial x}\int_z^\zeta uw dz - \rho w^2(z) \tag{3.60}$$

Assuming that u^2 is decomposed as

$$u^2(z) = \overline{u}^2(z) + u_w^2(z) + u'^2(z) \tag{3.61}$$

then, substituting these equations into the left-hand side of (3.54) yields

$$\text{LHS} = \frac{\partial}{\partial x}\{\frac{g}{2}\overline{(\zeta - \overline{\zeta})^2} + \overline{(\zeta - \overline{\zeta})\int_z^\zeta uw dz} - \overline{\int_{\overline{\zeta}}^\zeta uw dz}$$

$$+ \overline{(\bar{u}^2(\bar{\zeta}) + u_w^2(\bar{\zeta}) + u'^2(\bar{\zeta}))(\zeta-\bar{\zeta})\}} \tag{3.62}$$

It is then assumed that in the surface layer, the large scale turbulence exists whose velocity and surface fluctuation have dominant frequency in the spectral domain. If this dominant frequency is a harmonics of the wave, and other spectral components are negligiblly small, the turbulence components can be treated in the same manner as wave components. However, this assumption may be too bold to apply at this time since turbulence is usually characterized by multi-phase motion. However, eddies generated by breaking waves seem to have the same dominant frequency which is strongly related to the wave motion. If the above assumption is allowed, the brief expression of (3.62) can be obtained, as

$$\text{LHS} = \frac{\partial}{\partial x}\{\frac{g}{2}(\overline{\zeta_w\zeta_w} + \overline{\zeta'\zeta'})\} \tag{3.63}$$

Finally, from (3.9) and (3.63), the dynamic boundary condition at the surface of the inner layer is

$$\overline{u'(\bar{\zeta})w'(\bar{\zeta})} = \frac{\partial}{\partial x}\{\frac{g}{2}(\overline{\zeta_w\zeta_w} + \overline{\zeta'\zeta'})\} \tag{3.64}$$

In the equation, the first term on the right-hand side is approximated by (3.50) and, for the second term, the following assumption is made.

$$\overline{\zeta'\zeta'} \sim (\frac{A}{L})^2 \tag{3.65}$$

Furthermore, the shear stress due to turbulence is described by

$$\overline{u'(\bar{\zeta})w'(\bar{\zeta})} = -\frac{\tau_S}{\rho} \fallingdotseq -\nu_t \frac{\partial \bar{u}}{\partial z}\Big|_{z=\bar{\zeta}} \tag{3.66}$$

Consequently, the dynamic surface boundary condition, which is expressed by breaking wave quantities, is given as

$$\nu_t \frac{\partial \bar{u}}{\partial z}\Big|_{z=\bar{\zeta}} = -\frac{\partial}{\partial x}\left\{\frac{g}{2}\left(H^2 B_0 + \frac{A^2}{L^2}\right)\right\} \tag{3.67}$$

b) Bottom boundary condition

For the impermeable bottom, one boundary condition, the kinematic bottom boundary condition, is given by

$$\bar{u}(-h)\frac{\partial h}{\partial x} + \bar{w}(-h) = 0 \tag{3.68}$$

This condition means that the equation of stream function can be given on the bottom boundary, becase no flow is assumed through the bottom. The other is the dynamic boundary condition which depicts the fluid motion near the bottom. Essentially this problem is treated by employing the boundary layer theory. A simple and useful way is to assume a relationship between flow quantities and acting forces to the fluid element near the boundary, such as.

$$\frac{\partial \bar{u}}{\partial z}\Big|_{z=-h} = -\frac{\tau_b}{\nu_t} \tag{3.69}$$

c) Side boundary conditions

Side boundary conditons are also required at both the left and right

side boundaries of the calculation domain. Two types of condition are considered. One is a fixed wall at the shoreline, and the other is an open boundary at any place in the surf zone. In the former case, the problem is the same as that of the bottom boundary condition. In the case of the latter, the current field must be specified at the boundary as to obtain the boundary conditions of vorticity and stream function by the followingway: (i) the velocity vector (two components), (ii) one component of velocities and shear stress, or (iii) two shear stresses acting on the boundary column. This situation is the same as the surface boundary condition, however, it is often necessary to give the condition at the boundary where no kinematic or dynamic condition is specified. Because of this reason, side boundary conditions are usually difficult to be established. The condition (i) may be the easiest way to establish the side boundary conditions in this model, since, it is possible to measure the actual velocity vectors at both side boundaries in physical models or in the fields.

Only for the model test, the assumed velocity vectors are given at the side boundaries. For example, it is a way to assume a parabolic profile for both components u and w. A detail discussion about this problem along with the numerical calculation of the 2-D vertical circulation model are presented in the next section.

3.3 Numerical Model of 2DV Circulation in the Surf Zone

The numerical model of 2DV circulation in the surf zone is developed in this section. The coordinate transformation employed in the 2DV circulation model is based on the conformal mapping method by using the orthogonal function of a Fourier series expansion. This transformation technique makes the model applicable over a wide range of surf zone topography. The boundary conditions derived in the previous section for mean flow and turbulence are discussed in section 3.3.4. Finally, the computer coding of the numerical 2DV circulation model is developed and sample calculations are presented.

3.3.1 Coordinate transformation

The inner layer calculation domain is shaped by both the surface boundary (the mean water surface), which is determined by the given breaking wave fields, and the beach profile, which is also of arbitrary shape. Therefore, the coordinate transformation should simplify both calculation procedure and the expressions for the boundary conditions. The problem which arises is in the manner by which the surface boundary is specified. For this reason, the coordinate transformation method which was developed by Wanstrath, Whitaker and Reid (1976) and Wanstrath(1976), for storm surge calculation, is applied. This technique transforms the domain of calculation bounded by two arbitrarily curves and two parallel straight lines (Figure 3.2).

The inner layer (Z-plane) can be transformed into a rectangular shaped ζ^*-plane as is shown in Figure 3.2. The surface and bottom boundaries in Z-plane are transformed into straightline ($\eta = \pm\beta$) in the ζ^*-plane.

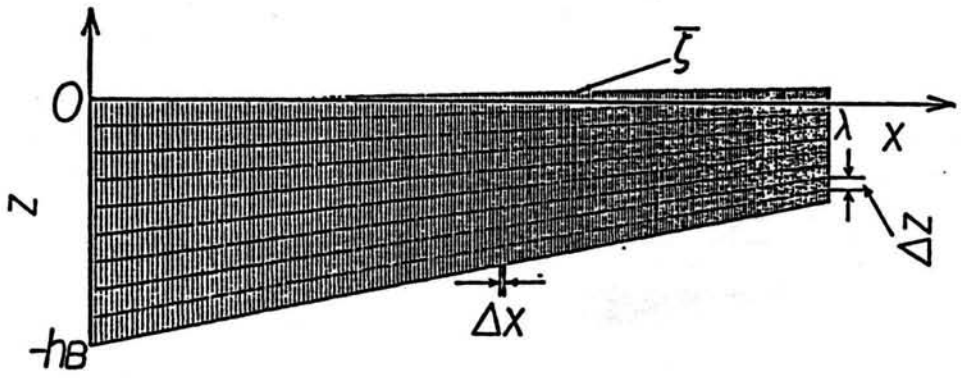

(a) z-plane

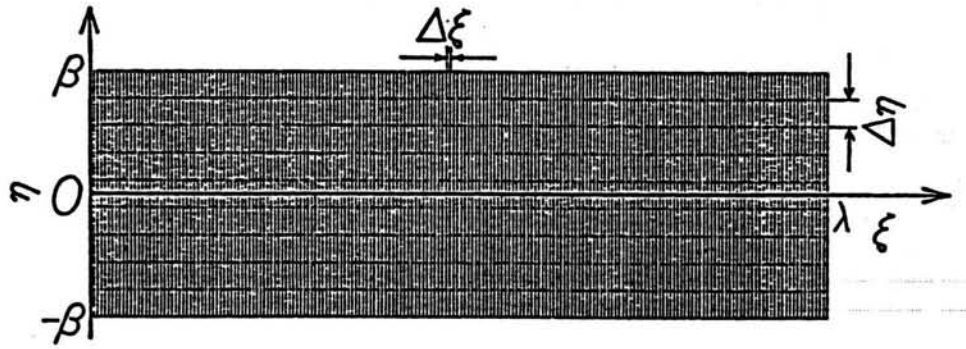

(b) ζ^*-plane

Figure 3.2 The z-plane and ζ^*-plane in the conformal mapping coordinates transformation.

By complex Fourier series expansion, the coordinates transformation relation is expressed in the form :

$$Z = F(\zeta^*) = P_0 + Q_0\zeta^* + \sum_{n=1}^{N}(P_n \cos nk_c\zeta^* + Q_n \sin nk_c\zeta^*) \tag{3.70}$$

where,

$$Z = x + iz, \quad \zeta^* = \xi + i\eta, \quad P_n = a_n + ib_n, \quad Q_n = c_n + id_n \tag{3.70.a}$$

$$k_c = \frac{\pi}{\lambda} \tag{3.70.b}$$

and λ is the region in the Z and ζ^* planes. By applying the condition $x = 0$ at $\xi = 0$, the Fourier coefficients a_n and b_n are determined as :

$$a_n = 0, \; d_n = 0. \tag{3.71}$$

Similarly, the condition for $x = \lambda$ at $\xi = \lambda$ gives

$$c_0 = 1. \tag{3.72}$$

The resulting relations for x and z in terms of ξ and η are:

$$x(\xi,\eta) = \xi + \sum_{n=1}^{N}(b_n \sinh nk_c\eta + c_n \cosh nk_c\eta) \sin nk_c\xi \tag{3.73}$$

$$z(\xi,\eta) = b_0 + \eta + \sum_{n=1}^{N}(b_n \cosh nk_c\eta + c_n \sinh nk_c\eta) \cos nk_c\xi. \tag{3.74}$$

The Fourier coefficients $b_n(n = 0,1,2,\cdots,N)$, and $c_n(n = 1,2,3,\cdots,N)$ are determined by matching the surface and bottom boundaries at $\eta = \pm\beta$, using the least square error.

The coordinates of the given surface or bottom boundaries, x and z, are specified parametrically in terms of the arc length, Δ, measured along each curve from the fixed point, $\xi = 0$. The complex values on the boundaries X_S, Z_S, X_B, and Z_B are defined as the functions of the parameter Δ, where the subscript S or B represents the surface and bottom boundaries, respectively.

To transform the surface and bottom curves into a rectangular region bounded by $\eta = \pm\beta$, $\xi = 0$ and $\xi = \lambda$, a least squares method is used. The error functions at the surface E_{SX}, E_{SZ} and at the bottom E_{BX}, E_{BZ} are defined by:

$$E_{SX}^{i+1} = \frac{1}{2\lambda}\int_{-\lambda}^{\lambda}\{X_S(\Delta^i(\xi,\beta)) - x_S^{i+1}(\xi,\beta)\}^2 d\xi \tag{3.75}$$

$$E_{SZ}^{i+1} = \frac{1}{2\lambda}\int_{-\lambda}^{\lambda}\{Z_S(\Delta^i(\xi,\beta)) - z_S^{i+1}(\xi,\beta)\}^2 d\xi \tag{3.76}$$

$$E_{BX}^{i+1} = \frac{1}{2\lambda}\int_{-\lambda}^{\lambda}\{X_B(\Delta^i(\xi,-\beta)) - x_B^{i+1}(\xi,-\beta)\}^2 d\xi \tag{3.77}$$

$$E_{BZ}^{i+1} = \frac{1}{2\lambda}\int_{-\lambda}^{\lambda}\{Z_B(\Delta^i(\xi,-\beta)) - z_B^{i+1}(\xi,-\beta)\}^2 d\xi \tag{3.78}$$

and then the total error function is defined by

$$E^{i+1} = W_{SX}^i E_{SX}^{i+1} + W_{SZ}^i E_{SZ}^{i+1} + W_{BX}^i E_{BX}^{i+1} + W_{BZ}^i E_{BZ}^{i+1} \tag{3.79}$$

where i indicates the iteration number, and W_{SX}, W_{SZ}, W_{BX} and W_{BZ} stand for weighting factors to be determined by the results of the previous iteration by:

$$W_{SX}^{i} = \frac{E_{SX}^{i}}{\bar{E}^{i}},\ W_{SZ}^{i} = \frac{E_{SZ}^{i}}{\bar{E}^{i}},\ W_{BX}^{i} = \frac{E_{BX}^{i}}{\bar{E}^{i}},\ W_{BZ}^{i} = \frac{E_{BZ}^{i}}{\bar{E}^{i}} \tag{3.80}$$

where,

$$\bar{E}^{i} = \frac{E_{SX}^{i} + E_{SZ}^{i} + E_{BX}^{i} + E_{BZ}^{i}}{4}. \tag{3.80.a}$$

The Fourier coefficients b_n and c_n and another unknown paramater β are firstly determined, so that the total error function can be minimized. Finally, they are given as:

$$\beta^{i+1} = \frac{1}{2\lambda}\int_0^{\lambda} \{Z_S(\Delta^{i}) - Z_B(\Delta^{i})\}\, d\xi \tag{3.81}$$

$$b_0^{i+1} = \frac{1}{2\lambda}\int_0^{\lambda} \{Z_S(\Delta^{i}) + Z_B(\Delta^{i})\}\, d\xi \tag{3.82}$$

$$b_n = \frac{\Psi_n\Omega_n - \Gamma_n\Phi_n}{\Upsilon_n\Omega_n - \Phi_n^2},\ c_n = \frac{\Gamma_n\Upsilon_n - \Psi_n\Phi_n}{\Upsilon_n\Omega_n - \Phi_n^2},\ (n = 1,2,3,\cdots,N) \tag{3.83}$$

where,

$$\Upsilon_n = \left(\frac{W_{SX}^{i} + W_{BX}^{i}}{2}\right)\sinh^2 nk_c\beta^{i+1} + \left(\frac{W_{SZ}^{i} + W_{BZ}^{i}}{2}\right)\cosh^2 nk_c\beta^{i+1} \tag{3.84}$$

$$\Omega_n = \left(\frac{W_{SZ}^{i} + W_{BZ}^{i}}{2}\right)\sinh^2 nk_c\beta^{i+1} + \left(\frac{W_{SX}^{i} + W_{BX}^{i}}{2}\right)\cosh^2 nk_c\beta^{i+1} \tag{3.85}$$

$$\Phi_n = \frac{(W_{SX}^i - W_{BX}^i) + (W_{SZ}^i - W_{BZ}^i)}{4} \sinh 2nk_c\beta^{i+1} \tag{3.86}$$

$$\begin{aligned}\Psi_n = \frac{\sinh nk_c\beta^{i+1}}{\lambda} \{ & W_{SX}^i \int_0^\lambda (X_S(\Delta^i) - \xi) \sin nk_c\xi d\xi \\ & - W_{BX}^i \int_0^\lambda (X_B(\Delta^i) - \xi) \sin nk_c\xi d\xi \} \\ & + \frac{\cosh nk_c\beta^{i+1}}{\lambda} \{ W_{SZ}^i \int_0^\lambda Z_S(\Delta^i) \cos nk_c\xi d\xi \\ & + W_{BZ}^i \int_0^\lambda Z_B(\Delta^i) \cos nk_c\xi d\xi \}\end{aligned} \tag{3.87}$$

$$\begin{aligned}\Gamma_n = \frac{\cosh nk_c\beta^{i+1}}{\lambda} \{ & W_{SX}^i \int_0^\lambda (X_S(\Delta^i) - \xi) \sin nk_c\xi d\xi \\ & + W_{BX}^i \int_0^\lambda (X_B(\Delta^i) - \xi) \sin nk_c\xi d\xi \} \\ & + \frac{\sinh nk_c\beta^{i+1}}{\lambda} \{ W_{SZ}^i \int_0^\lambda Z_S(\Delta^i) \cos nk_c\xi d\xi \\ & - W_{BZ}^i \int_0^\lambda Z_B(\Delta^i) \cos nk_c\xi d\xi \} .\end{aligned} \tag{3.88}$$

The iterative calculation is continued up to the allowable error range in order to obtain reasonable results.

3.3.2 Governing equations in the transformed coordinates

In the previous section, the governing equations were derived as (3.34), (3.36), (3.39) and (3.40). These equations in the transformed coordinates are derived as follows.

1) Partial differentiation operators in the ζ^*-plane

For transformation of the governing equations derived in the Z-plane, partial differentiation operators are defined as follows.

If φ is a function of x and z, the first order partial differentiation operators of φ are:

$$\frac{\partial \varphi}{\partial x} = -\frac{\partial(z,\varphi)}{\partial(\xi,\eta)} \Big/ \frac{\partial(x,z)}{\partial(\xi,\eta)}, \quad \frac{\partial \varphi}{\partial z} = -\frac{\partial(\varphi,x)}{\partial(\xi,\eta)} \Big/ \frac{\partial(x,z)}{\partial(\xi,\eta)} \tag{3.89}$$

where the transformation functions are defined as ;

$$\frac{\partial(x,z)}{\partial(\xi,\eta)} = \frac{\partial x}{\partial \xi}\frac{\partial z}{\partial \eta} - \frac{\partial x}{\partial \eta}\frac{\partial z}{\partial \xi}, \quad \frac{\partial(z,\varphi)}{\partial(\xi,\eta)} = \frac{\partial z}{\partial \xi}\frac{\partial \varphi}{\partial \eta} - \frac{\partial z}{\partial \eta}\frac{\partial \varphi}{\partial \xi},$$

$$\frac{\partial(\varphi,x)}{\partial(\xi,\eta)} = \frac{\partial x}{\partial \eta}\frac{\partial \varphi}{\partial \xi} - \frac{\partial x}{\partial \xi}\frac{\partial \varphi}{\partial \eta}. \tag{3.90}$$

In the transformation of (3.74.a) and (3.74.b), the partial differentiation of x, z with respect to ξ and η are given by:

$$\frac{\partial x}{\partial \xi} = \frac{\partial z}{\partial \eta} = 1 + \sum_{n=1}^{N} nk_c(b_n \sinh nk_c\eta + c_n \cosh nk_c\eta)\cos nk_c\xi \tag{3.91.a}$$

$$\frac{\partial x}{\partial \eta} = -\frac{\partial z}{\partial \xi} = \sum_{n=1}^{N} nk_c(b_n \cosh nk_c\eta + c_n \sinh nk_c\eta)\sin nk_c\xi. \tag{3.91.b}$$

Then, the transformation function $\partial(x,z)/\partial(\xi,\eta)$ is:

$$\frac{\partial(x,z)}{\partial(\xi,\eta)} = \left(\frac{\partial x}{\partial \xi}\right)^2 + \left(\frac{\partial z}{\partial \xi}\right)^2 = J^2. \tag{3.92}$$

Using these definitions, the relations of partial differentiations of φ with respect to (x, z) and (ξ, η) are:

$$\frac{\partial \varphi}{\partial x} = -\frac{1}{J^2}\left(\frac{\partial z}{\partial \xi}\frac{\partial \varphi}{\partial \eta} - \frac{\partial x}{\partial \xi}\frac{\partial \varphi}{\partial \xi}\right) = a\frac{\partial \varphi}{\partial \xi} - b\frac{\partial \varphi}{\partial \eta} \tag{3.93.a}$$

$$\frac{\partial \varphi}{\partial z} = -\frac{1}{J^2}\left(-\frac{\partial z}{\partial \xi}\frac{\partial \varphi}{\partial \xi} - \frac{\partial x}{\partial \xi}\frac{\partial \varphi}{\partial \eta}\right) = a\frac{\partial \varphi}{\partial \eta} + b\frac{\partial \varphi}{\partial \xi} \tag{3.93.b}$$

where,

$$a = \frac{1}{J^2}\left(\frac{\partial x}{\partial \xi}\right),\ b = \frac{1}{J^2}\left(\frac{\partial z}{\partial \xi}\right). \tag{3.94}$$

Finally, operators of the first order partial differentiation are given by:

$$\frac{\partial}{\partial x} = a\frac{\partial}{\partial \xi} - b\frac{\partial}{\partial \eta} = D_x, \quad \frac{\partial}{\partial z} = a\frac{\partial}{\partial \eta} + b\frac{\partial}{\partial \xi} = D_z. \tag{3.95}$$

Applying these operators to the second order partial differentiation, we get:

$$D_{xx}(\ ) = aD_{\xi\xi}(a,\ )\ +\ bD_{\eta\eta}(b,\ )\ -\ aD_{\xi\eta}(b,\ )\ -\ bD_{\eta\xi}(a,\ ) \tag{3.96.a}$$

$$D_{zz}(\ ) = aD_{\eta\eta}(a,\ )\ +\ bD_{\xi\xi}(b,\ )\ +\ aD_{\eta\xi}(b,\ )\ +\ bD_{\xi\eta}(a,\ ) \tag{3.96.b}$$

$$D_{xz}(\ ) = D_{zx}(\ ) = aD_{\xi\xi}(b,\ ) - bD_{\eta\eta}(a,\ ) + aD_{\xi\eta}(a,\ ) - bD_{\eta\xi}(b,) \tag{3.96.c}$$

where,

$$D_{\xi\xi}(a,\ ) = \frac{\partial}{\partial \xi}\left(a\frac{\partial}{\partial \xi}\right),\ D_{\xi\eta}(a,\ ) = \frac{\partial}{\partial \xi}\left(a\frac{\partial}{\partial \eta}\right),$$

$$D_{\eta\xi}(a, \ ) = \frac{\partial}{\partial \eta}(a\frac{\partial}{\partial \xi}), \ D_{\eta\eta}(a, \ ) = \frac{\partial}{\partial \eta}(a\frac{\partial}{\partial \eta}). \tag{3.97}$$

Furthermore, the Laplacian operator becomes:

$$\nabla^2 = \frac{\partial^2}{\partial x^2} + \frac{\partial^2}{\partial z^2}$$

$$= (a\frac{\partial}{\partial \xi} - b\frac{\partial}{\partial \eta})^2 + (a\frac{\partial}{\partial \eta} + b\frac{\partial}{\partial \xi})^2$$

$$-a\frac{\partial}{\partial \xi}(a\frac{\partial}{\partial \xi}) + b\frac{\partial}{\partial \eta}(b\frac{\partial}{\partial \eta}) - a\frac{\partial}{\partial \xi}(b\frac{\partial}{\partial \eta}) - b\frac{\partial}{\partial \eta}(a\frac{\partial}{\partial \xi})$$

$$+ a\frac{\partial}{\partial \eta}(a\frac{\partial}{\partial \eta}) + b\frac{\partial}{\partial \xi}(b\frac{\partial}{\partial \xi}) + a\frac{\partial}{\partial \eta}(b\frac{\partial}{\partial \xi})$$
$$+ b\frac{\partial}{\partial \xi}(a\frac{\partial}{\partial \eta}). \tag{3.98}$$

By using (3.94) and (3.97), the following relations can be obtained as:

$$\frac{\partial a}{\partial \eta} = \frac{\partial b}{\partial \xi}, \ \frac{\partial a}{\partial \xi} = -\frac{\partial b}{\partial \eta}. \tag{3.99}$$

Therefore, the Laplacian operator is given by:

$$\nabla^2 = \frac{1}{J^2}(\frac{\partial^2}{\partial \xi^2} + \frac{\partial^2}{\partial \eta^2}) = \frac{1}{J^2}\nabla_{(\xi,\eta)}^2. \tag{3.100}$$

2) Governing equations in the transformed coordinates

The governing equations derived in the Z-plane are transformed to the ζ^*-plane by applying the above mentioned operators. The stream function (3.34) and the vorticity (3.36) equations are rewritten as:

$$\nabla^2_{(\xi,\eta)}\psi = J^2\Omega \tag{3.101}$$

$$D_z(\psi)\left(a\frac{\partial\Omega}{\partial\xi} - b\frac{\partial\Omega}{\partial\eta}\right) - D_x(\psi)\left(a\frac{\partial\Omega}{\partial\eta} + b\frac{\partial\Omega}{\partial\xi}\right)$$

$$+ F^*(\Omega,\nu_t) = \frac{\nu_t}{J^2}\nabla^2_{(\xi,\eta)}\Omega \tag{3.102}$$

where,

$$F^*(\Omega,\nu_t) = -4D_{xz}\psi D_{xz}\nu_t + \{D_{zz}(\nu_t) - D_{xx}(\nu_t)\}\{\Omega - 2D_{xz}(\psi)\} \tag{3.103}$$

Similarly, the k-equation (3.39) and the ε-equation (3.40) are transformed to the ζ^*-plane as, respectively:

$$a\frac{\partial}{\partial\xi}(\bar{u}k) - b\frac{\partial}{\partial\eta}(\bar{u}k) + a\frac{\partial}{\partial\eta}(\bar{w}k) + b\frac{\partial}{\partial\xi}(\bar{w}k)$$

$$- \left\{a\frac{\partial}{\partial\xi}\left(\frac{\nu_t}{\sigma_k}\right) - b\frac{\partial}{\partial\eta}\left(\frac{\nu_t}{\sigma_k}\right)\right\}\left(a\frac{\partial k}{\partial\xi} - b\frac{\partial k}{\partial\eta}\right)$$

$$- \left\{a\frac{\partial}{\partial\eta}\left(\frac{\nu_t}{\sigma_k}\right) + b\frac{\partial}{\partial\xi}\left(\frac{\nu_t}{\sigma_k}\right)\right\}\left(a\frac{\partial k}{\partial\eta} + b\frac{\partial k}{\partial\xi}\right)$$

$$- \frac{\nu_t}{\sigma_k J^2}\nabla^2_{(\xi,\eta)}k$$

$$= \text{Prod} - \varepsilon \tag{3.104}$$

$$a\frac{\partial}{\partial\xi}(\bar{u}\varepsilon) - b\frac{\partial}{\partial\eta}(\bar{u}\varepsilon) + a\frac{\partial}{\partial\eta}(\bar{w}\varepsilon) + b\frac{\partial}{\partial\xi}(\bar{w}\varepsilon)$$

$$- \left\{a\frac{\partial}{\partial\xi}\left(\frac{\nu_t}{\sigma_\varepsilon}\right) - b\frac{\partial}{\partial\eta}\left(\frac{\nu_t}{\sigma_\varepsilon}\right)\right\}\left(a\frac{\partial\varepsilon}{\partial\xi} - b\frac{\partial\varepsilon}{\partial\eta}\right)$$

$$- \left\{a\frac{\partial}{\partial\eta}\left(\frac{\nu_t}{\sigma_\varepsilon}\right) + b\frac{\partial}{\partial\xi}\left(\frac{\nu_t}{\sigma_\varepsilon}\right)\right\}\left(a\frac{\partial\varepsilon}{\partial\eta} - b\frac{\partial\varepsilon}{\partial\xi}\right)$$

$$- \frac{\nu_t}{\sigma_\varepsilon J^2} \nabla^2_{(\xi,\eta)} \varepsilon$$

$$= \frac{\varepsilon}{k}(C_{1\varepsilon}\mathrm{Prod} - C_{2\varepsilon}\varepsilon) \qquad (3.105)$$

where,

$$\mathrm{Prod} = \nu_t \left[2D_x(\overline{u})^2 + 2D_z(\overline{w})^2 + \{D_z(\overline{u}) + D_x(\overline{w})\}^2 \right]. \qquad (3.106)$$

3.3.3 Finite difference method

The governing equations can be numerically solved in the two-dimensional calculation domain using a finite difference method. The technique used to solved the finite difference equations are the SOR (Successive Over Relxation) method and the Dennis-Chang method. The SOR method is applied for the stream function (continuity) equation (3.101), k-equation (3.104) and ε-equation (3.105), which are elliptic partial differential equations. Dennis-Chang method is employed to solve the vorticity (momentum) equation (3.102), which is an advection and diffusion equation.

The domain of calculation is subdivided into the rectangular grids in the transformed ζ^*-plane. Nodes i is alloted in the ξ direction and j in the η direction. The model equations in the ζ^*-plane are then expressed in the following finite difference form.

1) Stream function equation

The continuity equation (3.101) is the Poisson equation whose SOR

finite difference forms is expressed as

$$\psi_{i,j}^{n+1} = \psi_{i,j}^{n} + \frac{\alpha}{2(1+\gamma^2)}\{\psi_{i+1,j}^{n} + \psi_{i-1,j}^{n+1} + \gamma^2\psi_{i,j+1}^{n} + \gamma^2\psi_{i,j-1}^{n+1}$$

$$- \Delta\xi^2(J^2\Omega)_{i,j} - 2(1+\gamma^2)\psi_{i,j}^{n}\} \qquad (3.107)$$

where n denotes the iteration number, γ is the aspect ratio given by

$$\gamma = \frac{\Delta\xi}{\Delta\eta} \qquad (3.108)$$

and α is an acceleration parameter. For convergency, it should be ranged as

$$1 < \alpha < 2. \qquad (3.109)$$

2) Vorticity equation

Numerical solution to an advection and diffusion equation, such as the vorticity equation (3.102), suffers from the numerical (artificial) diffusion as well as wiggles when the FTCS (Forward Time Centered Space) scheme is employed. The Dennis-Chang method, however, is known as one of methods which can overcome this type of numerical problem in the advection-diffusion equation with the second order accuracy. An iteration form of (3.104) is discretized by this scheme and calculated up to the converged solution, which gives the boundary value problem solution of the original equation. The Dennis-Chang method makes the following finite difference equation.

$$\mathcal{A}_{UD}(\Omega^{n+1}) - \mathcal{D}(\Omega) = \mathcal{A}_{UD}(\Omega^{n}) - \mathcal{A}_{CD}(\Omega^{n}) \qquad (3.110)$$

where $\mathcal{A}_{UD}(\ )$ and $\mathcal{A}_{CD}(\ )$ are the upwind and centered difference operators, respectively, which given by:

$$\mathcal{A}_{UD}(\Omega) = \frac{U + |U|}{2\Delta x}(\Omega_{i,j} - \Omega_{i-1,j}) + \frac{U - |U|}{2\Delta x}(\Omega_{i+1,j} - \Omega_{i,j})$$

$$+ \frac{V + |V|}{2\Delta z}(\Omega_{i,j} - \Omega_{i,j-1}) + \frac{V - |V|}{2\Delta z}(\Omega_{i,j+1} - \Omega_{i,j}) \qquad (3.111.a)$$

$$\mathcal{A}_{CD}(\Omega) = \frac{1}{2\Delta x}\{(U\Omega)_{i+1,j} - (U\Omega)_{i-1,j}\} +$$

$$\frac{1}{2\Delta z}\{(V\Omega)_{i,j+1} - (V\Omega)_{i,j-1}\} \qquad (3.111.b)$$

and for the diffusion term :

$$\mathcal{D}(\Omega) = \frac{1}{\Delta x^2}\{(\nu_t\Omega)_{i+1,j} - 2(\nu_t\Omega)i,j\& + (\nu_t\Omega)_{i-1,j}\}$$

$$+ \frac{1}{\Delta z^2}\{(\nu_T\Omega)_{i,j+1} - 2(\nu_t\Omega)_{i,j+1} + (\nu_t\Omega)_{i,j-1}\} \qquad (3.112.a)$$

where the advection velocity U and V are written as:

$$U = aD_z(\psi) - bD_x(\psi) \quad , \quad V = -\{aD_x(\psi) + bD_z(\psi)\} \qquad (3.112.b)$$

For stable calculation, the dumping coefficient α_* is used at each iteration step as

$$\Omega^{n+1} = \alpha_* \Omega^n \tag{3.113}$$

In the case of Dirichlet boundary problem, Woods boundary condition is applicable as:

$$\Omega_0 = -\frac{1}{2}\Omega_1 - \frac{3}{\Delta x^2}(\Omega_1 - \Omega_0) + 0(\Delta x^3) \tag{3.114}$$

where the suffix 0 indicates the value at the boundary, and 1 indicates the value just inside the boundary.

On the other hand, differentiation operators D_x, D_z, D_{xx}, D_{zz} and D_{xz} are given as (3.95) and (3.96). The operators of the second order partial differentiation with respect to ξ and η in (3.96) are expressed by the difference forms.

$$D_{\xi\xi}(a,f) = \frac{\partial}{\partial \xi}\left(a\frac{\partial f}{\partial \xi}\right)$$

$$\doteq \frac{1}{\Delta \xi}\left(a_{i+1/2,j}\frac{f_{i+1,j} - f_{i,j}}{\Delta \xi} - a_{i-1/2,j}\frac{f_{i,j} - f_{i-1,j}}{\Delta \xi}\right)$$

$$= \frac{1}{(\Delta \xi)^2}\{a_{i+1/2,j}f_{i+1,j} - (a_{i+1/2,j} + a_{i-1/2,j})f_{i,j}$$

$$+ a_{i-1/2,j}f_{i-1,j}\} \tag{3.115.a}$$

$$D_{\xi\eta}(a,f) = \frac{\partial}{\partial \xi}\left(a\frac{\partial f}{\partial \eta}\right)$$

$$\doteq \frac{1}{\Delta\xi}\left(a_{i+1/2,j}\frac{f_{i+1/2,j+1/2} - f_{i+1/2,j-1/2}}{\Delta\eta}\right.$$

$$\left. - a_{i-1/2,j}\frac{f_{i-1/2,j+1/2} - f_{i-1/2,j-1/2}}{\Delta\eta}\right)$$

$$= \frac{1}{\Delta\xi\Delta\eta}\left\{a_{i+1/2,j}\left(\frac{f_{i+1,j+1} - f_{i,j+1}}{2} - \frac{f_{i+1,j} - f_{i,j}}{2}\right)\right.$$

$$\left. - a_{i-1/2,j}\left(\frac{f_{i,j} - f_{i-1,j}}{2} - \frac{f_{i,j-1} - f_{i-1,j-1}}{2}\right)\right\} \qquad (3.115.b)$$

$$D_{\eta\xi}(a,f) = \frac{\partial}{\partial \eta}\left(a\frac{\partial f}{\partial \xi}\right)$$

$$\doteq \frac{1}{\Delta\eta}\left(a_{i,j+1/2}\frac{f_{i+1/2,j+1/2} - f_{i-1/2,j+1/2}}{\Delta\xi}\right.$$

$$\left. - a_{i,j-1/2}\frac{f_{i+1/2,j-1/2} - f_{i-1/2,j-1/2}}{\Delta\xi}\right)$$

$$= \frac{1}{\Delta\xi\Delta\eta}\left\{a_{i,j+1/2}\left(\frac{f_{i+1,j+1} - f_{i+1,j}}{2} - \frac{f_{i,j+1} - f_{i,j}}{2}\right)\right.$$

$$\left. - a_{i,j-1/2}\left(\frac{f_{i,j} - f_{i,j-1}}{2} - \frac{f_{i-1,j} - f_{i-1,j-1}}{2}\right)\right\} \qquad (3.115.c)$$

$$D_{\eta\eta}(a,f) = \frac{\partial}{\partial \eta}\left(a\frac{\partial f}{\partial \eta}\right)$$

$$\doteq \frac{1}{\Delta\eta}\left(a_{i,j+1/2}\frac{f_{i,j+1} - f_{i,j}}{\Delta\eta} - a_{i,j-1/2}\frac{f_{i,j} - f_{i,j-1}}{\Delta\eta}\right)$$

$$= \frac{1}{(\Delta\eta)^2}\left\{a_{i,j+1/2}f_{i,j+1} - (a_{i,j+1/2} + a_{i,j-1/2})f_{i,j}\right.$$

$$+ a_{i,j-1/2} f_{i,j-1} \} \qquad (3.115.d)$$

where,

$$a_{i+1/2,j} = \frac{1}{2}(a_{i+1,j} + a_{i,j}),\ a_{i-1/2,j} = \frac{1}{2}(a_{i,j} + a_{i-1,j}) \qquad (3.116)$$

3) k-ε equations

Because the k-equation (3.104) and the ε-equation (3.105) are elliptic partial differential equations, the SOR method is employed in the numerical calculation. The finite difference form of the k-equation is given by:

$$k_{i,j}^{n+1} = k_{i,j}^{n} + \frac{\alpha}{2(1+\gamma^2)} \{ k_{i+1,j}^{n} + k_{i+1,j}^{n} + k_{i-1,j}^{n+1} + \gamma^2 k_{i,j+1}^{n} + \gamma^2 k_{i,j-1}^{n+1}$$

$$- 2(1+\gamma^2) k_{i,j}^{n} - \frac{\sigma_k J^2}{\nu_t} W \} \qquad (3.117)$$

where,

$$W = - \frac{a\Delta\xi}{2} \mathfrak{L}_\xi(\bar{u}k) + \frac{b\gamma\Delta\xi}{2} \mathfrak{L}_\eta(\bar{u}k) - \frac{a\gamma\Delta\xi}{2} \mathfrak{L}_\eta(\bar{w}k) - \frac{b\gamma\Delta\xi}{2} \mathfrak{L}_\xi(\bar{w}k)$$

$$+ \frac{1}{\sigma_k} \{ \frac{a}{2} \mathfrak{L}_\xi(\nu_t) - b\frac{\gamma}{2} \mathfrak{L}_\eta(\nu_t) \} \{ \frac{a}{2} \mathfrak{L}_\xi(k) - b\frac{\gamma}{2} \mathfrak{L}_\eta(k) \}$$

$$+ \frac{1}{\sigma_k} \{ a\frac{\gamma}{2} \mathfrak{L}_\eta(\nu_t) + \frac{b}{2} \mathfrak{L}_\xi(\nu_t) \} \{ a\frac{\gamma}{2} \mathfrak{L}_\eta(k) + \frac{b}{2} \mathfrak{L}_\xi(k) \}$$

$$+ \mathrm{Prod}_{i,j} - \varepsilon_{i,j} \qquad (3.118.a)$$

$$\mathfrak{L}_\eta = \varphi_{i,j+1} - \varphi_{i,j-1}, \qquad \mathfrak{L}_\xi = \varphi_{i+1,j} - \varphi_{i-1,j} \qquad (3.118.b)$$

In the same manner, the finite difference form of the ε-equation is obtained, as:

$$\varepsilon_{i,j}^{n+1} = \varepsilon_{i,j}^{n} + \frac{\alpha}{2(1+\gamma^2)}\{\varepsilon_{i+1,j}^{n} + \varepsilon_{i+1,j}^{n+1} + \varepsilon_{i-1,j}^{n+1} + \gamma^2\varepsilon_{i,j+1}^{n} + \gamma^2\varepsilon_{i,j-1}^{n+1}$$

$$- 2(1+\gamma^2)\varepsilon_{i,j}^{n} - \frac{\sigma_\varepsilon J^2}{\nu_t}W\} \qquad (3.119)$$

where,

$$W = -\frac{a\Delta\xi}{2}\mathfrak{L}_\xi(\bar{u}\varepsilon) + \frac{b\gamma\Delta\xi}{2}\mathfrak{L}_\eta(\bar{u}\varepsilon) - \frac{a\gamma\Delta\xi}{2}\mathfrak{L}_\eta(\bar{w}\varepsilon) - \frac{b\gamma\Delta\xi}{2}\mathfrak{L}_\xi(\bar{w}\varepsilon)$$

$$+ \frac{1}{\sigma_\varepsilon}\{\frac{a}{2}\mathfrak{L}_\xi(\nu_t) - b\frac{\gamma}{2}\mathfrak{L}_\eta(\nu_t)\}\{\frac{a}{2}\mathfrak{L}_\xi(\varepsilon) - b\frac{\gamma}{2}\mathfrak{L}_\eta(\varepsilon)\}$$

$$+ \frac{1}{\sigma_\varepsilon}\{a\frac{\gamma}{2}\mathfrak{L}_\eta(\nu_t) + \frac{b}{2}\mathfrak{L}_\xi(\nu_t)\}\{a\frac{\gamma}{2}\mathfrak{L}_\eta(\varepsilon) + \frac{b}{2}\mathfrak{L}_\xi(\varepsilon)\}$$

$$+ \frac{\varepsilon_{i,j}}{k_{i,j}}(\mathrm{Prod}_{i,j}C_{1\varepsilon} - \varepsilon_{i,j}C_{2\varepsilon}) \qquad (3.120.a)$$

$$\nu_{ti,j} = C_\mu\frac{(k_{i,j}^{n})^2}{\varepsilon_{i,j}} \qquad (3.120.b)$$

3.3.4 Boundary conditions

As discussed in the previous section, the boundary conditions have to be given at all the boundaries with consistency, for mean-flow equations and k-ε equations. In the 2DV circulation model, there are four unknown variables to be solved, ψ, Ω, k and ε.

1) Surface boundary conditions

At the surface, both the kinematic and dynamic boundary conditions for mean flow variables, ψ and Ω, are determined by the approximate expressions of the momentum and mass conservation equations in the surface layer.

The kinematic boundary condition derived in Section 2.2.4 in the Z-plane determines the stream function in the transformed coordinates. One possible example can be given as follows.

If the velocity components u^*, w^* are determined in the ζ^*-plane as:

$$w^* = -\frac{\partial \psi}{\partial \xi}, \quad u^* = \frac{\partial \psi}{\partial \eta} \tag{3.121}$$

the equation (3.121) can be transformed to:

$$\overline{u}^* = -\frac{\partial x}{\partial \eta}\left(\overline{w}_s - \overline{u}_s \frac{\partial \zeta}{\partial x}\right) = -\frac{\partial M_S}{\partial \eta} \tag{3.122.a}$$

$$\overline{w}^* = \frac{\partial x}{\partial \xi}\left(\overline{w}_s - \overline{u}_s \frac{\partial \zeta}{\partial x}\right) = \frac{\partial M_S}{\partial \xi} \tag{3.122.b}$$

In equations (3.122.a) and (3.122.b) $-M_S$ is the stream function in the transformed coordinates system, which gives the surface boundary condition for the ψ-equation.

The boundary condition for the vorticity equation is

$$\Omega_s^* = \frac{\partial \overline{u}^*}{\partial \eta}\Big|_s - \frac{\partial \overline{w}^*}{\partial \xi}\Big|_s \tag{3.123}$$

The dynamic boundary condition derived in the Z-plane gives the shear stress

τ_s/ρ at the surface, and equation (3.120.a) gives the $\partial \overline{w}^*/\partial \xi|_s$. Then, the surface boundary condition of vorticity is given as

$$\Omega_s^* = \frac{\tau_s}{\rho \nu_t}\Big|_s - \frac{\partial^2 M}{\partial \xi^2}\Big|_s \tag{3.124}$$

The boundary condition for the k-equation at the surface can be given in terms of the energy production due to breaking waves.

$$P_s = \frac{gH^3 D}{4h^2 T_w} \tag{3.125}$$

where D is the nondimensional energy dissipation rate due to breaking waves which is given by hydraulic jump approximation. The turbulent production term Prod is defined as

$$\text{Prod} = \nu_t\{2(\frac{\partial \overline{u}}{\partial x})^2 + 2(\frac{\partial \overline{w}}{\partial z})^2 + (\frac{\partial \overline{u}}{\partial z} + \frac{\partial \overline{w}}{\partial x})^2\} \tag{3.126}$$

Assuming the term $\partial \overline{u}/\partial z$ is much larger than others, the boundary condition for the k-equation is given by

$$P = \nu_t(\frac{\partial \overline{u}}{\partial z})^2 = \nu_t D_z^2(\overline{u}) \tag{3.127}$$

To determine the boundary condition for the ε-equation, some reasonable approximation is needed. In the case of the 2DV circulation model of surf zone, the turbulent property must be introduced into this approximation. If we assume that breaking waves generate turbulence which

eventually diffuses into the entire inner layer, then it is possible to relate the diffusion term in k-equation $\mathfrak{L}(k)$ to the energy dissipation term in the following manner:

$$\mathfrak{L}(k) = \alpha\varepsilon = \text{Prod} - \varepsilon, \qquad \varepsilon = \gamma\ \text{Prod} \tag{3.128}$$

Where the factors α and γ are used to determine the relation between turbulence dissipation and diffusion, and turbulence dissipation and production, respectively. If α is proportional to the distance from the surface boundary and $\gamma_s = 1$ at the bottom boundary, α and γ distributions are obtained as:

$$\alpha = \frac{1 - \gamma_s}{2\gamma_s}\left(\frac{\eta}{\beta} + 1\right), \qquad \gamma = \left\{1 + \frac{1 - \gamma_s}{2\gamma_s}\left(\frac{\eta}{\beta} + 1\right)\right\}^{-1} \tag{3.129}$$

where γ_s is the turbulence dissipation factor at the surface. These assumed factors satisfy the following physical properties of turbulence and its transport. 1) When no turbulence diffusion exists at the wall boundary, turbulence dissipation is balanced with turbulent production, i.e., $\varepsilon = P_b$. 2) The magnitude of diffusion is proportional to the distance from the turbulent source which is supplied by breaking waves.

From (3.127), the surface boundary condition for the k-equation is given by

$$k_s = \sqrt{\frac{\gamma_s}{C_\mu}}\left|\frac{\tau_s}{\rho}\right| \tag{3.130}$$

where τ_s is shear stress at the surface. The boundary condition is

$$\varepsilon = \gamma_s P_s \tag{3.131}$$

where γ_s is the coefficient to be determined by turbulence properties.

2) Bottom boundary conditions

The bottom boundary condition for the stream function can be determined by the same way as the surface boundary. The kinematic boundary condition in the Z-plane (3.68) leads the expressions of $\overline{u}^*$, $\overline{w}^*$ in the transformed coordinates as:

$$\overline{u}^* = -\frac{\partial x}{\partial \xi}\left(\overline{w}_b + \overline{u}_b \frac{\partial h}{\partial x}\right) = 0 \tag{3.132.a}$$

$$\overline{w}^* = \frac{\partial x}{\partial \eta}\left(\overline{w}_b + \overline{u}_b \frac{\partial h}{\partial x}\right) = 0 \tag{3.132.b}$$

Equations (3.130.a) and (3.130.b) depict that the stream function becomes an arbitrary constant at the bottom boundary. The bottom boundary condition for the vorticity equation can be determined when the bottom shear stress τ_b/ρ is given by:

$$\Omega_b^* = \frac{\partial \overline{u}^*}{\partial \eta}\bigg|_b - \frac{\partial \overline{w}^*}{\partial \xi}\bigg|_b = \frac{\partial \overline{u}^*}{\partial \eta}\bigg|_b = \frac{\tau_b}{\rho \nu_{tb}} \tag{3.133}$$

In this model, the bottom shear stress is estimated by

$$\tau_b = \rho f \overline{u}_b^2 \tag{3.134}$$

On the other hand, from (3.127) to (3.129), the bottom boundary conditions of k and ε equations are given respectively as:

$$k_b = \sqrt{\frac{1}{C_\mu}} \left| \frac{\tau_b}{\rho} \right| \tag{3.135}$$

$$\varepsilon_b = P_b, \quad P_b = \frac{\tau_b}{\rho \nu_{tb}} \tag{3.136}$$

3) Side boundary conditions

As was discussed in the previous section, the velocity vector type boundary condition is employed here. If the distribution of the eddy viscosity is assumed as

$$\nu_t = \frac{-2\nu_{ts}\nu_{tb}\beta}{\nu_{ts}(\eta - \beta) - \nu_{tb}(\eta + \beta)} \tag{3.137}$$

the velocity profile at the side boundary is a third order polynomial function of η and the stream function is a forth order. The stream function can be determined by using the following conditions:

$$\psi_s = -M_S, \qquad \psi_b = 0, \qquad \left.\frac{\partial^2 \psi}{\partial \eta^2}\right|_s = -\frac{\tau_s}{\nu_t},$$

$$\left.\frac{\partial^2 \psi}{\partial \eta^2}\right|_b = -\frac{\tau_b}{\nu_t}, \qquad \left.\frac{\partial \psi}{\partial \eta}\right|_s = \bar{u}_s^* \tag{3.138}$$

The stream function at $\xi = 0, \lambda$ is then given by:

$$\psi = a\eta^4 + b\eta^3 + c\eta^2 + d\eta + e \tag{3.139.a}$$

where,

$$a = -\frac{\bar{u}_s}{8\beta^3} - \frac{M_S}{16\beta^4} - \frac{1}{24\beta^2\nu_t}(T_B + 2T_S) \tag{3.139.b}$$

$$b = \frac{1}{12\beta\nu_t}(T_B - T_S) \tag{3.139.c}$$

$$c = \frac{3\bar{u}_s}{4\beta} + \frac{3M_S}{8\beta^2} + \frac{T_S}{4\nu_t} \tag{3.139.d}$$

$$d = \frac{M_S}{2\beta} - \frac{\beta}{12\nu_t}(T_B - T_S) \tag{3.139.e}$$

$$e = -\frac{13}{16}M_S - \frac{5}{8}\bar{u}_s\beta + \frac{\beta^2}{24\nu_t}(T_B - 4T_S) \tag{3.139.f}$$

and

$$T_S = \frac{\tau_s}{\rho} = \frac{g}{2}\frac{\partial}{\partial x}\left(H^2B_0 + 0.81\frac{H^4}{L^2}\right) \tag{3.140.a}$$

$$T_B = \frac{\tau_b}{\rho} = f\bar{u}_B^2, \quad f = 0.0026 \tag{3.140.b}$$

To determine the boundary condition for the vorticity equation, the distribution of $\partial\bar{w}^*/\partial\xi$ must be given at the side boundary. In this model, linear interpolation of $\partial\bar{w}^*/\partial\xi$ between surface and bottom is assumed. By this, the boundary condition at the side boundary is then given by

$$\Omega = \frac{\partial \overline{u}^*}{\partial \eta} - \frac{\partial \overline{w}^*}{\partial \xi} \tag{3.141}$$

3.3.5 Calculation Algorithm and Examples

The numerical model of 2DV nearshore circulation is established in terms of the finite difference method with alignment of variables shown in Figure 3.3. The stream function ψ and vorticity Ω are defined at the grids corners k, ε, ν_t are at the cell-centers, where ν_t is calculated in the ψ-Ω system by a four-point interpolation. The flow chart for calculation is shown in Figure 3.4.

In order to verify the applicability of the numerical model explained in the previous section, some numerical examples are shown and compared with experiments of Stive and Wind (1982). Whose conditions are, the beach slope s = 1/40, wave period T = 1.79, deep water steepness Ho/Lo = 0.032. The changes in wave heights relative to breaker height in the Z and ζ^* planes are shown in Figure 3.5. Figure 3.6 shows the changes in the relative values of wave celerity c/c_B, wave heights H/H_B and mean water level ζ/h_B with the relative water depth h/h_B to compare with the experiments by Hansen and Svendsen (1979). The figure shows that the calculations are in reasonable agreement with the experiments.

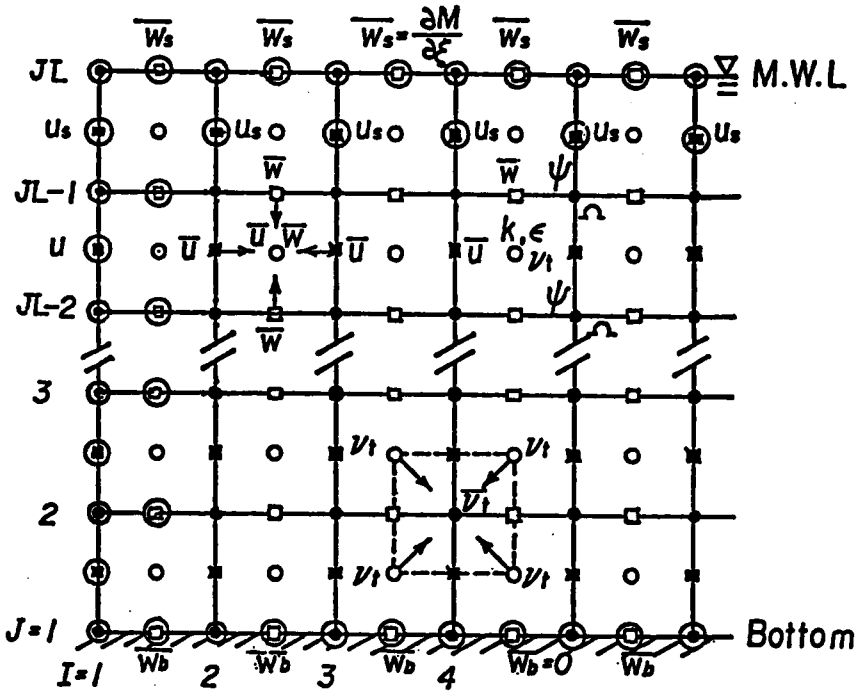

Figure 3.3 Grid system and alignment of variable used in the numerical calculation.

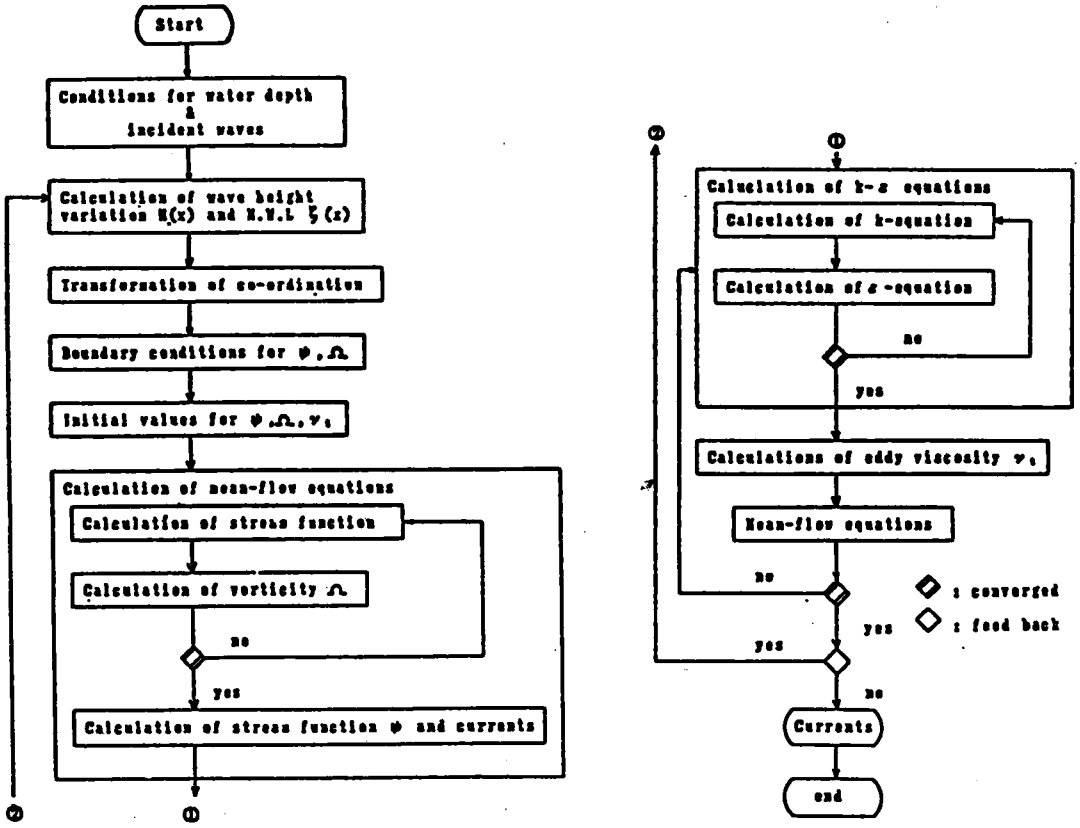

Figure 3.4 Flowchart of the numerical model of the 2-D Vertical nearshore circulation.

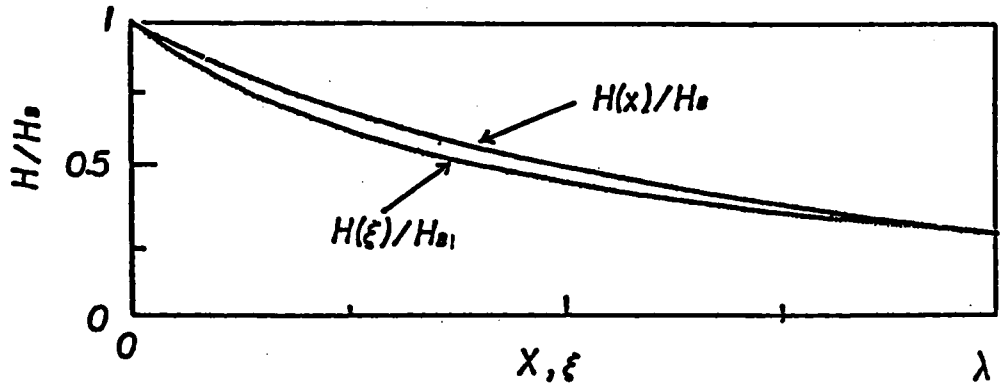

Figure 3.5 Changes in wave heights calculated numerically in the Z and ζ^*-planes, respectively.

The undertow velocity field in the surf zone, especially in the inner region (quasi-steady bore region), can be calculated by using the 2-DV model developed in this study. Difficulty, however still exists in improving the side boundary conditions which are in consistency with both mean and turbulent flow fields including bottom and surface boundary conditions. In other words, further extension of the proposed 2-DV model is required to clarify the treatment of the bottom boundary conditions which can satisfy the no-slip condition of mean flow and wall boundary condition of the k-ε equations. To verify the mean flow (undertow) model, test calculation is performed by using the same assumption of ν_t as Svendsen (1984) which was also attempted the comparison between his undertow model and Stive and Wind's (1982) experiments. In assuming the slip condition for the undertow on the bottom, and that the undertow velocity distributions at both side boundaries are third order polynomial functions, the two dimensional vertical circulation was calculated as shown in Figure 3.7, in which all wave parameters used of Stive and Wind (1982).

Furthermore, the vertical velocity distribution of undertow in the inner layer region is compared with experiments by Stive and Wind (1982) in the relative water depth range of h/h_B = 0.88. 0.765, 0.647 and 0.53. Comparisons between the calculated velocity vectors and the experiments are shown in the Figure 3.8, where solid circles indicate the experimental data.

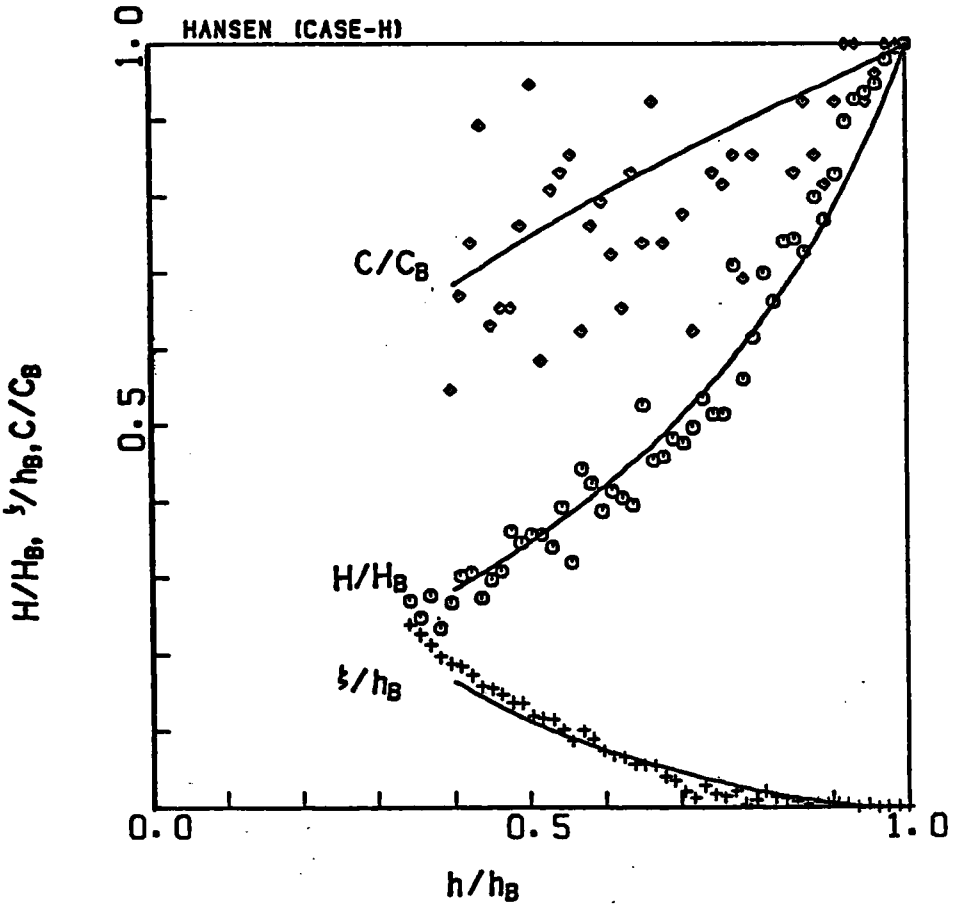

Figure 3.6 Changes in the calculated relative wave celerity c/c_B, wave height H/H_B and mean water level ζ/h_B in the Z-plane versus the relative water depth h/h_B in the Z-plane in comparison with Hansen and Svendsen's (1979) experiments.

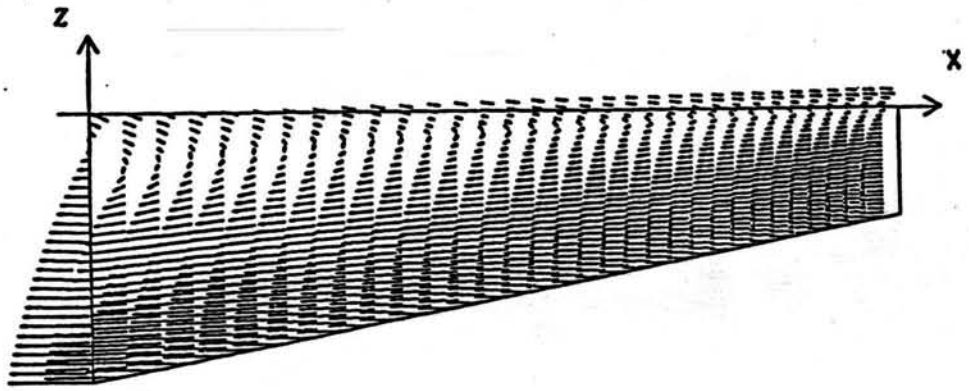

Figure 3.7 The vertical circulation pattern calculated by the 2-D vertical circulation model under the experimental condition of Stive and Wind (1985).

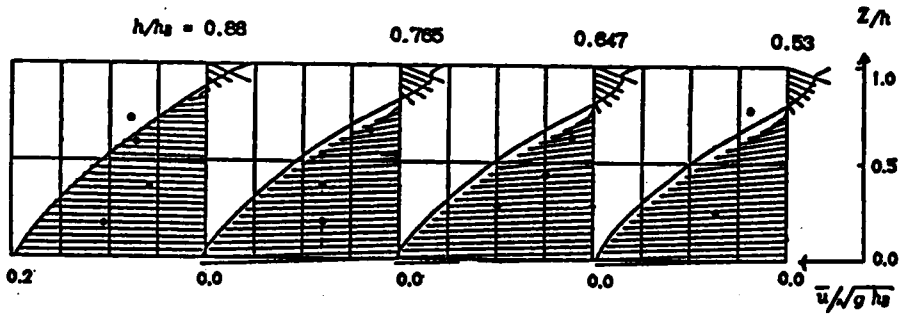

Figure 3.8 The vertical distributions of undertow velocity vectors and horizontal velocity profiles (solid curves) calculated by the 2-D vertical circulation model in comparison with the experiments of stive and wind (1985).

Because of an insufficient quantity of experimental data verification is not possible, however, the theoretical curves agree resonably well with experimens. From the comparison between undertow test calculations and Stive and Wind's laboratory experiment, it could be concluded that the proposed 2-DV nearshore circulation model is applicable to predict the undertow in the whole inner region. For the case of arbitrary bathymetry, the 2-DV model developed in this study is more applicable than the previous 1-DV model.

3.4 Conclusions

The 2-D vertical nearshore circulation for the inner region was proposed using a simplified two layer model, i.e., the surface and inner layers. The results of this study are summarized as follows.

The governing equations describing the mean flow motion of the inner region were established in terms of the vorticity and stream functions which were derived from the mass and momentum equations. While the governing equations of turbulent motion were derived based on the k-ε equation. This 2-D vertical circulation model was not only able to provide the vertical distribution of undertow velocity but also the vector components in vertical plane. In the calculation, the kinematic boundary condition, the dynamic boundary condition and the wave energy dissipation along the mean water level were determined to specify the stream function, the vorticity and the production of TKE, respectively. To formulate the required boundary conditions for the dynamics of the inner region along mean water level, the method developed by Madsen and Svendsen (1979) was employed. In order to quantify the boundary conditions, the variation of wave height and wave

set-up were first calculated using Svendsen's (1984) model. In which the wave energy dissipation is assumed analogous to that of hydraulic jump.

In performing the numerical calculation, the conformal mapping method was used to transform the coordinate of a planar beach into two parallel straight lines. In the transformed coordinates, the boundary condition for the stream function was defined as the shoreward mass transport due to wave evaluated along the M.W.L., while for the vorticity by both the dynamic and kinematic boundary conditions.

In order to overcome the remaining closure problems, two factors α and γ were proposed based on the assumption that turbulence generated by breaking waves eventually diffuses into the entire inner layer, and considered to be proportional to the distance from the surface boundary. Where α and γ were used to relate the diffusion term of TKE, and the production term of TKE, to the turbulence dissipation, respectively. They could be justified as when no turbulence diffusion at the wall boundary, α=0, the production term of TKE was equivalent to the turbulence dissipation, which agreed with the usual boundary condition.

The numerical calculation using the beach slope s = 1/40, wave period T = 1.79 sec and deep water steepness Ho/Lo = 0.032 resulted in dimensionless variation of wave celerity, wave heights, and mean water level. These results agreed reasonably well with the experiments of Hansen and Svendsen (1979). A test calculation of the mean flow in the inner layer was performed using: ν_t assumption of Svendsen (1984), third order polynomial functions of the undertow at both side of boundaries, and the slip condition for undertow on the bottom. The undertow test calculation in the relative water depth range of h/h_B = 0.88, 0.765 0.647, 0.53, were compared to to the results of Stive and Wind's laboratory experiment. From

this comparison, the applicability of the present model in reasonably predicting the undertow appeared to have been justified.

REFERENCE

Buhr-Hansen, J. and I.A. Svendsen, 1984, A thoretical and experimental study of undertow, Proc. 19th Inter. Conf. on Coastal Eng., pp.2246-2262.

Buhr-Hansen, J. and I.A. Svendsen, 1979, Regular waves in shoaling water - experimental data, Ins. Hydrodyn. Hydraulic Eng., Series paper 21, Tech. University of Denmark, Lyngby.

Daly, B.J. and F.H. Harlow, 1970, Transport equations in turbulence, The Physics of Fluids, Vol.13, Number 11,

Duncan, J.H., 1981, An experimental investigation of breaking waves produced by a towed hydrofoil, Proc. R. Soc., London, Ser. A, 377, pp.331-348.

Dyhr-Nielsen, M. and T. Sørensen, 1970, Sand transport phenomena on coasts with bars, Proc. 12th Inter. Conf. on Coastal Eng., pp.855-866.

Hanjalic, K. and B.E. Launder, 1972, A Reynolds stress model of turbulence and its application to thin shear flows, Jour. Fluid Mech., Vol.52, pp.609-638.

Hanjalic, K. and B.E. Launder, 1976, Contribution towards a Reynolds-stress closure for low-Reynolds-number turbulence, Jour. Fluid Mech., Vol.74, pp.593-610.

Madsen, P.A. and I.A. Svendsen, 1979, On the form of the integrated conservation equations for waves in the surf zone, Inst. Hydrodyn. and Hydraulic Engrg. Tech. Univ. Denmark, Prog. Rep.48, pp.31-39.

Rodi, W., 1984, Turbulence models and their application in hydraulics, IAHR-Publication, Delft, 104p.

Stive, M.J.F. and H.G. Wind, 1982, A STudy of radiation stress and set-up in the nearshore region, Coastal Engineering, Vol.6, pp.1-25

Stive, M.J.F. and H.G. Wind, 1985, Cross-shore mean flow in the surf zone, Delft Hydraulics Laboratory-Report R1351, 15p.

Svendsen, I.A., 1984a, Wave heights and set-up in a surf zone, Coastal Engineering, Vol.8, pp.303-329.

Svendsen, I.A., 1984b, Mass flux and undertow in a surf zone, Coastal Engineering, Vol.8, pp.347-365.

Svensson, U., 1978, A mathematical model of the seasonal thermocline, 187p.

Tsuchiya, Y., T. Yamashita, M. Uemoto, 1986, On the undertow in the surf zone, Conf. on Coastal Eng. in Japan, pp. 31-35. (in Japanese)

Yamashita,T., A.S. Dadang, T. Shishikura and Y. Tsuchiya, 1988, The 2DV circulation model in the surf zone, Proc.35th Japanese Conf. on Coastal Eng., pp. 267-271.

Wanstrath, J.J., R.E. Whitaker, R.O. Reid, A.C. Vastano, 1976, Storm surge simulation in transformed coordinates, Volume I, Technical Report No.76-3, U.S. Coastal Engineering Research Center, 166p.

Wanstrath, J.J., 1976, Storm surge simulation in transformed coordinates, Volume II, Technical Report No.76-3, U.S. Coastal Engineering Research Center, 176p.

CHAPTER 4 CONCLUDING REMARKS

Nearshore circulation such as rip currents and undertow are of great importance in the so called nearshore dynamics. Sediment transport in the nearshore zone is a complex three dimensional phenomenon resulting from the combined actions of both waves and nearshore currents. In formulating the nearshore sediment transport it is necessary to investigate the effects of both horizontal and vertical circulations and the action of waves.

In this 3-D nearshore circulation investigation, the horizontzal(2-DH) and vertical(2-DV) circulations such as rip current and undertow in the nearshore zone are independently formulated. Problems which had previously impeded a mathematical solution to the nearshore circultaion were solved deriving the field equations of rip currents both in the shoaling and surf zones. zones. Furthermore a new formulation of the dynamics of the vertical circulation in the surf zone was developed, which describes the vertical flow pattern in the so-called inner region.

In Chapter 2, the rip current field equations are formulated using the expressions of wave induced nearshore driving forces, which are derived employing the MSE. The MSE is capable of expressing both wave refraction and amplitude decay. By introducing the wave-current interaction into the MSE, and employing a perturbation method with a scale parameter of the beach slope, a set of rip current field equations was mathematically derived for both the shoaling and surf zones. The eigenvalues for the rip current spacings were determined by the matching condition at the breaking point. Furthermore, the integration constant for the solution was solved using the wave energy flux conservation between prebreaking and postbreaking state.

The rip current spacings were then expressed in terms of Dalrymple and Lozano's parameter and by the so-called surf similarity parameter. The theoretical rip current spacings agreed well with field data in the region of $0.2< \xi_B$. Compared with laboratory data, however, the theoretical spacings were about half. This discrepancy was believed to exist due to the influence of the littoral boundaries in the laboratory basins. Therefore, a series of rip current formation experiment were performed to determine the littoral boundary influence. A theoretical solution of the rip currents, which includes the littoral boundary effect, was then developed. Consequently, the theoretical curve of rip spacings agreed well with the experiments.

Numerical calculations of the theoretical rip current solutions were performed in order to display velocity profiles along the center line of the rip current and the rip current circulation patterns at the scale of laboratory and field. The rip currents of this mathematical solution flowed seaward from the minimum run-up point, attained a maximum velocity in the middle of the surf zone and gradually decayed seaward. The magnitude of rip current decreases as its spacing increases, and the circulation pattern is extended seaward. The theoretical velocities of rip current were found to reasonably compare with laboratory and field measurements.

In Chapter 3, the 2DV model for the nearshore circulation such as undertow in the so-called inner region was proposed based on the governing equations of mass and momentums as well as the so-called k-ε equations. From the governing equations in the surface layer, the kinematic and dynamic boundary conditions for the inner layer were derived. The mathematical model consists of three sub-model, (1) calculation of breaking wave height variation, (2) calculation of mean flow, and (3) calculation of turbulent

eddy viscosity field in terms of the k-ε equations. These three sub-models are related to each other through the eddy viscosity and mean flow fields. The combined kinematic and dynamic boundary conditions for the mean flow field resulted in a Dirichlet boundary value problem of all equations to be solved in the inner layer.

For numerical calculation, a coordinate transformation technique was employed, which allows the use of realistic bottom and surface boundaries as well as the generation an effective grid system. The numerical calculation method was presented for each equation, and the Dennis-Chang method was applied to solve the set of undertow equations. Under the experimental condition of Stive and Wind, numerical calculation was performed for the set of equations in order to determine the applicability of the 2DV circulation (undertow) model. The calculated mean flow patterns of undertow generally agreed with experimental results, except in the vicinity of the sea bed. Further developments in the application of the k-ε equations are needed before improvements in near bed predictions are possible.

Finally, several suggestion are made towards the development of future nearshore circulation models. In the present horizontal nearshore circulation model, the lateral mixing terms in the governing equations were not introduced, therefore, the calculated circulation patterns extend offshore of the breaker line due to the bottom friction effect only. By introducing these terms effectively into the governing equations, the nearshore circulation patterns will extend more offshore. It is however noted that difficulty in the formulation of rip currents may exist in the higher order partial differential equations.

In the vertical nearshore circulation, as previously stated,

improvement of the proposed 2DV model is required by applying the k-ε equations to calculate the realistic undertow flow patterns in the vicinity of the sea bed. Since the mathematical formulation was already made in the present investigation, such improvement will be made in the near future.